Università degli Studi di Messina

Dipartimento di Scienze Chimiche, Biologiche, Farmaceutiche ed Ambientali

Dottorato di Ricerca in "Scienze Chimiche"

Doctor of Philosophy in "Chemical Sciences"

Chromatographic Separation Techniques coupled to Mass Spectrometry for the Analysis of Complex Samples

---

PhD Thesis of:

Veronica Inferrera

Supervisor:

Prof. **Paola Dugo**

Coordinator:

Prof. **Sebastiano Campagna**

SSD CHIM/10
XXIX Ciclo 2014-2016

TABLE OF CONTENTS

Chapter IX
On-line coupling of ultra performance convergence chromatography and ultra high pressure liquid chromatography for enhancing orthogonality in comprehensive separations

Chapter X

Multidimensional preparative liquid chromatography to isolate flavonoids from Citrus products

CHAPTER I
General Introduction

1.1. Introduction

Liquid chromatography (LC) was defined in 1903 by the work of the Russian botanist Tswett. His pioneering studies focused on separating compounds (leaf pigments), extracted from plants using a solvent, in a column of calcium carbonate. Tswett coined the name chromatography (from the Greek words *chroma* and *graph* literally meaning *color writing*) to describe his colourful experiment (curiously, the name Tswett means color). Further development of chromatography came in 1941 with the work of Martin and Synge (Martin & Synge, 1941). They established the basics of partition chromatography with the separation of acetyl derivatives of natural amino-acids, and also developed "plate theory" for which they won the Nobel Prize in 1952. However, the modern LC owes its present to the scientist Horváth, who in 1965 packed a 1 mm internal diameter (I.D.) column with such μ-porous particles (Horváth & Lipsky, 1966). The mobile phase was flushed into the column at different flow rates (in the range of μL-mL/min), depending on the column characteristics (length, I.D. and particles size), with rather high back pressures. As a consequence, "high pressure liquid chromatography" (HPLC) or "high performance liquid chromatography" was the name of the modern LC techniques. Currently, every liquid chromatography application can be considered a HPLC application, therefore in this thesis the acronym LC or HPLC will be used. Today, LC, in its various forms, is one of the most powerful methods commonly applied for the separation of real-world samples, in several fields. By using LC, it is possible to analyze a wide range of compounds with various molecular weights, from hundreds to hundreds of thousands. This technique allows to determine the quali-quantitative profile of

different compounds; at present, analytes in trace concentrations as low as parts per trillion (ppt) may be easily identified. HPLC can be also applied to isolate specific molecules by using preparative system. Compared to the gas chromatography (GC) technique, LC allow to analyze thermolable and non-volatile molecules.

1.2. Columns

The first stationary phases used in LC were based on very polar chemicals, like cellulose, silica or alumina. In 1950 Howard and Martin observed that very apolar compounds, such as long chain fatty acids, were not sufficiently separated on a polar support, regardless on the mobile phase employed (Howard & Martin, 1950). Subsequently, they used a cellulose acetate stationary phase and water in combination with a very apolar solvent, like octane, to attain a good quality separation (high chromatographic resolution). Such a stationary phase, less polar than the mobile phase, was named "reversed phase" (RP) to differentiate it from the conventional "normal phase" (NP). The use of RP chromatography has gained enormous popularity, since the discovery of bonded phase, i.e. with the possibility to functionalize the silica particles. Nowadays, RP-LC covers more than 80% of applications.

The most common columns used in LC have I.D. 2-2.1 mm or 4-4.6 mm and a length of 10-25 cm. The choice of the column mainly depends on the application. In general, columns with smaller I.D. allow detecting very low quantity of sample and reducing the amount of mobile phases, but they show a low sample capacity. Wider columns are normally employed for preparative LC. Table I-1 reports the classification of analytical LC columns according to their I.D. (Saito, *et al.*, 2004).

Table 1-1. *Classification of LC columns according to I.D.*

Column designation	Typical I.D. (mm)
Preparative LC	Higher than 20
Semi-preparative LC	6-20
Conventional LC	3-5
Narrow-bore LC	2
Micro LC	0.5-1
Capillary LC	0.1-0.5
Nano LC	0.01-0.1
Open tubular LC	0.005-0.05

1.2.1. Column efficiency

To achieve optimal separations, sharp and symmetrical chromatographic peaks should be obtained, thus band broadening must be limited. Column efficiency is used to compare the performance of different columns. It can be expressed as the theoretical plate number (N), which is calculated by:

$$N = 16\left(\frac{t_R}{w}\right)^2 = 5.54\left(\frac{t_R}{w_{1/2}}\right)^2 \quad \textbf{(Eq. I-1)}$$

where t_R is the retention time, and $w_{1/2}$ is the peak width at half height. The number of theoretical plates depends on column length L: the longer the column, the higher the number of the plates. The plate height H (HETP = height equivalent to a theoretical plate) has also been introduced to relate the plate number to column length:

$$H = \frac{L}{N} \qquad \textbf{(Eq. I-2)}$$

To improve the efficiency and reduce the band broadening phenomenon, a series of factors must be considered, which are all included in the van Deemter equation:

$$H = A + \frac{B}{u} + Cu \qquad \textbf{(Eq. I-3)}$$

- The term A reflects the contribution of the multi-path dispersion along the column, due to inhomogeneities in column packing and small variations in the particle size of the packing material so that multiple diffusion channels are formed. This term is also known as Eddy diffusion and can be calculated as $A=2\lambda d_p$, where λ depends on the quality of the packing and d_p is the particle diameter.
- The factor B, the longitudinal diffusion, is related to the solute concentration gradient, and is responsible for the Gaussian shape of each chromatographic peak. It can be expressed as $B=2\gamma D_M/u$, where γ refers to possible irregularities in the stationary phase (like λ), D_M is the solute diffusivity in the mobile phase and u is the mobile phase linear velocity. To minimize the B contribution, D_M should be reduced and high flow rate should be used.
- The term C represents the resistance to mass transfer and takes into account the transfer to both mobile (C_m) and stationary (C_s) phase, so $C=C_m+C_s$, where $C_m=f_1K'd_p^2u/D_M$ and $C_s=f_2K'd_f^2u/D_s$. The f_1 and f_2 parameters are associated to the stationary phase shape, K' is the capacity factor of the column proportional to the solute retention, d_p and d_f are respectively the diameter of particles and of

the total packing, D_M and D_s are the diffusivity of the solute in the mobile and stationary phase, respectively, and u is the mobile phase flow rate.

The optimal flow rate, for which both B and C terms are minimized, corresponds to the minimum of the curve plotting H against linear velocity u (Figure I-1).

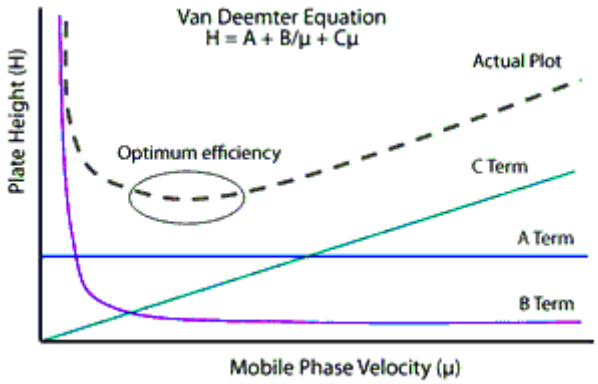

Figure I-1. *Typical Van Deemter Plot.*

Evidently, the reduction in both particle diameter (d_p) and stationary phase thickness (d_f) should cause a significant decrease of H, since both A and C terms are correlated to these parameters.

1.2.2. Resolution

Resolution represents the capability of a column to separate the peaks of interest, and so the higher the resolution, the simpler it is to achieve baseline separation between two peaks (Equation I-4).

$$Rs = \frac{\sqrt{N}}{4}\,\frac{\alpha - 1}{\alpha}\,\frac{k}{k+1} \qquad \textbf{(Eq. I-4)}$$

The Fundamental Resolution Equation indicates that resolution is affected by three important parameters: efficiency (*N*), selectivity (α) and retention factor (*k*) (Figure I-2). One can improve resolution by improving any one of these parameters. A value of 1 is the minimum for a measurable separation to occur and to allow adequate quantitation. Compared to gas chromatography (GC), HPLC is characterized by a relatively low resolving power which is mainly caused by the restricted length of the analytical columns.

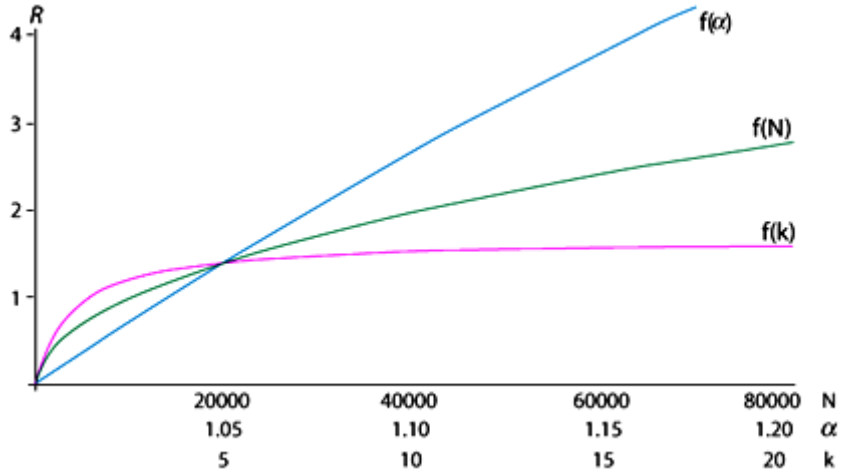

Figure I-2. *Resolution as a function of efficiency, selectivity and retention factor.*

Various approaches have been reported to establish an increase in LC resolving power and they will be discussed in the following chapters II and IV.

1.3. Detection

The chromatographic detector is able of determining both the identity and concentration of eluting components in the mobile phase stream. A wide range of detectors is available to meet different sample requirements, among which there are UV detectors, evaporative light scattering detectors (ELSD), mass

spectrometers (MS), refractive index (RI) detectors, fluorescence detectors, and electrochemical detectors. The most popular detectors in LC are UV-type, based on the solute adsorption of UV-VIS wavelengths, and MS, capable to measure with different accuracy the mass of a component. UV detectors can work either at a fixed wavelength, usually corresponding to the analyte maximum absorption (UV detectors), and at variable wavelength (photo diode array, PDA), making possible simultaneous monitoring of more than one absorbing component at different wavelengths. This detector extracts more information from the chromatogram and provides important data for the qualitative analyses of unknown samples, even if non-absorbing compounds cannot be detected at all. On the contrary, MS is an universal detector, specific enough to support the positive identification of a compound, offering structural information and/or the molecular weight (MS technique will be the subject of the chapter V). Beside, the ELSD is often used in HPLC; such detector enables the non-selective detection of non-volatile analytes. After removal of mobile phase by passing through a heated zone, the solute molecules are detected by light scattering depending on molecular sizes.

1.4. General trends

Since its advent, LC is being exploited by separation scientists and applied to a wider and wider range of sample matrices for the separation, identification and quantification of ever more compounds. The unceasing progresses in columns and stationary phases production, and the enormous developments in detection techniques, have contributed to the outstanding success of chromatography, as an invaluable tool in analytical chemistry, in many different fields including nutraceutical, food, environmental, clinical, forensic, and pharmaceutical applications. The great advantages to be gained by the use of LC are especially increased with the hyphenation to MS (LC-MS). Recent trends in the area of

LC-MS and related techniques involve: (*i*) the shift from conventional HPLC-MS to ultra high pressure liquid chromatography (UHPLC)-MS or other fast LC-MS techniques (core-shell particles, high-temperature LC and monolithic columns), requiring fast MS analyzers (typically time-of-flight (ToF)-based systems); (*ii*) the use of supercritical fluid chromatography (SFC) for fast and "green" separations, with reduction in solvents consumption; (*iii*) the use of multidimensional liquid chromatography techniques (MDLC) for complex samples, and other dimension also in MS, such as ion mobility spectrometry (IMS)-MS and the coupling of two or more mass analyzers (tandem MS); (*iv*) the shift from low-resolution to (ultra)high-resolution MS to allow accurate mass measurements. Each of these techniques will be described in detail in the following chapters.

REFERENCES

- Horváth C., Lipsky S. R., Nature 1966, 211, 748-749.
- Howard G.A., Martin A. J. P., Biochem. J. 1950, 46, 532-538.
- Martin A.J.P., Synge R.L.M., Biochem. J. 1941, 35, 1358-1368.
- Saito Y., Jinno K., Greibrokk T., J. Sep. Sci 2004, 27,1379-1390.

CHAPTER II
Ultra High Pressure Liquid Chromatography

2.1. Introduction

Over recent decades, different advances in the development of comprehensive solutions to increase the separation efficiency and reduce the analysis time have been made. Different approaches have been reported to provide improved chromatographic separation. Among these, silica-based monolith columns, which consist of a single piece of porous material with several unique features in terms of high permeability and efficiency, plus low resistance to mass transfer, could be interesting (Luo, *et al.*, 2005; Miyamoto, *et al.*, 2008). However, the limited number of available columns dimensions and surface chemistries has restricted the progress of this technology. Another possible way to increase the efficiency on standard LC instrumentation consists in the use of long columns by coupling standard LC columns with totally porous particles and operation at high temperatures, allowed by the reduced mobile phase viscosity and hence lower pressure drop along the analytical column (Lestremau, *et al.*, 2006; Plumb, *et al.*, 2007; Sandra & Vanhoenacker, 2007). Unfortunately, the technical constraints as the longer analysis time, the limited number of available stationary phases capable of withstanding elevated temperatures, and the question of stability of the analytes, make this approach difficult to practice. Analogously, the use of partially porous stationary phases, also known as fused core or core-shell particles, allows to serially couple columns and boost the separation efficiency (Wang, *et al.*, 2006; Cunliffe & Maloney, 2007; Cabooter, *et al.*, 2008). The stationary phase particle consists of a thin layer of porous shell fused to a solid particle (Figure II-1). This technology drastically reduces the pressure drop when compared to fully porous (sub-2 μm) stationary phases, mainly when high temperatures are applied,

making it possible to operate such phases on a conventional LC instrument (Fekete, *et al.*, 2014).

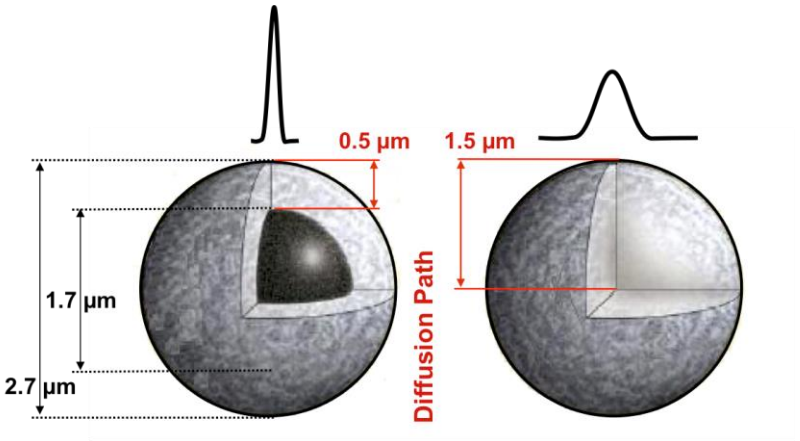

Figure II-1. *Partially porous technology (Fused core, on the left) and totally porous particles (on the right).*

Since the introduction of the first commercially available HPLC columns packed with 10 µm particles in the early 1970s, the use of ever smaller particles has become the most popular way to improve chromatographic separations (Snyder, 2000; Gritti & Guiochon, 2012; Unger, *et al.*, 2000; Eeltink, *et al.*, 2004).

As reported by Giddings in 1991, there is a linear correlation between the pressure drop (ΔP) and the linear velocity (u) in the column (Giddings, 1991) (Equation II-1):

$$\Delta P = \frac{\varphi \eta u L}{d^2_p} \quad \textbf{(Eq. II-1)}$$

where φ, η, L, and d are the flow resistance, viscosity of the mobile phase, length of the column, and particles diameter, respectively. It has been

demonstrated that using a column 25 cm long packed with 5 μm particles an inlet pressure <25 bar is required for the chromatographic analysis, whereas reducing at 1 μm the particles diameter needs an inlet pressure of 2000 bar (Colon, *et al.*, 2004; Anspach, *et al.*, 2007). Consequently, dedicated instrumentation and columns are necessary (MacNair, *et al.*, 1999; Shen, *et al.*, 2005; Plumb, *et al.*, 2006; de Villiers, *et al.*, 2006a). Recent HPLC developments have been focusing, on the one hand, on the design of pumping devices, injection system and flow paths, capable of operating at very high pressures (600 to 1000 bar) and detectors capable of high acquisition rate; on the other hand, on the manufacturing of stationary phase particles that are stable enough to tolerate such elevated pressures. The term "ultra-high pressure liquid chromatography" (UHPLC) to describe the higher performance achieved by the novel instrumentation, in combination with small particles, was coined by Jorgensen in 1997 (MacNair, *et al.*, 1997). Nowadays this technique is also known with the name of "ultra-high performance liquid chromatography" (UPLC). The first commercially available UHPLC system was introduced in 2004. The real success of any UHPLC system is correlated to the use of columns packed with sub-2 μm particles. The Van Deemter plot (Figure II-2) shows that smaller particles have the advantage of much flatter H values at higher flow velocities. This result means that speed can not only be doubled by halving particle diameter, but can also be doubled and doubled again by operating at higher flow velocities, without any efficiency loss. The numerous applications on UHPLC suggest a considerable enthusiasm towards this technique (Aguilera-Luiz, *et al.*, 2008; Motilva, *et al.*, 2013; Beltrán, et al., 2009; Wilson, *et al.*, 2005; Cai, *et al.*, 2009). Compared to conventional HPLC, it offers a series of advantages such as improved resolution, higher peak efficiency, shorter retention times, and reduced solvent consumption. Furthermore the narrower peaks (sharper peaks) and the lower detection limits

(LODs), due to the higher peak efficiency, provide for a greater sensitivity than HPLC. On the other hand, the technique is easily prone to several deficits. One of the major problems associated to the application of elevated pressures is the heating of the mobile phase due to viscous friction losses (Martin & Guiochon, 2005; de Villiers, *et al.*, 2006b; Neue & Kele, 2007). This could produce radial or axial temperature gradients inside the column related to the thermal conditions under which the analysis is performed (isothermal or adiabatic operation, respectively). Both temperature gradients may compromise the separation efficiency.

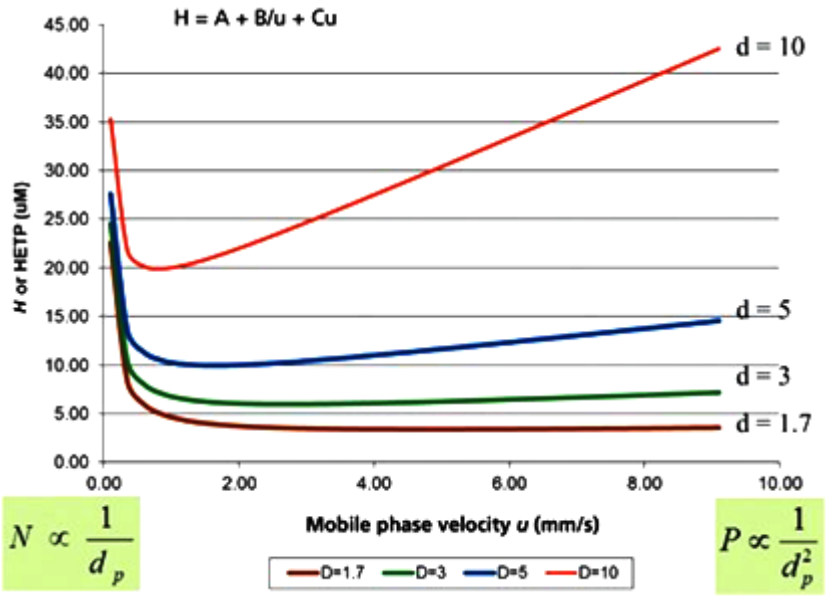

Figure II-2. *Van Deemter Plot at different d_p.*

2.2. UHPLC system requirements

The development of UHPLC systems represents an engineering challenge, since these instruments have to be designed to take advantage of the greater speed, higher resolution and superior sensitivity offered by small particles.

Various instrumental characteristics need to be considered for satisfactory

operation of UHPLC:

- Instrument performance. It must be able to withstand the increased higher pressures than HPLC system, by improving the pressure capabilities of the pumping device.
- Extra-column volume. The tubing volume, the mixer volume, the detector cell volume must be reduced as much as possible. A system plumbed with 0.005'' I.D. stainless steel tubing and zero dead volume fittings is preferred for UHPLC experiments.
- Dwell volume. It represents the volume of liquid contained in the system between the point where the gradient is formed and the point where the mobile phase enters the column. This volume includes the mixer, transfer lines, and any swept volume (including the sample loop) in the injection system. After the gradient has started, a delay is observed until the selected proportion of solvent reaches the column inlet, on account of this the sample is subjected to an unwanted additional isocratic migration. The dwell volume may differ from one instrument to another, but it can be easily measured (Dolan, 2006).
- Mobile phases. It is recommended the use of high-grade organic solvents (recognized UPLC or LC-MS grade), Milli-Q water or similar, being careful to microbiological growth, and store the column with pure organic solvent, because of the size of the frits and particles that are much smaller than HPLC (0.2 μm versus 2 μm).
- Column dimension. The separation is made faster by using shorter columns, but the same should still offer sufficient column efficiency to allow at least a baseline separation of analytes. If the primary goal is speed, it is recommended the use of a column with a length of 50 mm, otherwise it is preferable a column of 100 mm, if the main purpose is resolution. Reducing the column diameter does not shorten the analysis time, but decreases mobile

phase consumption and sample volume. It is possible to find UHPLC columns with 1.0, 2.1, 4.6 mm I.D. The 2.1 mm I.D. column should be considered as optimal, while 4.6 mm I.D. can generate significant frictional heating. Concerning the 1.0 mm I.D., the compatibility between the column geometry and any UHPLC instrument is critical, and it is only used for specific reasons (e.g. severely sample limited or direct flow to MS).

- Detector acquisition rate. The narrow peaks generated in UHPLC have to be monitored by detectors that offer acquisition rates high enough to record a reasonable data points (20 points per peak are recommended) across the chromatographic peak. Only the latest generation of instruments meets these requirements.

2.3. Moving a HPLC method to an UHPLC

When transferring methods from HPLC to UHPLC, it is usually sufficient to maintain the resolution of the original method. A widespread approach consists in the employment of shorter columns packed with smaller particles; this strategy maintains resolution and allows faster separations. Several calculations are required to adapt some parameters, such as injection volume, flow rate, dwell volume, in both isocratic and gradient modes, to the new column characteristics.

2.3.1. Isocratic mode

In isocratic mode it is important to consider and thus adjust the flow rate and the injection volume. The linear velocity of the mobile phase has to be increased while decreasing the particle size to work within the Van Deemter optimum. In addition, the new flow rate is scaled to the change of column cross section if the column inner diameter changes. Specifically, it must be decreased as column internal diameter decreases. The UHPLC flow rate (F_2) can be

calculated with the following equation:

$$F_2 = F_1 \cdot \left(\frac{d^2_{c2}}{d^2_{c1}} . \frac{d_{p1}}{d_{p2}} \right) \qquad \textbf{(Eq. II-2)}$$

where d_p is the particle size. Also the injection volume should be adapted to the new column dimension, since it is proportional to the column volume. Indeed, decreasing the column internal diameter and length decreases the overall column volume and sample capacity. The new injection volume (V_{I2}) can be calculated with the Equation II-3:

$$V_{I2} = V_{I1} \ . \frac{d^2_{c2}}{d^2_{c1}} . \frac{L_2}{L_1} \qquad \textbf{(Eq. II-3)}$$

where d_c and L represent the diameter and the length of the column, respectively. Practically it is important to maintain the ratio of column dead volume and injection volume constant.

2.3.2. Gradient mode

Transferring an optimized gradient elution method between instruments, columns, etc. is more difficult than transferring isocratic elution method. Gradient methods can introduce variables that may not be easy to control. First of all, the same considerations about the flow rate and volume injection (Eq. II-2 and II-3) should be made. Either linear gradient or step gradient can be dissected into a combination of isocratic or gradient walks (Stoll, *et al.*, 2006). For the isocratic step (t_{iso2}) can be applied the following equation:

$$t_{iso2} = t_{iso1} \cdot \left(\frac{F_1}{F_2} \cdot \frac{d^2_{c2}}{d^2_{c1}} \cdot \frac{L_2}{L_1} \right) \qquad \textbf{(Eq. II-4)}$$

this is useful also for the re-equilibration time. For the gradient step, the guidelines proposed by Schellinger and Carr should be followed (Schellinger & Carr, 2005). In order to maintain a constant selectivity, the start and the final composition of the mobile phase in the gradient should be the same than the original method:

$$t_{grad2} = \frac{(\%B_{final1} - \%B_{start1})}{slope_2} \qquad \textbf{(Eq. II-5)}$$

where $slope_2$ is the slop of the new gradient and it is can be calculated with the Equation II-6:

$$slope_2 = slope_1 \cdot \left(\frac{F_1}{F_2} \cdot \frac{d^2_{c2}}{d^2_{c1}} \cdot \frac{L_2}{L_1} \right) \qquad \textbf{(Eq. II-6)}$$

even if this ploys is employed, the selectivity could be different because of different dwell volume (Guillarme, *et al.*, 2012). In view of this, one must adjust the "effective" dwell volume, which is the total volume of starting eluent delivered to the column inlet after injecting the solutes. The "intrinsic" dwell volume is the gradient delay volume delivered to the column before the front of the gradient arrives at the column inlet. The latter is obviously an instrument constant, while the former is a modifiable parameter by delaying the injection or using an initial isocratic step (Schellinger & Carr, 2005).

REFERENCES

- Aguilera-Luiz M.M., J.L.M. Vidal, R. Romero-González, A. Garrido Frenich, J. Chromatogr. A 2008, 1205, 10-16.
- Anspach J.A., Maloney T.D., Colon L.A., J. Sep. Sci. 2007, 30, 1207-1213.
- Beltrán E., Ibáñez M., Sancho J.V., Hernández F., Rapid Commun. Mass Spectrom. 2009, 23, 1801-1809.
- Cabooter D., Lestremau F., Lynen F., Sandra P., Desmet G., J. Chromatogr. A 2008, 1212, 23-34.
- Cai S.S., Syage J.A., Hanold K.A., Balogh M.P., Anal. Chem. 2009, 81, 2123-2128.
- Colon L.A., Cintron J.M., Anspach J.A., Fermier A.M., Swinney K.A., Analyst 2004, 129, 503-504.
- Cunliffe J.M., Maloney T.D., J. Sep. Sci. 2007, 30, 3104-3109.
- de Villiers A., Lestremau F., Szucs R., Gelebart S., David F., Sandra P., J. Chromatogr. A 2006, 1127, 60-69.
- de Villiers A., Lauer H., Szucs R., Goodall S., Sandra P., J. Chromatogr. A 2006, 1113, 84-91.
- Dolan J.W., LCGC North Am. 2006, 24, 458-466.
- Eeltink S., Decrop W.M.C., Rozing G.P., Schoenmakers P.J., Kok W.Th., J. Sep. Sci. 2004, 27, 1431-1440.
- Fekete S., Guillarme D., Dong M.W., LC GC N. Am. 2014, 32, 2-12.
- Giddings J.C., Unified separation Science, Wiley, New York, 1991.
- Gritti F., Guiochon G., J. Chromatogr. A 2012, 1228, 2-19.
- Guillarme D., Veuthey J.L., Smith R.M., Royal Society of Chemistry 2012.
- Lestremau F., Cooper A., Szucs R., David F., Sandra P., J. Chromatogr. A 2006, 1109, 191-196.
- Luo Q.Z., Shen Y.F., Hixson K.K., Zhao R., Yang F., Moore R.J., Mottaz H. M., Smith R.D., Anal. Chem. 2005, 77, 5028-5035.
- MacNair J.E., Lewis K.C., Jorgenson J.W., Anal. Chem. 1997, 69, 983-989.
- MacNair J.E., Patel K.D., Jorgenson J.W., Anal. Chem. 1999,71, 700-708.
- Martin M., Guiochon G., J. Chromatogr. A 2005, 1090,16-38.

- Miyamoto K., Hara T., Kobayashi H., Morisaka H., Tokuda D., Horie K., Koduki K., Makino S., Nunez O., Yang C., Kawabe T., Ikegami T., Takubo H., Ishihama Y., Tanaka N., Anal. Chem. 2008, 80, 8741-8750.
- Motilva M.J., Serra A., Macià A., J. Chromatogr. A 2013, 1292, 66-82.
- Neue U., Kele M., J. Chromatogr. A 2007, 1149, 236-244.
- Plumb R.S., Rainville P., Smith B.W., Johnson K. A., Castro-Perez J., Wilson I.D., Nicholson J.K., Anal. Chem. 2006, 78, 7278-7283.
- Plumb R.S., Mazzeo J.R., Grumbach E.S., Rainville P., Jones M., Wheat T., Neue U.D., Smith B., Johnson K.A., J. Sep. Sci. 2007,30, 1158-1166.
- Sandra P., Vanhoenacker G., J. Sep. Sci. 2007, 30, 241-244.
- Schellinger A.P., Carr, P.W., J. Chromatogr. A 2005, 1077, 110-119.
- Shen Y., Zhang R., Moore R.J., Kim J., Metz T.O., Hixon K.K., Zhao R., Livesay E.A., Udseth H.R., Smith R.D., Anal. Chem. 2005, 77, 3090-3100.
- Snyder L.R., Anal. Chem. 2000, 72, 412-420.
- Stoll D.R., Paek C., Carr P.W., J. Chromatogr. A 2006, 1137, 153-162.
- Unger K.K., Kumar D., Grun M., Buchel G., Ludtke S., Adam T., Schumacher K., Renker S.J., Chromatogr. A 2000, 892, 47-55.
- Wang X., Barber W.E., Carr P.W., J. Chromatogr. A 2006, 1107, 139-151.
- Wilson I.D., Nicholson J.K., Castro-Perez J., Granger J.H., Johnson K.A., Smith B.W., Plumb R.S., J. Proteom Res. 2005, 4, 591-598.

CHAPTER III
Supercritical Fluid Chromatography

3.1. Introduction

The use of supercritical fluids (SFs) for chromatography was first reported in 1962 by Klesper (Klesper, *et al.*, 1962). In that study supercritical dichlorodifluoromethane and monochlorodifluoromethane were used as mobile phases to separate nickel etiporphyrin II from nickel mesoporphorin IX dimethyl ester. Since its introduction, SFC had a rapid rise as a new separation topic in the late 1980s and 1990s, before starting a slow decrease and almost waning for over a twenty-year span, in the shadow of other separation techniques. The last decade has been characterized by a renewed interest in this technique, as the introduction of a new generation of commercial instruments has given new stimulus to the development and application of SFC-based methodologies. SFC may be considered as a valuable alternative to conventional chromatographic techniques, and as such is being exploited by separation scientists and employed for a wide range of sample matrices. In the 1980s, SFC was mainly used with capillary columns and FID, while nowadays packed columns and LC type detectors are preferred, as this configuration is more robust and can be easily adapted to a broad range of analytes. Lee et al. (Lee & Markides, 1987) and Novotny (Novotny, 1989) were the first to introduce long capillaries or open tubular stationary phases for SFC in 1981, contributing in this way to the propagation of SFC among GC chromatographers. The latter were strongly attracted by the possibility to widen the power of GC techniques in terms of range of compounds that could be analyzed, while making only slight modifications to GC hardware to properly function with a supercritical fluid. Capillary SFC (cSFC) required pure CO_2 as mobile phase and was coupled with flame ionization detector (FID), while

temperature and pressure ramps were programmed to modify the elution strength in separations. Various passive devices were adopted for maintaining the critical pressure within the chromatographic instrument, from capillary tubing of small I.D. to integral frits; however, such homemade systems were often little rugged and suffered from poor reproducibility. Moreover, the properties of pure SF CO_2 limited its use to only lipophilic compounds, and the strong restrictions in terms of application caused the decline of cSFC in the 1990s. At the same time, a radical change of philosophy occurred based on works of Gere et al. (Gere, *et al.*, 1982) and Berger (Berger & Deye, 1990a; Deye, *et al.*, 1990; Berger & Deye 1990b). Enormous efforts were done for the development of SFC instruments dedicated to the use of LC-like packed columns (pSFC). The first commercial SFC system, based on LC equipment, was commercialized in 1983 by Hewlett Packard. The configuration included an innovative binary pump, offering the capability to modulate the properties of pure SF CO_2 by directly modifying the mobile phase composition with the addition of a modifier. Moreover, the backpressure could be maintained constant within the system, thanks to the presence of an active backpressure regulator (BPR), even under gradient elution. The technique was reported to provide better selectivity, shorter analysis times, and broader applicability also to polar compounds (Saito, 2013) than cSFC. However, the poor compatibility of pSFC with FID and the lower efficiency afforded by the use of short columns and 5 or 10 μm particles, beside the commercial success of LC characterized by superior repeatability and more rugged design of instrumentation, have contributed to the almost disappearance of SFC for nearly 20 years from analytical laboratories. Over the last decade, a renewed interest arouse within the chromatographic community, following the introduction of a new generation of instruments by a number of manufacturers (Waters, Agilent, Shimadzu). These pioneering systems are well suited to different analytical

purposes, and are capable to deliver efficiency and sensitivity rivaling with those offered by UHPLC. The novel BPR design, the higher upper pressure limits, and the reduced void volumes in fact make these instruments fully compatible with low diameter particles (<2 μm) and core-shell columns (Nováková, *et al.*, 2014; Lesellier, 2012). On the other hand, preparative SFC (prep-SFC) has also proved to be a valuable tool for the isolation of sample constituents, or the purification of extracts (Pettinello, *et al.*, 2000; Alkio, *et al.*, 2000), strongly supported from the industry, to replace toxic and expensive normal phase solvents commonly employed at a preparative scale in HPLC.

3.2. Supercritical fluids and physico-chemical properties

Supercritical fluids were firstly defined by Cagniard de la Tour in his famous cannon barrel experiments in 1822 (Cagniard de la Tour, 1822), while the term "critical point" was coined by Andrews in 1869 (Andrews, 1869), as the end point of a liquid-vapor equilibrium curve, above which the heat of vaporization is null. This means that, above the critical point, there exists a state of matter that is continuously connected with both the liquid and the gaseous state: that is called a supercritical fluid. In SFC separation, the mobile phase consists of supercritical fluids, which are kept above their critical pressure and temperature; the nature of SFs vary markedly from that of liquid or gases, and the properties are considered to be a hybrid of these two physical states, which can be manipulated by changing some experimental parameters. The viscosity and diffusivity are similar to those of a gas, providing high solute diffusion coefficients (and limited pressure drop in the system) and faster separation kinetics (at increased flow rates without any loss in resolution). The density and solvating power of SFs are comparable to those of liquids, leading to good solubility and transportation of analytes; nevertheless SFs are more compressible than liquids, and that implies their density will severely change

with pressure and temperature. The latter will also affect the elution strength of the mobile phase, since the polarity of SFs directly increases with density. There are a number of possible fluids that may be used in SFC, but CO_2 is by far the most commonly used supercritical mobile phase nowadays, for various reasons. Ammonia, N_2O, light hydrocarbons, water, and chlorofluorocarbons cause serious problem related to toxicity, environmental pollution, and hardware corrosion, apart from being unsuitable for the analysis of thermolabile compounds (high critical temperature and critical pressure); instead, the use of CO_2 has attracted particular attention because it is safe (low toxicity, non-inflammable, non-corrosive), inert (no hardware damage), and easily available at high quality at a low price, (though it is abundant in the atmosphere, a large amount is also available as a by-product from NH_3, H_2 and ethanol production). Moreover, CO_2 offers good miscibility with both apolar (hexane, toluene, etc.) and polar (water, alcohols, acetonitrile) organic solvents, and is also UV transparent down to 190 nm. Other advantages can be observed for preparative-scale separations in terms of recovery of concentrated fractions after separation (requiring less effort to evaporate solvents and thus recover pure fractions) and non-toxicity of residual amounts in human-contact products (Lesellier & West, 2015). But the real success of CO_2 compared to other fluids consists in its low critical point (31°C and 74 bar), as shown in Figure III-1, because these mild conditions are easily reached by conventional instrumentation and furthermore cause no degradation of the analytes (Taylor, 2010).

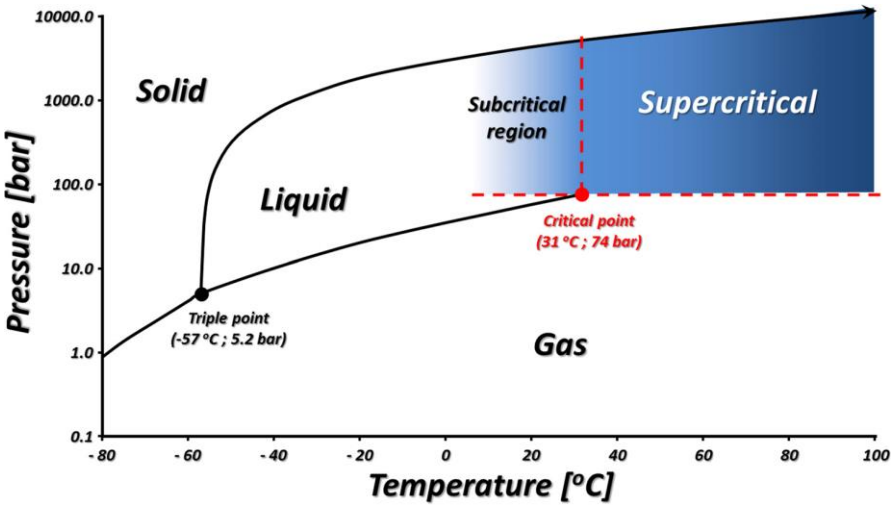

Figure III-1. *Phase diagram of carbon dioxide (Nováková, et al., 2014).*

CO_2 is a highly nonpolar solvent, and its solvating power is considered similar to that of hydrocarbons such as pentane or hexane. The non-polar character of SF CO_2 favors the solubility of hydrophobic compounds, but limits the application for the more polar analytes. In order to increase the elution strength of the mobile phase, small amounts (typically, 2-40%, *v/v*) of a polar solvent, called modifier or co-solvent, is usually added to SF CO_2. Increased proportions of modifier most often result in decreased retention, and peaks elute from lower to higher polarity. Most common used modifiers are isopropanol (IPA), methanol (MeOH), acetonitrile (ACN), ethanol (EtOH), and *n*-hexane; modifier addition will also improve peak shape and minimize peak tailing, either due to solubility improvement, or by masking some residual silanol groups on stationary phases of silica bonded with octadecyl groups and, thus, reducing the extent of unwanted interactions between the analytes and high energy sites. The modifier will change some physico-chemical properties of the mobile phase such as the viscosity and dielectric constant, and can generate further interactions such as hydrogen bonding or dipole-dipole, leading to modifications in selectivity. Therefore, the interactions with the stationary

phase may be too strong, and highly polar solutes may fail to elute, or elute with poor peak shapes. In order to overcome this drawback, a highly polar additive, such as a strong acid or base, is often dissolved in the modifier. The first use of additives to SFC eluent was reported in 1988 (Ashraf-Khorassani, *et al.*, 1988). The critical point of the mobile phase will considerably shift with modifier addition: both the critical temperature and the critical pressure will increase, depending on the percentage and the nature of the modifier added to carbon dioxide, as shown in Figure III-2 (e.g. to reach 135°C and 168 bar for a 70:30 *v/v* CO_2/MeOH mobile phase). This means that in most SFC separations, the state of the mobile phase should be defined as "subcritical", rather than "supercritical", as with a working temperature typically not exceeding 60°C, whatever the gradient program, a subcritical fluid will be obtained very quickly upon increasing the proportion of modifier (Pinkston, *et al.*, 2004). On the other hand, the increased elution strength produced by the presence of polar modifiers would be mostly connected to the proportion of the latter, rather than to the density modification associated with their presence; meantime the co-solvent will poorly influence the GC-like diffusivity and low viscosity.

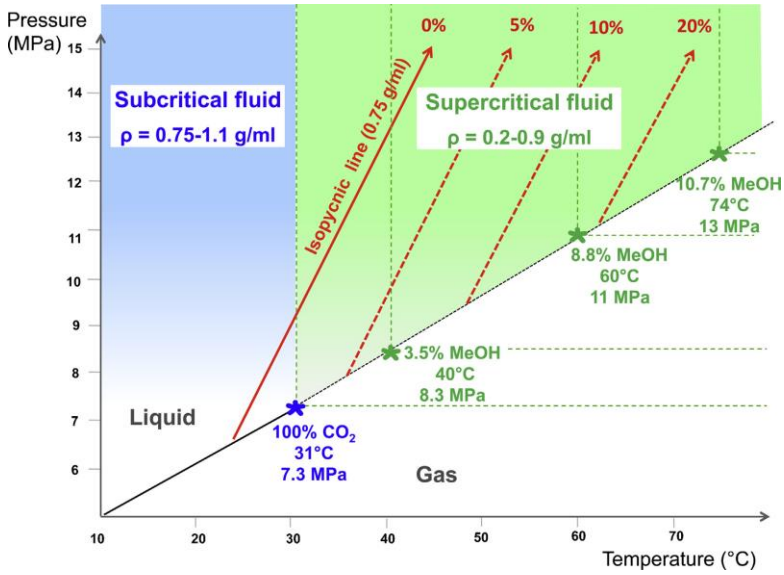

Figure III-2. *Phase diagram for pure carbon dioxide (in blue) or carbon dioxide mixed with methanol at different proportions (in green). The slanting red arrows indicate isopycnic lines (Lesellier & West, 2015).*

3.3. Stationary phase types

Fused-silica capillary columns with cross-linked chemically bonded stationary phases, traditionally employed for high-resolution gas chromatography (HR-GC), have also been successfully exploited for SFC applications (King & List, 1996; King, 2003). Most of the recent work however is being described with packed HPLC columns. The absence of water in the mobile phase makes SFC a unified separation method because it allows the employment of both non-polar and polar stationary phases with the same mobile phase (Lesellier, 2009; Lesellier, 2008). SFC can replace RP-LC, non aqueous reversed phase liquid chromatography (NARP-LC), NP-LC, and hydrophilic interaction chromatography (HILIC), provided that the compounds of interest are soluble in the CO_2. This means that practically all HPLC stationary phases are also suitable to use in SFC, from octadecyl silica (ODS)-bonded silica to pure silica. However, they showed a number of inconveniences/limitations, the major being

poor selectivity and low sample capacity in SFC separations compared to the HPLC counterpart; moreover, the poor peak shape obtained for the separation of acidic or basic analytes required the use of additives in the mobile phase. More recently, new stationary phases especially designed for SFC have been developed, in the attempt to overcome such issues (Poole, 2012). The silica-based polymer-encapsulated has been probably the first type of stationary phase to find larger use in SFC than in HPLC, consisting of fully porous silica particles coated with a polysiloxane layer functionalized with polar groups or alkyl substituents. Such columns are not more in use nowadays, mainly because of problem associated to the free residual silanol activity, which was hampering the separation of more polar compounds. A number of novel SFC-specific stationary phases have been recently introduced to minimize such inconvenience, which include bonding and ligands designed and optimized for use in CO_2-based separations. One of the most popular is a chemically bonded phase with a 2-ethylpyridine substituent, affording decreased undesirable interactions among the silanol groups and the polar compounds, since the hydrogen-bonding between free silanol groups and the nitrogen atom of the pyridine ring, or partial protonation of the pyridine group (due to the acidity of carbon dioxide-methanol mobile phases) would repel positively charged analytes from the stationary phase, reducing interactions with the silanol groups. The use of such a phase decreases or eliminates the need for additives, and it is well suited to the analysis of a wide range of basic, as well as neutral and acidic compounds. The same mechanism of interaction (hydrogen-bonding or steric protection) can be encontered with silica-based support having amino, amide, urea and sulfonamide groups (Poole, 2012).

3.4. Instrumentation

A system for SFC can be easily developed starting from GC or LC equipment, on condition that facilities for temperature and pressure programming are available. In SFC separations it is very important to maintain the column outlet at a pressure above the critical one; in this regard a backpressure regulator is located after the column. This can be a simple capillary tube (passive backpressure regulator) or a device allowing the modification of this parameter (dynamic backpressure regulator). Most remarkably, some detectors must operate at elevated pressures, e.g. with UV detection pressure resistant cells are necessary (upto 400 bar). Commonly, SFC instruments consist of a binary pumping system: one pump is used to propel the CO_2 and the other one is dedicated to the organic modifier. The former is usually supplied from steel cylinders containing liquefied CO_2 in contact with a gaseous headspace at 55 to 85 bar near room temperature, since reciprocating pumps cannot compress a low density gas because of a low compression ratios. Instead the modifier is a liquid at room temperature and pressure; separate pumps are hence required to avoid mismatches in pressure. It is necessary to cool the CO_2 pump to below 4°C (generally, through an electronic cooling unit), to prevent any decrease in pressure or increase in temperature during the pump refill stroke; this would bring to vaporization of the liquid, and the pump would produce gaseous cavities in the liquid flow. Usually, a sample loop injection device is employed, and the column oven is nearly identical to that of an LC system. Finally, both GC type and LC type detectors can be coupled, the latter being more used nowadays. Specifically, in a GC-like SFC set-up, where only pure CO_2 is used as the mobile phase, FID, IR, electron capture detection (ECD), chemiluminescence, and various other detection approaches are possible, instead in a LC-like set-up, in the presence of a modifier, ELSD, UV, MS and, sometimes, charged aerosol detection (CAD) and acoustic flame detection

(AFD) are employed. Earlier implementations of SFC-MS followed the evolution of both HPLC-MS and GC-MS interfaces (Zaugg, *et al.*, 1987; Arpino, *et al.*, 1990; Crowther & Henion, 1985). The hyphenation of SFC to the mass analyzers is provided by means of electrospray ionization (ESI) or atmospheric pressure chemical ionization (APCI), much like in HPLC-MS (Lesellier & West, 2015).

3.4.1. Towards ultra high performance SFC

The ACN (the most widely used solvent in RP-LC) shortage of 2008 has had a direct negative impact on HPLC, in ways such as increases in the cost of solvent reprocessing, forcing chromatography users to consider solutions that consume less solvent. Based on these needs, important instrument manufacturers considered it vital to turn to greener technologies that have to be able to preserve high performance and productivity.

A number of improvements in the design of new systems have led to the introduction of the first instrument fully dedicated to high-performance analytical SFC, developed by Waters Corporation and commercialized with the name of Ultra-Performance Convergence Chromatography (UPC²). Compared to old generation SFC instruments, with this technology, the reliability and precision of pumping system and backpressure regulation, required for controlling the delivery of mixtures of CO_2 and organic modifier over a broad range of flow rates and pressures, were drastically enhanced. A two-stage back pressure regulator (BPR) (passive + active) was assembled on the UPC^2 instrument, in which the passive component maintains pressure at 104 bar, while the active component provides for further backpressure increase and fine adjustments. This device ensures repeatable mobile phase density conditions and retention times between successive analyses, adapting itself fairly quickly to modifications in mobile phase composition or flow.

The new instrument design also includes reductions in injection volume and detector-cell volume, and minimized connector tubing length and diameter. All these improvements offer increases in throughput and in the efficiency of the analyses, especially when used in combination with sub 2-µm particles at the limit pressure tolerate by the system. In this regard, it must be pointed out that this system allow for a maximum pressure of 400 bar. Despite its lower inlet pressure limit, the optimum linear velocity is higher by a factor of 3-5-fold than in UHPLC, allowing ultra-fast and/or highly efficient analysis (Grand-Guillaume Perrenoud, *et al.*, 2012b). This justifies introduction of the term ultra high performance SFC (UHPSFC) as an appellation for the combination of state-of-the-art SFC set-up and columns packed with sub-2 µm particles (Grand-Guillaume Perrenoud, *et al.*, 2012a). A schematic of UPC^2 instrumentation is illustrated in Figure III-3.

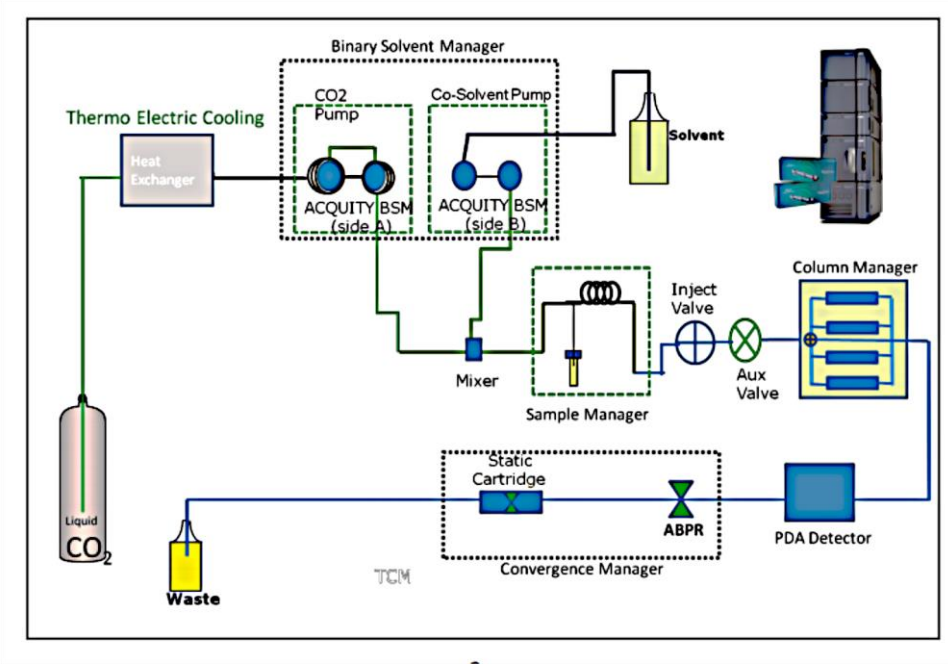

Figure III-3. *A schematic of UPC^2 instrumentation.*

REFERENCES

- Alkio M., Gonzalez C., Jännti M., Aaltonen O., JAOCS 2000, 77, 315-321.
- Andrews T., Philosophical Transactions of the Royal Society (London) 1869, 159, 575-590.
- Arpino P.J., Dilettato D., Nguyen K., Bruchet, A., J. High Res. Chromatog. 1990, 13, 5-12.
- Ashraf-Khorassani M., Fessahaie M.G., Taylor L.T., Berger T.A., Deye J. F., J. High Res. Chromatog. 1988, 11, 352-353.
- Berger T.A., Deye J.F., Anal. Chem. 1990, 62, 1181-1185.
- Berger T.A., Deye J.F., Chromatographia 1990, 30, 57-60.
- Cagniard de la Tour C., Annales de chimieet de physique 1822, 21, 127-132.
- Crowther J.B., Henion J.D., Anal. Chem. 1985, 57, 2711-2716.
- Deye J.F., Berger T.A., Anderson A.G., Anal. Chem. 1990, 62,615-622.
- Gere D.R., Board R., McManigill D., Anal. Chem. 1982, 54, 736-740.
- Grand-Guillaume Perrenoud A., Boccard J., Veuthey J.-L., Guillarme D., J. Chromatogr. A 2012, 1262, 205-213.
- Grand-Guillaume Perrenoud A., Veuthey J.-L., Guillarme D., J. Chromatogr. A 2012, 1266, 158-167.
- King J.W., List G.R., AOCS Press, Champaign 1996.
- King J.W., (R. O. Adlof, ed.) Oily Press, Bridgewater 2003, 301-366.
- Klesper K., Corwin A.H., Turner D.A., J. Org. Chem. 1962, 27, 700-706.
- Lee M.L., Markides K.E., Science 1987, 235, 1342-1347.
- Lesellier E., J. Chromatogr. A 2009, 1216, 1881-1890.
- Lesellier E., J. Chromatogr. A 2012, 1228, 89-98.
- Lesellier E., J. Sep. Sci. 2008, 31, 1238-1251.
- Lesellier E., West C., J. Chromatogr. A 2015, 1386, 2-46.
- Nováková L., Perrenoud A.G-G., François I., West C., Lesellier E., Guillarme D., Anal.Chim. Acta 2014, 824, 18-35.
- Novotny M.V., Science 1989, 246, 51-57.
- Pettinello G., Bertucco A., Pallado P., Stassi A., J. Supercrit. Fluids 2000, 19, 51-60.

- Pinkston J.D., Stanton D.T., Wen D., J. Sep. Sci. 2004, 27, 115-123.
- Poole C.F., J. Chromatogr. A 2012, 1250, 157-171.
- Saito M., J. Biosci. Bioeng. 2013, 115, 590-599.
- Taylor L.T., Anal. Chem. 2010, 82, 4925-4935.
- Zaugg S.D., Deluca S.J., Holzer G.U., Voorhees K.J., J. High Res. Chromatog. 1987, 10, 100-101.

CHAPTER IV
Multidimensional Liquid Chromatography

4.1. Introduction

There are a whole host of real mixtures that are profitable to separate for qualitative and quantitative analysis, but simply can not be due to their complex nature. Obviously, these mixtures can be separated to some extent by using one-dimensional chromatography (1D-LC), but even in optimum conditions and with the most efficient column, full separation from single column chromatography will never be achieved. Moreover, even in samples of low complexity there is generally a random peak distribution, which requires high plate number values for total peak resolution (Guichon, 2006; Davis, *et al.*, 1983). In particular, if the number of components exceeds 37% of the peak capacity, peak resolution is statistically compromised (Davis, *et al.*, 1983). The limited resolving power of 1D-LC has incited the development of multidimensional LC (MDLC), in which the sample is subjected to two different separation mechanisms. The largest benefit of pairing columns, with different selectivity in a MDLC configuration, is the dramatic increase of the peak capacity, which is reflected in the reduction of component overlap. The first recorded use of two-dimensional chromatography was reported by Consden et al. (Consden, *et al.*, 1947), who separated 22 hydrochlorides of amino acids by using paper chromatography. Combinations of chromatography ×electrophoresis (Haugaard & Kroner, 1948) and electrophoresis×electrophoresis (Durrum, *et al.,* 1951) were also made early in the life of multidimensional separations. Two-dimensional thin-layer chromatography (2D-TLC) was pioneered by Kirchner et al. (Kirchner, *et al.*, 1951) and quickly became a popular technique. Following, great efforts were made to develop two-dimensional gas chromatography (2D-GC) (Deans, 1968;

Deans, 1971). In 1978 Enri and Frei (Erni & Frei, 1978) described the usage of off-line and on-line approaches to two-dimensional liquid chromatography (2D-LC). However, the first truly comprehensive 2D-LC work did not occur until 1990, when Bushey and Jorgenson performed the separation of a protein sample with a microbore cation-exchange column in the first dimension (^{1}D) and a exclusion column in the second dimension (^{2}D) (Bushey & Jorgenson, 1990). This publication has experienced large interest in the technique in different fields, and in recent years, because of commercially available systems, has been the subject of various reviews (Liu & Lee, 2000; Evans & Jorgenson, 2004; Shellie & Haddad, 2006; Jandera, 2006; Tranchida, *et al.*, 2007; Dugo, *et al.*, 2008a; Dugo, *et al.*, 2008c).

4.2. Multidimensional chromatography approaches

Several approaches may be used when coupling different separation mechanisms in 2D-LC, namely off-line, on-line, and stop-flow (also known as stop-and-go) methods, which can be distinguished on the basis of the transfer mode from the ^{1}D to the ^{2}D.

In off-line approach, fractions from the first dimension column are collected (manually or via a fraction collector) and stored indefinitely after concentration by partial or complete evaporation (if necessary), and finally injected onto the second dimension column. In off-line mode, only a single liquid chromatograph is sufficient to perform a 2D-LC separation and only a little attention is required regarding the compatibility of the mobile phases (immiscible solvents can be evaporated after which the sample components are re-dissolved in the appropriate second dimension injection solvent). Furthermore, there is no time constraint for either dimension and therefore, practically no high limit to the separation power available. The main drawbacks are the possibility of sample contamination, degradation or loss during handling (making this approach

almost useless for quantitative trace analyses), lack of automation (often causing poor reproducibility), its time consuming and operative intensive character.

In on-line coupling, fractions from the first dimension are sequentially transferred to the second dimension through an appropriate interface, typically a high-pressure switching valve. This approach is characterized by a high reproducibility, since the whole process is completely automated, and high sample throughput, but a number of technical requirements need to be fulfilled, in order to avoid mismatches arising from mobile phase miscibility employed in the two dimensions and the compatibility between the ^{1}D mobile phase with ^{2}D stationary phase. On-line method requires that analysis in the second dimension be completed before transfer of the following fraction. This constrains the separation in the second dimension to be concluded in what is usually a very short amount of time (generally, on the order of several seconds to one or two minutes). The ^{2}D analysis time should be at least equal or less than the duration of a modulation period; this can often result in a limited separation power in the second dimension. To overcome such an issue, it is possible to speed up the separation in ^{2}D by using a very high flow rate or a short column. In fact, the enhancements in LC column technologies (fused-core or sub-2 μm particles) and instrumentation (UHPLC instruments able to work at pressure of 1000 bar and higher) allow to carry out very fast analysis in ^{2}D with acceptable efficiency. Alternatively, the stop-flow strategy can be adopted. This set-up involves direct transfer of each fraction to the second dimension column, followed by stopping the flow in the first dimension whereas operating the separation in the second dimension, and replaying this process throughout the entire first dimension separation. This approach attenuates the time constraints of the second-dimension, but can result in overly long “peak parking” times,

which decreases the efficiency of the first-dimension separation (Gritti & Guiochon, 2006; Miyabe, *et al.*, 2007).

Evidently, the high complexity of on-line system, the need for specific interfaces and software, the expertise degree of the analysts and also economic implications, make this technique less easy to use with respect to the off-line approach that can be easily accomplished, since both analytical dimensions can be optimized as two independent methods.

Both off-line and on-line 2D-LC can be distinguished on heart-cutting (LC-LC) and comprehensive (LC×LC) techniques (Schoenmakers, *et al.*, 2003). The principal difference between the two approaches is the number of fractions that are transferred from the primary column effluent. In heart-cutting 2D-LC, only significant parts of the effluent, containing the compounds of interest, are transferred to the second dimension, permitting the rest of the first column effluent to exit the system through the waste, while comprehensive LC allows the separation of the complete (comprehensive) sample by the two dimensions.

As stated, all these techniques are associated with a number of advantages and disadvantages, and normally the choice of configuration depends on the one hand by the purpose or problem of the separation, and on the other hand by the availability of instrumentation.

4.3. Theoretical concepts: peak capacity, orthogonality and sampling rate

The basic metric that represents the separation capability is the peak capacity (n_c) which is defined as the maximum number of peaks that can fit side by side between the first (or unretained) and last peak of interest, at a fixed resolution between all these peaks. For one-dimensional gradient separation, the peak capacity can be calculated using the well-known method defined by Neue (Neue, 2005):

$$n_c = 1 + \frac{t_g}{(1/n)\sum_1^n \omega_n} \qquad \textbf{(Eq. IV-1)}$$

where t_g is the gradient time, ω is the baseline peak width, and n represents the number of peaks selected for the calculation.

In a fully orthogonal 2D system, ideally the total peak capacity ($n_{c,2D}$) is equal to the product of the peak capacities in the first (^1n_c) and in the second (^2n_c) dimensions:

$$n_{c,2D} = {}^1n_c \times {}^2n_c \qquad \textbf{(Eq. IV-2)}$$

However, the real increase in peak capacity is usually lower than predicted from Equation IV-2, depending on the degree of similarity of the coupled columns, as this value includes a region where there is retention correlation between the dimensions. In the calculation of the "practical peak capacity" ($n'_{c,2D}$) interrelated factors, including orthogonality and sampling rate, must be taken into consideration. Methods for calculating a truer $n_{c,2D}$ were proposed and reviewed by Dixon and Perrett (Dixon & Perrett, 2006). The maximum gain in resolving power is achieved in so-called "orthogonal" systems, in which the minimum correlation between the two retention mechanisms must occur. This means that the two used separation principles have to be independent of each other and show distinct retention profiles. Practically, truly orthogonal systems are hard to achieve, as orthogonality not only depends on the separation mechanisms, but also on the properties of the analytes and the separation conditions. The best orthogonal combinations can be attained when the appropriate stationary and mobile phases are carefully selected with respect to the physico-chemical properties of the sample constituents like molecular

size, charge, acid-base nature, polarity, hydrophobicity, etc. A number of various stationary phases is nowadays available, with different characteristics regarding surface chemistries, support material, pore size, and carbon load, while mobile phase composition can be modified by adding ion pair agents or changing the modifier, pH, temperature. Some example of orthogonal combinations are: NP-LC×RP-LC, in which the separation occurs respectively on the basis of polarity and hydrophobicity (Dugo, *et al.*, 2004), silver-ion (SI) LC×NARP-LC, which provides separation according to degree of saturation and hydrophobicity (Mondello, *et al.*, 2005), and also the coupling of two RP-LC dimensions can give high orthogonality, despite the degree of correlation between similar or even identical stationary phases that may be reduced by adequately tuning analytes interactions; this can be accomplished through the use of different mobile phase pH values (Dugo, *et al.*, 2013; Donato, *et al.*, 2011) or by varying the gradient composition between subsequent 2D runs, according to the properties of the analytes being transferred from ^{1}D (Leme, *et al.*, 2014). On the other hand, retention in orthogonal combination could be slightly related because of similar physico-chemical properties of some molecule in the sample. For example, size exclusion chromatography (SEC)×RP-LC or SEC×NP-LC may exhibit some selectivity correlation as the high contribution of hydrophobic or polar interactions in large molecules; in the same way ion-exchange (IEX) LC separates analytes mainly on the basis of charge, but might show hydrophobic or polar interactions.

The concept and meaning of orthogonality are better illustrated in Figure IV-1 and are clarified by practical examples of RP-LC×RP-LC (on the right: not orthogonal set-up due to the same retention mechanisms and same pH mobile phases) and HILIC×RP-LC (on the left: orthogonal set-up due to two independent retention mechanisms).

Evidently, low orthogonality is observed when the blobs obtained by plotting the retention times of the two dimensions are spread in the two-dimensional space mostly along a line, usually over a diagonal of the contour plot, instead of a random peak distribution able to completely cover the 2D map. Consequently, the determination of orthogonality is essential in order to evaluate the efficiency of the technique in terms of peak capacity and maximize the separation space available for the separation of complex samples. Various approaches have been studied for the calculation of the 2D system orthogonality, among which: the spreading angle method of Liu et al. (Liu, *et al.*, 1995), the informational theory of Slonecker et al. (Slonecker, *et al.*, 1996; Gray, *et al.*, 2002), and a more recent approach proposed by Camenzuli and Schoenmakers (Camenzuli & Schoenmakers, 2014).

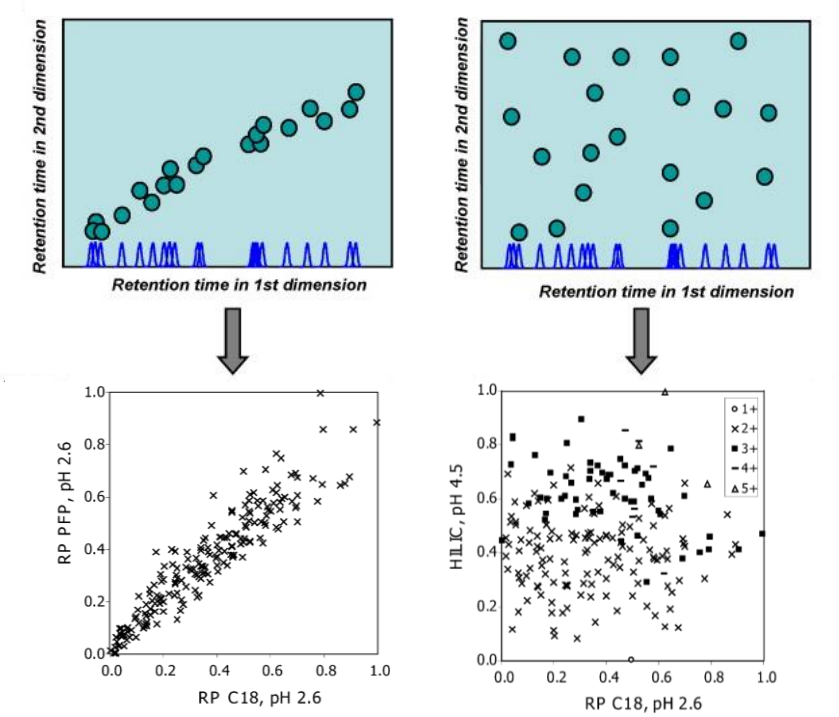

Figure IV-1. *Representation of orthogonality in comprehensive LC (François, et al., 2009; Gilar, et al., 2005).*

As well as the low orthogonality, an additional decrease in peak capacity can result from ^{1}D band broadening due to re-mixing in a loop or trap of sampling interface between the first and the second column. Usually, the sampling or modulation time is equal to the analysis time in ^{2}D so that each fraction is transferred when the previous one has been totally eluted. The standard deviation (σ_{D1}), which characterizes the overall first dimension peak dispersion, is contributed to both the column dispersion (σ_1) and the dispersion of the modulator interface (σ_M):

$$\sigma^2_{D1} = \sigma^2_1 + \sigma^2_M \qquad \textbf{(Eq. IV-3)}$$

Average band width of a ^{1}D peak before sampling, σ_1, is broadened by re-mixing of the collected fraction, and is characterized by a factor $\beta' = \sigma_{D1}/\sigma_1$, which decreases at shorter sampling times (t_S):

$$\beta' = \sqrt{\kappa \frac{t_s}{\sigma_1} + 1} \qquad \textbf{(Eq. IV-4)}$$

where k is a parameter that proportionally increase with the sampling rate (in LC×LC, k=3.35). Thus, the real peak capacity of ^{1}D (^1n_c') can be calculated by the ratio of uncorrected ^1n_c value to β' factor, and the total practical peak capacity by the following Equation:

$$n'_{c,2D} = {}^1n'_c \times {}^2n_c \times f_{coverage} \qquad \textbf{(Eq. IV-5)}$$

where $f_{coverage}$ is the above mentioned orthogonality value, corresponding to the peak distribution on the 2D separation space (Gu, *et al.*, 2011); β' is also called

under-sampling factor, considering its intrinsic relationship with the sampling rate. However, to achieve "ideal" conditions and maintain ^{1}D resolution, the "under-sampling" effects must be considered. Murphy et al. suggested that 3 fractions should be sampled for each first dimension peak to avoid severe loss of first dimension resolution. This number is only acceptable when the sampling is 'in-phase', which entails that the sampling should start exactly at the beginning of the peak. Practically, this cannot be ensured, therefore a minimum of 4 samplings is recommended (Murphy, *et al.*, 1998a). During method optimization, it is advisable evaluating the average peak width in order to set the appropriate sampling time. In essence, the separation in ^{2}D should be fast enough to ensure an adequate number of samplings. On the other hand, an "over-sampling" can cause loss in sensitivity because of the fact that some fractions (like the front and the tail of the peak) will be too much diluted and will not be detected after ^{2}D separation.

4.4. Method optimization and instrumentation

4.4.1. General overview

Multidimensional separation is a multi-step process that requires selecting and developing of the two dimensions, the fraction collection and detection. To optimize a 2D-LC technique, one should consider the many parameters that affect the separation power of the whole system. Therefore, before coupling, the methods in both dimensions should be optimized independently, considering also the sample characteristics. Therefore, the type, the composition and the flow rate of the mobile phase, the gradient program and the temperature of the separation must be carefully chosen. The analyst should take into account the retention patterns, basically the degree of correlation between the retention mechanisms used in the two dimensions and the number of collected fractions from the first dimension.

A typical LC×LC system is composed of at least two pumps, two columns, an injector, an interface and a detector (Figure IV-2).

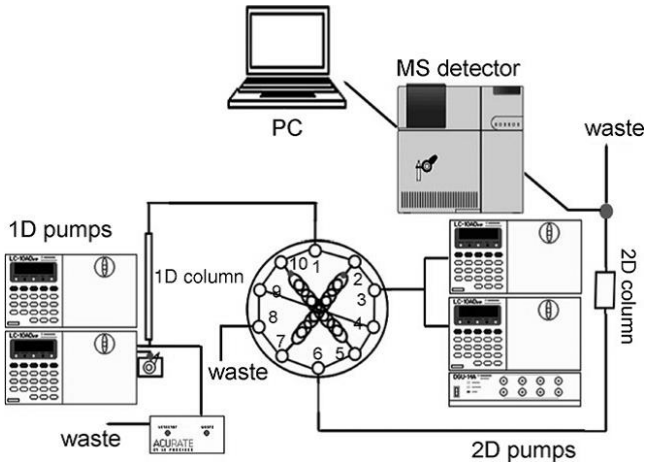

Figure IV-2. *Common set-up for comprehensive 2D-LC (Dugo, et al., 2006).*

The interface is the heart component in all comprehensive 2D-LC set-ups, since it has the function to hyphen the two dimensions and provides the continuous transfer of aliquots of predefined volumes from the ^{1}D to the ^{2}D in an automated way.

The following paragraphs highlight the properties of the individual dimensions and diverse issues that may be encountered during the development of comprehensive LC separations.

4.4.2. First dimension

The separation in the first dimension has no time restrictions, hence it is characterized by satisfactory resolution. In order to reduce band broadening and diminish signal interferences caused by solvent incompatibilities, in the first dimension is usually employed a micro- or narrow-bore column. The small column I.D. guarantees a minimization of dilution and provides low flow rates

(10-100 μL/min) that are compatible with the conventional bore columns of 4.6 mm I.D. in the second dimension. Furthermore, a pre-concentration step at the head of the secondary column is not essential and solvent incompatibility between different separation modes is avoided (Cortes, 1992; Dugo *et al.*, 2004). The use of micro-bore columns allows low mobile phase consumption and higher separation efficiency. Despite the lower sample capacity of these columns can be considered a disadvantage, it should be taken into account that a large volume injection could be performed with an acceptable decrease in efficiency. An alternative is to use a wider bore column and to split the effluent prior to the interface, but in this way a large part of the sample components is wasted through which the sensitivity is compromised. In order to obtain an enough number of samplings per first dimension peak, the flow rate applied on these columns is reduced to below its optimum value. This means that the first dimension resolution and, thus, global peak capacity are in this case sacrificed.
For the first dimension, both isocratic and gradient elution can be used, depending on the application.

4.4.3. Second dimension

The time for analysis in ^{2}D, including re-conditioning time when a gradient is applied, is dictated by the sampling and flow rates used in ^{1}D.
As stated before, fast second dimension analyses should be performed at high flow rate, ensuring that each separation can be completed before transfer of the following fraction. The sampling rate usually ranges from several seconds to 1-2 minutes, depending on the application, at the expense of the resolution. A number of possibilities are exploited to speed up the separation in ^{2}D.
The use of monolithic columns is well suited because of their brief re-conditioning times, that allow the application of gradient programs during successive second dimension runs (Cacciola, *et al.*, 2006; Mondello, *et al.*,

2005; Dugo, *et al.*, 2006a; Dugo, *et al.*, 2006b; François, *et al.*, 2006; Tanaka, *et al.*, 2002), and high permeability (Eeltink, *et al.*, 2005). Moreover, they can be operated at elevated flow rates without loss of resolution.

Sub-2 μm and fused core particles packed columns have been all successfully employed to speed up the second dimension analysis. Both these column technologies offer an increase of the resolution, but the columns packed with sub-2 μm particles, unlike the fused core, require sophisticated instrumentation capable of delivering high pressures (600 to 1000 bar).

In addition to changing the morphology of the stationary phase, it is also possible to modify the properties of the mobile phase for increasing the speed in the ^{2}D analysis. It has already been demonstrated that by increasing mobile phase temperatures to more than 100 °C, ultra-fast gradient elution separations on narrow-bore wide pore carbon-coated zirconia columns, with excellent retention times repeatability, can be obtained (Stoll & Carr, 2005; Stoll, *et al.*, 2006). The decrease of eluent viscosity allows higher flow rate at the same maximum pressure and, consequently, fast column re-equilibration. Moreover, high temperatures mitigate the loss in efficiency, which usually occurs at higher than optimum linear velocities. However, this strategy could suffer from a possible thermal degradation of both stationary phase and the analyzed compounds.

Usually, the second columns I.D. are 4.6 mm (optimal flow rate 1.8 mL/min) and they are operated up to 4-5 mL/min with satisfactory resolution. Such large diameter allows the introduction of relatively large volumes, generally equal to the mobile phase eluting from the first dimension per modulation time. As a rule, the ^{2}D column I.D. is always 4-8 times larger than the one of the column used for the primary separation (Schoenmakers, *et al.*, 2006).

The second dimension can be performed both in gradient or isocratic modes. Isocratic elution provides fast runs, avoids column conditioning steps and

eliminates the presence of undesirable effects on the background signals of UV or MS detectors due to the rapid changes of the mobile phase composition. Instead, gradient elution is more advantageous, since it reduces the possibility of wrap-around phenomenon. This one occurs when the elution times of the analytes in the ^{2}D separation exceed the modulation time. In that case, the compound elutes together with components from the successive modulation cycle, at a retention time different than its real retention time. This results in several co-elutions and broader peaks. Very steep gradients should be used to allow a fast elution, but slower gradients provide major resolution (Cacciola, *et al.*, 2007). During the years, various gradient elution strategies have been investigated to improve the peak distribution in the 2D-LC.

In "full in fraction" (FIF) gradient a very rapid gradient is cyclically applied in all the fractions (Stoll, *et al.*, 2007). The main advantages of FIF elution mode include larger sample retention range avoiding the possibility of accumulation in column and better analyte re-focusing on the transfer from the first to the second dimension. On the other hand, the main disadvantages are the difficulty for a fast column re-equilibration to the initial gradient condition and the possibility to poorly resolve the peaks due to the high slope of the gradient.

In Continuously Shifting (CS) gradient, only one single gradient spanning during the whole ^{2}D separation time is adopted simultaneously to the ^{1}D gradient (Cacciola, *et al.*, 2007; Cesla, *et al.*, 2009). This approach is particularly useful for 2D systems with moderately correlated retention, where the average elution times in the second dimension increase for compounds more strongly retained in the first dimension.

Finally, segmented in fraction (SIF) employs different gradient ranges in different segments of the ^{1}D separation; this combines the benefits of the CS and FIF gradients.

4.4.4. Interface

As mentioned before, the interface is the key component of any comprehensive LC system, since it enables the continuous transmission of the primary column effluent to the second dimension in an automated mode. In the last years, different configurations have been investigated.

The most commonly used is the loop interface, based on a two-position/ten- or eight-port switching valve equipped with two identical-volume sampling loops (Dugo, *et al.*, 2004; Mondello, *et al.*, 2005; Dugo, *et al.*, 2006c; Cacciola, *et al.*, 2007; Dugo, *et al.*, 2008a; Dugo, *et al.*, 2008b; Hu, *et al.*, 2005; Murphy, *et al.*, 1998b; Chen, *et al.*, 2004), one of which collects the effluent from the first dimension, while the previous effluent fraction contained in the second loop is transferred onto the second dimension and is subjected to separation (Schoenmakers, *et al.*, 2003; van der Horst & Schoenmakers, 2003). Both dimensions are operated continuously, as the two loops are periodically and alternately switched between the collection and the re-injection modes; the modulation period is controlled by the switching valve frequency.

A modification of the sampling loops is represented by the packed loops, which are filled with stationary phase. Here, each fraction is adsorbed alternately on one of the trapping columns; in the following cycle the retained compounds are back-flushed from the trapping columns onto the second dimension analytical column. The characteristics of the adsorbent in the loops depending on the application, especially on the properties of the components of interest and the solvents employed in both dimensions. The development of such arrangement is complicated by the fact that trapping efficiency and rapid desorption are inversely related. In order to allow a good focusing, a weak solvent for the stationary phase in the loop should be used as mobile phase in the ^{1}D dimension, whereas fast desorption by a strong solvent should be accomplished by the secondary mobile phase. Evidently, changes in retention order of the

sample components should be taken into account, because of the possibility of chromatographic separation inside the trapping columns. Various interface set-ups equipped with packed loops were used, consisting of: two-position/ten-port switching valve assembled with two guard columns (Cacciola, *et al.*, 2007; Cacciola, *et al.*, 2006); a six-port switching valve with a solid-phase extraction (SPE) column selector that incorporated eighteen trapping columns collecting the same number of fractions throughout the first dimension chromatogram (Wilson, *et al.*, 2007); a two-position/twelve-port switching valve equipped with three identical packed loops (Venkatramani & Patel, 2006).

In the stop-flow approach, the columns are coupled via an interface without sampling loops. The conventional loop interface is also employable in this case, but since the sampling loops have no function and negatively affect the extra-column band broadening is not recommended. It is possible the use of one or several two-position/six-port switching valves, all following the same criterion (Köhne & Welsch, 1999; Blahova, *et al.*, 2006). In one position, the interface directly connects the two columns and drives the ^{1}D column effluent to the ^{2}D. When the transfer of the wanted fraction is accomplished, the interface is switched back and, simultaneously the ^{1}D flow is interrupted, allowing the ^{2}D separation of the fraction. In this configuration, the mobile phases in both dimensions have a great importance, because a focusing of the solutes at the head of the second dimension column is essential to avert peak shape deterioration.

Lately, an innovative interface was developed by Tian et al. (Tian, *et al.*, 2006; Tian, *et al.*, 2008), namely vacuum evaporation interface (VEI), suitable for the coupling of NP-LC and RP-LC. The interface valve not only provided the collection of the fractions eluting from the ^{1}D, but also allowed the evaporation of the mobile phase solvents by applying elevated temperatures under vacuum conditions. On the one hand, this approach solves the problem of

incompatibility of mobile phases that plagues the NP-LC×RP-LC coupling; on the other hand it was not capable to obtain full recovery of all sample compounds, especially for solutes with a low boiling point.

4.5. 2D comprehensive SFC-based separations

Notwithstanding the advantages of SFC as one of the dimensions in comprehensive separations, only few applications have been described.

Hirata and co-workers (Hirata, *et al.*, 2003; Hirata & Sogabe, 2004) performed on-line comprehensive 2D-SFC (SFC×SFC) by means of a double three-port and a ten-port switching valve. The latter was used as a modulator to connect the two columns, and was equipped with a capillary trapping tube consisting of methyl silicone material on which the analytes were trapped after elution from the ^{1}D and depressurization through the BPR. The double three-port valve was used for the change-over between 1D and 2D measurements, so that changing the plumbing of the system was not necessary. A schematic diagram of the configuration is shown in Figure IV-3. The first dimension was operated in the stopped-flow mode, and the mobile phase consisted of pure CO_2; the selectivity in both dimensions was achieved through the application of different stationary phases and/or a significant change in column temperature.

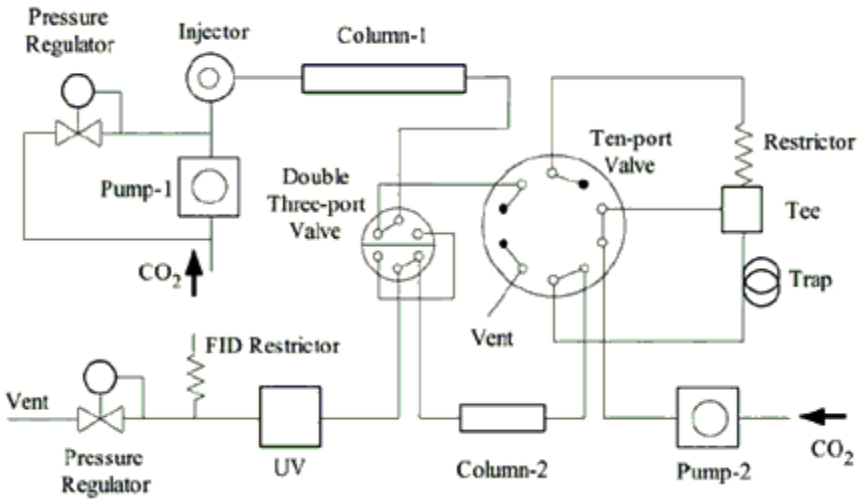

Figure IV-3. *SFC×SFC interface by Hirata et al.*

Liu et al. (Liu, *et al.*, 1993) coupled capillary SFC to GC by using the decompressed CO_2 gas after the BPR as the gaseous mobile phase. Both columns were in the same oven, therefore undergone at the same temperature programs, meaning that each second dimension chromatogram was acquired under isothermal conditions. This was profitable in terms of column re-equilibration time, but the first dimension separation was negatively affected by the increasing temperature. Besides, the separation in high-speed GC is largely jeopardized by using CO_2 gas as mobile phase due to slow diffusion coefficients (Fuller, *et al.*, 1966).

François et al. (François, *et al.*, 2008; François, *et al.*, 2009b; François, *et al.*, 2010) developed a new interface to hyphen SFC and RP-LC in a comprehensive configuration. The interface consisted of a two-position/ten-port switching valve equipped with two packed ODS loops for trapping and focusing of the analytes after elution from the SFC dimension. An additional flow of water to the SFC eluent, before entering the packed loops, ensured the focus of the solutes on the ODS material, and at the same time the removal of residual

supercritical CO_2 expanded in the loops, thus limiting the occurrence of signal interferences.

During this Ph.D. research, a similar approach to that proposed by François et al. was used to combine SFC and RP-LC in a comprehensive configuration. This coupling offered an interesting alternative to the highly orthogonal NP-LC×RP-LC separations with the additional advantages of the reduction of signal interferences and incompatibility problems (chapter IX).

4.6. Detectors

A comprehensive 2D-LC separation is easily hyphenated with the most conventional HPLC detectors, such as ELSD, PDA and MS. Usually only one detector is installed after the second dimension column with the first dimension separation monitored only during the optimization step. Because of the high speed of the ^{2}D analysis, the detector has to provide acquisition rate very fast, ensuring the acquisition of narrow peaks, and then the proper reconstruction of the 2D chromatogram; no loss in resolution can be accepted deriving from a low number of data points. Both PDA and MS detectors can add a third dimension to the 2D system, offering supplementary information for a comprehensive identification of the analytes. When using MS for detection, the flow is generally split to values of 1 mL/min and lowers prior to entrance in the ion source, since the high flow rates employed in ^{2}D to quicken the analysis speed are not tolerated from the ion source. The flow splitting negatively affects the sensitivity and leads to peak broadening, because of the addition of the extra volume of the splitter. ESI and APCI are the most frequently used ionization techniques for on-line analyses, while matrix assisted laser desorption ionization (MALDI) can be applied to off-line collected fractions (François, *et al.*, 2009a). Concerning to the analyzers, the high scanning rates and high resolution concurred to make time-of-flight (ToF) MS the detector of choice in

LC×LC applications (scan speed 20000 amu/sec). Nevertheless, the latest generation of quadrupole (Q)-type instruments allows for high speed scanning and ultrafast polarity switching. A number of hybrid instruments, characterized by enhanced resolution, high sensitivity, as well as increased mass accuracy over a wide dynamic range, must be also considered because they enable for a confident identification by performing tandem MS experiments and accurate quantification by increasing the signal-to-noise ratio and also the selectivity of the analytical method (for example, triple quadrupole (QqQ) MS for ultrasensitive target analysis and high resolution MS such as Q-ToF or quadrupole-ion mobility-time of flight (Q-IMS-ToF) for non-target approaches).

4.7. Data processing

The huge amount of data generated from the 2D chromatography requires the use of informatics tools capable of processing and converting the raw analytical data into useful chemical information, and then elaborate two-dimensional or three-dimensional plots. Problems increase if peak quantification needs to be executed. Peak integration and quantitation can be performed by summing the areas of individual second dimension peaks belonging to one analyte, which are integrated using specific integration algorithms. Therefore, the availability of tables including retention times, panels for the visualization of MS and UV spectra (for qualitative analysis), and integration functions for building regression curve (for quantitative analysis) of all detected peaks is highly desirable.

Typically, in a 2D plot or contour plot, the retention times in the first and second dimensions are plotted along the *x*- and *y*- axes, respectively; each peak (blob) is characterized by a colour of intensity proportional to the concentration in the sample, as well as in a 3D plot the peak height is directly related to the

compound amount (Figure IV-4). The scarcity of software available for data acquisition and handling in 2D chromatography is one of the most significant obstacles for a generalized implementation of this separation technique.

In the last years, great progresses are being made in this field, that also concern the combination of multidimensional separation with chemometric data analysis, as recently reviewed by Dixon and Perrett (Dixon & Perrett, 2006).

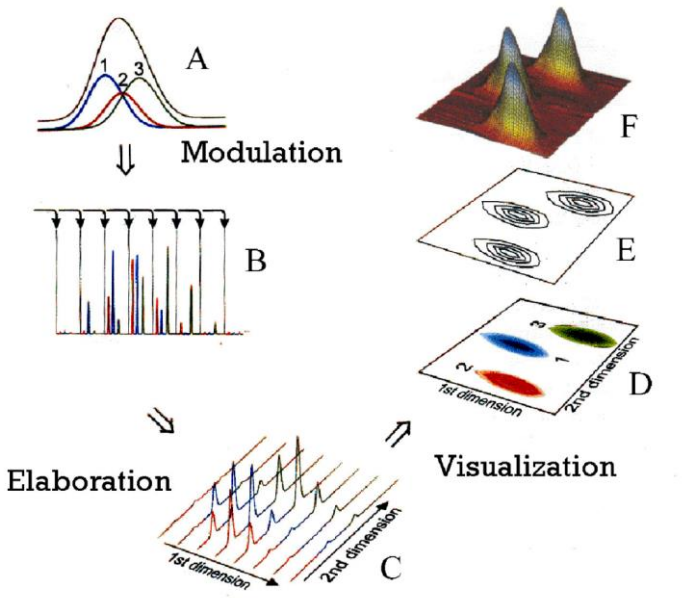

Figure IV-4. *Scheme representing the LC×LC data manipulation and visualization process.*

In this thesis, the functions of a 2D software, namely Chromsquare (Chromaleont, Messina, Italy), will be utilized for the characterization of a complex sample by using complementary informations gathered from retention times, PDA spectra, and high resolution ToF MS data.

REFERENCES

- Blahova E., Jandera P., Cacciola F., Mondello L., J. Sep. Sci. 2006, 29, 555-566.
- Bushey M.M., Jorgenson J.W., Anal. Chem. 1990, 2262, 161-167.
- Cacciola F., Jandera P., Blahova´E., Mondello L., J. Sep. Sci. 2006, 29, 2500-2513.
- Cacciola F., Jandera P., Hajdú Z., Česla P., Mondello L., J. Chromatogr. A 2007, 1149, 73-87.
- Camenzuli M., Schoenmakers P.J., Anal. Chim. Acta 2014, 838, 93-101.
- Česla P., Hájek T., Jandera P., J. Chromatogr. A 2009, 1216, 3443-3457.
- Chen X.G., Kong L., Su X.Y., Fu H.J., Ni J.Y., Zhao R.H., Zou H.F., J. Chromatogr. A 2004, 1040, 169-178.
- Consden R., Gordon A.H., Martin A.J.P., Biochem J. 1947, 41, 590-596.
- Cortes H.J., J. Chromatogr. 1992, 626, 3-23.
- Davis J.M., Giddings J.C., Anal. Chem. 1983, 55, 418-424.
- Deans D.R., Chromatographia 1968, 1, 18-22.
- Deans D.R., Chromatographia 1971, 4, 279-285.
- Dixon S.P., Perrett I.A.D., Biomed. Chromatogr. 2006, 20, 508-529.
- Donato P., Cacciola F., Sommella E., Fanali C., Dugo L., Dacha M., Campiglia P., Novellino E., Dugo P., Mondello L., Anal. Chem. 2011, 83, 2485-2491.
- Dugo P., Cacciola F., Kumm T., Dugo G., Mondello L., J. Chromatogr. A 2008, 1184, 353-368.
- Dugo P., Favoino O., Luppino R., Dugo G., Mondello L., Anal. Chem. 2004, 76, 2525-2530.
- Dugo P., Fawzy N., Cichello F., Cacciola F., Donato P., Mondello L., J. Chromatogr. A 2013, 1278, 46-53.
- Dugo P., Herrero M., Kumm T., Giuffrida D., Dugo G., Mondello L., J. Chromatogr. A 2008, 1189, 196-206.
- Dugo P., Kumm T., Cacciola F., Dugo G., Mondello L., J. Liq. Chromatogr. Relat. Technol. 2008, 31, 1758-1807.

- Dugo P., Kumm T., Chiofalo B., Cotroneo A., Mondello L., J. Sep. Sci. 2006, 29, 1146-1154.
- Dugo P., Kumm T., Crupi M. L., Cotroneo A., Mondello L., J. Chromatogr. A 2006, 1112, 269-275.
- Dugo P., Skerikova V., Kumm T., Trozzi A., Jandera P., Mondello L., Anal. Chem. 2006, 78, 7743-7750.
- Durrum E.L., J. Colloid Sci. 1951,6, 274-290.
- Eeltink S., Desmet G., Vivó-Truyols G., Rozing G. P., Schoenmakers P. J., Kok W.T., J. Chromatogr. A 2005, 1104, 256-262.
- Erni F., Frei R.W., J. Chromatogr. 1978,149, 561-569.
- Evans C.R., Jorgenson J.W., Anal. Bioanal. Chem. 2004, 378, 1952-1961.
- François I., de Villiers A., Sandra P., J. Sep. Sci. 2006, 29, 492-498.
- François I., dos Santos Pereira A., Sandra P., J. Sep. Sci. 2010, 33, 1504-1512.
- François I., Pereira A.S., Lynen F., Sandra P., J Sep Sci. 2008, 31, 3473-3478.
- François I., Sandra K., Sandra P., Anal. Chim. Acta 2009, 641, 14-31.
- François I., Sandra P., J. Chromatogr. A 2009, 1216, 4005-4012.
- Fuller E.N., Schettle P.N., Giddings J.C., Ind. Eng. Chem. 1966, 58, 19-35.
- Gilar M., Olivova P., Daly A.E., Gebler J.C., Anal. Chem. 2005, 77, 6426-6434.
- Gray M., Dennis G.R., Wormell P., Shalliker R.A., Slonecker P., J. Chromatogr. A 2002, 975, 285-297.
- Gritti F., Guiochon G., Anal. Chem. 2006, 78, 5329-5347.
- Gu H., Huang Y., Carr P.W., J.Chromatogr. A, 2011, 1218, 64-73.
- Guichon G., J. Chromatogr. A 2006, 1126, 6-49.
- Haugaard G., Kroner T., J. Am. Chem. Soc. 1948, 70, 2135-2137.
- Hirata Y., Hashiguchi T., Kawata E., J. Sep. Sci. 2003, 26, 531-535.
- Hirata Y., Sogabe I., Anal. Bioanal. Chem. 2004, 378, 1999-2003.
- Hu L.H., Chen X.G., Kong L., Su X.Y., Ye M.L., Zou H.F., J. Chromatogr. A 2005, 1092, 191-198.
- Jandera P., J. Sep. Sci. 2006,29, 1763-1783.
- Kirchner J.G., Miller J.M., Keller G., Anal. Chem. 1951, 23, 420-425.

- Köhne A.P., Welsch T., J. Chromatogr. A 1999, 845, 463-469.
- Leme G.M., Cacciola F., Donato P., Cavalheiro A.J., Dugo P., Mondello L., Anal. Bioanal. Chem. 2014, 406, 4315-4324.
- Liu Z., Lee M.L., J. Microcolumn Sep. 2000,12, 241-254.
- Liu Z., Ostrovsky I., Farnsworth P.B., Lee M.L., Chromatographia 1993, 35, 567-573.
- Liu Z., Patterson Jr. D.G., Lee M.L., Anal. Chem. 1995, 67, 3840-3845.
- Miyabe K., Matsumoto Y., Guiochon G., Anal. Chem. 2007, 79, 1970-1982.
- Mondello L., Tranchida P.Q., Stanek V., Jandera P., Dugo G., Dugo P., J. Chromatogr. A 2005, 1086, 91-98.
- Murphy R.E., Schure M.R., Foley J.P., Anal. Chem. 1998, 70, 1585-1594
- Murphy R.E., Schure M.R., Foley J.P., Anal. Chem. 1998, 70, 4353-4360.
- Neue U.W., J. Chromatogr. A 2005, 1079, 153-161.
- Schoenmakers P.J., Vivo-Truyols G., Decrop W.M.C., J. Chromatogr. A 2006, 1120, 282-290.
- Schoenmakers P., Marriott P., Beens J., LC-GC Eur. 2003, 16, 335-339.
- Shellie R.A., Haddad P.R., Anal. Bioanal. Chem. 2006, 386, 405-415.
- Slonecker P.J., Li X., Ridgway T.H., Dorsey J.G., Anal. Chem. 1996, 68, 682-689.
- Stoll D.R., Carr P.W., J. Am. Chem. Soc. 2005, 127, 5034-5035.
- Stoll D.R., Cohen J.D., Carr P.W., J. Chromatogr. A 2006, 1122, 123-137.
- Stoll D.R., Li X., Wang X., Carr P.W., Porter S.E.G., Rutan S.C.J., J. Chromatogr. A 2007, 1168, 3-43.
- Tanaka N., Kobayashi H., Ishizuka N., Minatuchi H., Nakanishi K., Hosoya K., Ikegami T., J. Chromatogr. A 2002, 965, 35-49.
- Tian H., Xu J., Guan Y., J. Sep. Sci. 2008, 31, 1677-1685.
- Tian H., Xu J., Xu Y., Guan Y., J. Chromatogr. A 2006, 1137, 42-48.
- Tranchida P.Q., Donato P., Dugo P., Dugo G., Mondello L., Trends Anal. Chem. 2007, 26, 191-205.
- van der Horst A., Schoenmakers P.J., J. Chromatogr. A 2003, 1000, 693-709.
- Venkatramani C.J., Patel A., J. Sep. Sci. 2006, 29, 510-518.

- Wilson S.R., Jankowski M., Pepaj M., Mihailova A., Boix F., Vivo-Truyols G., Lundanes E., Greibrokk T., Chromatographia 2007, 66, 469-474.

CHAPTER V
Mass Spectrometry

5.1. Introduction

Of the many powerful analytical techniques, which govern the life science panorama, MS has raised a pivotal position in several fields. Analytical applications concerning to quality control of drugs and foods, environmental and forensic analyses, are now routinely accomplished by using mass spectrometry (Cooper & Marshall, 2001; Hughey, *et al.*, 2002; Zuccato, *et al.*, 2005). Regardless of the analytical purpose, mass spectrometry aims to provide structural information of a compound for an unambiguous identification. The central principle for a profitable mass spectrometric experiment is the generation of stable ions of the molecules of interest able to "survive" along their path inside the mass spectrometer and, hence, to become detectable. In this regard, the molecule has to be firstly transferred from its existing physical state to the gas phase into the vacuum of an ion source block, and secondly it has to acquire one or more charges to be separated according to their mass-to-charge (*m/z*) and detected, into a mass analyzer, in proportion to its abundance. The analytes may be ionized thermally, by electric field or by impacting energetic electrons, ions or photons. During the last decades, mass spectrometry has dramatically grown in terms of developing of new and/or improving existing methodologies of ion sampling, generation and transfer into mass analyzers, as well as data recording and generation of mass spectra (Harris, *et al.*, 2007). Nowadays, mass spectrometry is the most used technique coupled to the chromatographic systems, GC, LC and SFC; such "hyphenation", i.e., as GC-MS, LC-MS and SFC-MS, delivers high selectivity and low detection limits for the analysis of trace compounds, or the possibility to resolve complex samples, high throughput and high accuracy.

A mass spectrometer consists of the following fundamental elements, as illustrated in Figure V-1: a *sample inlet* to introduce the compound that is analyzed, an *ionization source* to produce ions from the sample, a *mass analyzer* to separate the various ions, and a *detector* to 'count' the ions emerging. At the bottom end of such a scheme, a data processing system produces the mass spectrum in a suitable form.

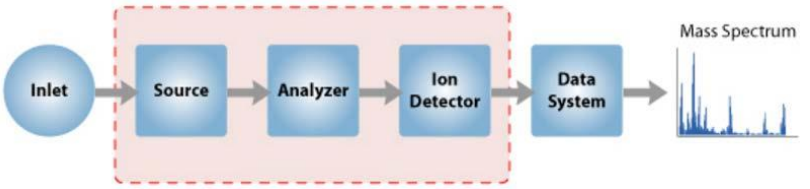

Figure V-1. *Diagram scheme of a mass spectrometer instrument.*

Moreover, the instrument is made up also of a pumping system, which is essential component of a mass spectrometer. The ions formation and manipulation must be operated under high vacuum because they are very reactive and short-lived. The pressure under which ions may be handled is approximately 10^{-3} to 10^{-10} torr. This is fundamental to avoid the possibility that the ions undergo collisions with other gaseous molecules and reach the detector. In fact, the collisions would change the trajectory and the ion would release its charge against the walls of the instrument. In addition, ion-molecule collisions could produce undesirable reactions and thus destroy the molecule and lose the mass information.

Generally, MS systems can be operated in the full scan mode (total ion current chromatogram, TIC, are obtained), in tandem MS experiments or in the selected ion monitoring (SIM) mode where only ions with a specific *m/z* values reach the detector. The latter approach is usually used for the development of

selective and sensitive quantitative assays, due to the reduction of the baseline noise, and thus the gain in the signal-to-noise ratio (S/N).

5.2. Mass resolution and mass accuracy

5.2.1. Resolution and resolving power

The term *mass resolution*, R, or just *resolution*, commonly denotes the ability of a mass spectrometer of separating two narrow mass spectral peaks. The capability of an instrument to distinguish between ions differing by a small increment in their *m/z* value ($\Delta m/z$) is named *resolving power* (RP):

$$R = \frac{m}{\Delta m} = \frac{m/z}{\Delta m/z} \qquad \textbf{(Eq. V-1)}$$

where Δm is the peak full width at half maximum (FWHM), as shown in Figure V-2. The older definition of RP (established for magnetic sector analyzers) based on two neighboring peaks of identical heights and 10% valley is not used in the current LC-MS practice.

At present, it is possible to differentiate mass analyzers between three basic categories of RP: low-RP (<10000), high-RP (10000-100000), and ultrahigh-RP (>100000). However, there is no exact definition of these terms. Furthermore, one should be aware that increased settings of resolving power are usually obtained at the cost of transmission of the analyzer, thereby reducing the absolute signal intensity.

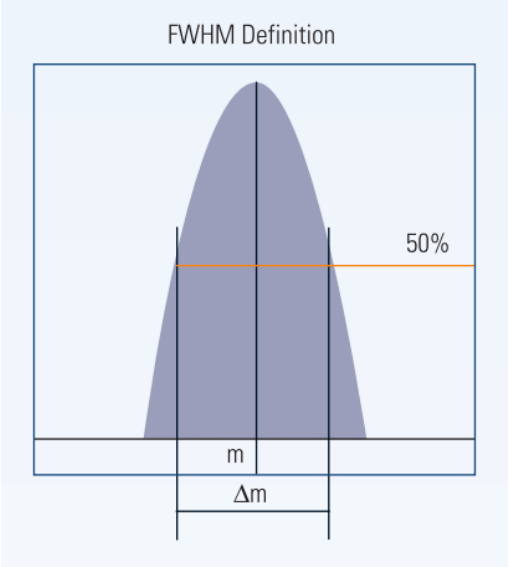

Figure V-2. *FWHM definition.*

5.2.2. Mass accuracy

The measurement of the mass of an atom, molecule or ion, is an important tool for scientists over a wide range of disciplines. For stoichiometric calculations, chemists use the average mass that is the result of the weighted average of the atomic masses of the different isotopes of each element in the molecule. In mass spectrometry, the nominal mass is generally used, and it is calculated using the mass of the most abundant isotope of each element rounded to the nearest integer value and equivalent to the sum of the mass numbers of all constituent atoms. However, the exact masses of isotopes are not exact whole numbers. They differ slightly from the nominal mass by a specific value, so-called mass defect, which is unique for each isotope. The monoisotopic mass is calculated by using the exact mass of the most abundant natural isotope of each constituent element.

Mass accuracy (MA) is defined as the relative difference between the experimental *m/z* value and theoretical (calculated exact mass) *m/z* value related

to this theoretical value including the sign (plus or minus) and expressed as parts per million (ppm):

$$\mathrm{MA} = \left(\frac{(m/z)_{\mathrm{exp}} - (m/z)_{\mathrm{theor}}}{(m/z)_{\mathrm{theor}}} \right) \times 10^6 \qquad \textbf{(Eq. V-2)}$$

Accurate mass measurements allow to determine the elemental composition of an analyte, and thus to confirm the identification of target compounds or to support the identification of unknowns.

The conventional definition of high-MA is 5 ppm and better. Technical specifications report for mass spectrometers with the internal calibration or the lock-mass approach values below 1 ppm (ultrahigh-MA) (Holcapek, *et al.*, 2012).

5.2.3. High-resolution mass spectrometry

The advancement of state of the art MS instrumentation now comprises the high-resolution mass spectrometry (HR-MS) capable of separating mass fragments at the fourth or fifth decimal place (exact mass) where previous instrumentation was limited to single-digit mass units (integer mass). High-resolution mass spectrometers have developed through many steps. The advent of orthogonal ion introduction and kinetic energy focusing by the use of a reflectron device brought the already existing linear ToF mass analyzers to dramatic improvements in terms of accurate mass measurements (Wiley & McLaren, 1955; Mamyrin, 1994; Morgan, *et al.*, 1978; Wollnik, 1987). Other important innovations contributed to the development of the HR-MS that correspond to the introduction of Fourier transform ion cyclotrone resonance (FT-ICR) and Orbitrap analyzers (Xian, *et al.*, 2012).

All of these remarkable novelties allowed the possibility not only to accurately measure analyte ions, but also improved sensitivity. The acquisition HR-MS data always requires the mass calibration. The best values of MA are reached with the internal calibration, in which the sample and the internal calibrant are introduced into the ion source simultaneously. The introduction of internal calibrant during LC-MS is not always possible, because of interference of calibrant with the chromatographic separation or identical masses of calibrant and analyte. The "lock-mass" calibration is based on well-defined ion with known elemental composition coming from the background (known impurities resulting from previous samples, mobile phase, air components, etc.), introduced by a second inlet system, which permits real-time recalibration by correction of *m/z* shifts arising from instrumental drift (Holcapek, *et al.*, 2012). Otherwise, an external mass calibration procedure can be performed; in this procedure the sample and the calibrant are not present in the ion source at the same time, but it can also provide for accurate measurements, particularly if the time difference between the sample and the calibrant introduction is rather low.

5.3. A mass spectrometer's building block

The basic type of mass spectrometer consists of three major parts: the ion source, the mass analyzer, and the detector.

5.3.1. Ion sources

The kind of information inferable from an MS spectrum depends principally on the ionization process occurring into the ion source, which can be classified in hard and soft. The choice of the ion source heavily depends on the application, and thus on the physico-chemical properties of the analyte that must be investigated. Hard sources impart sufficient energy to the molecules and their relaxation involves break of bonds, producing fragment ions with mass-to-

charge ratios less than the molecular ion, making easy the structural elucidation. On the contrary, soft sources cause little fragmentation, generating the molecular ion peak (in GC-MS) or (de)protonated molecular ion (in LC-MS). In these cases, the resulting mass spectrum provides only the molecular weight information. The first application of MS was carried out on hard ionization process based on electron impact (EI), becoming soon the most used in organic mass spectrometry. However, since its discovery, it has proven useful for gas phase low-mass thermally stable molecules and unsuitable for large molecules (Bleakney, 1929; Nier, 1947). Moreover, because of a low compatibility of the liquid phase with the vacuum region of a MS, the hyphenation with GC was easier compared to the hyphenation with LC, which necessitated the removal of the mobile phase before the analyte entered the MS, thus jeopardizing the analytical performances. The development of more versatile ionization techniques allowed to extend the range of applicability of MS to also large non-volatile molecules. Among these are the plasma desorption ionization method (Macfarlane & Torgerson, 1976) involving the bombardment with ionic or neutral atoms formed as a result of the nuclear fission of a suitable nuclide, typically the californium isotope ^{252}Cf, and the fast atom bombardment (FAB) technique (Barber, *et al.*, 1981) where the bombardment take place by means argon or xenon atoms, all soft techniques operating under vacuum conditions.

Later, the introduction of atmospheric pressure ionization (API) techniques, specifically ESI, APCI and atmospheric pressure photo ionization (APPI), beside MALDI, marked a dramatic breakthrough in the expansion of the range of applications, thanks to the their capability to handle the high amount of liquid phase involved (Horning, *et al.*, 1974; Whitehouse, *et al.*, 1985). Briefly, in ESI the ionization occurs after the analytes passage through a needle held at high voltage (kV) placed at the entrance to the MS; it represents the technique of choice for highly polar compounds ranging in molecular weight from 100 to

150000 Da, but, considering that such technique generates, especially for large molecules, multiply charged ions, a conventional mass range of 3000 Da is sufficient. Instead, APCI is applied to medium polarity compounds ranging in a molecular weight from 100 to 2000 Da. Unlike ESI that is a liquid phase ionization, APCI occurs in gas phase conditions, after the nebulization (favored by N_2) and the vaporization of the LC effluent at a temperature of 350-550° C. The resulting vapor is ionized using a corona discharge (source of electrons) and the mobile phase behaves as a reagent gas to ionize the sample. Finally, the APPI technique is applicable to highly apolar solutes (Robb, *et al.*, 2000). Basically, APPI is like an APCI source where the corona discharge has been replaced with a Kr lamp which produces electromagnetic radiations capable to excite and ionize the mobile phase, an additive or the analytes themselves. There are some differences in the flow rates applicable to each ionization technique. In particular, conventional ESI ion source can tolerate flow rates ranging from 20 μL/min to 1 mL/min (or even smaller, if a high amount of water is used), whereas the ionization in both APCI and APPI sources can be operated at higher flow rates (up to 2 mL/min). However, elevated flow rates can be also used in ESI, but in that case a splitting is required prior to the entrance in the source (Naegele, 2011). Furthermore, it is possible combine ion sources, merging the advantages and application ranges of each; for instance the combinations ESI/APCI (Zhou, *et al.*, 2008) or ESI/APPI ion sources (Short & Syage, 2008) can provide detection of both polar and non-polar analytes in one run, which can increase the number of identified components for highly complex matrices. At present, ESI and MALDI (Tanaka, *et al.*, 1988) are the most widespread methods in the analysis of macromolecules. MALDI approach usually generates only singly charged ions, over an unlimited mass range and it is well suitable for synthetic polymers, as well as for protein, carbohydrate and lipid fingerprinting (Karas, *et al.*, 2000). Concisely, the compounds to be

analyzed are dissolved in a solvent containing small organic molecules, called matrix, capable to absorb a laser pulse that induces the desorption of the matrix-sample cluster and the ionization of the matrix, which, due to its acidity properties, is able to exchange ions with the analyte molecules.

5.3.2. Mass analyzers

The mass analyzer is the device of the mass spectrometer dedicated to ions' separation according to their *m/z* values. It can be considered the key component of any MS, since important characteristics like mass range, resolution, mass accuracy, dynamic range, sensitivity and analysis speed, depend on it. Currently, the analyzers widely used are Q, ion-trap (IT) and ToF, mostly because a low-moderate economic cost: the Q analyzer is the simplest and cheapest, followed by the IT; on the other hand, the ToF analyzer is the cheapest high-resolution mass analyzer, with outstanding features in terms of acquisition speed, *m/z* range and rather good resolution and mass accuracy. The general trend in mass analyzer development is to combine different devices in sequence in order to allow multiple experiments to be performed. Table V-1 shows an overview of mass spectrometers and their technical specifications currently offered by the main manufacturers under LC-MS (and also MALDI-MS) configuration (Di Girolamo, *et al.*, 2013). Among these, the most employed are Q-ToF, IT-ToF and QqQ, alongside a series of other hybrid mass spectrometers of more recent introduction such as Q-IMS-ToF, FT-ICR and Orbitrap analyzers.

These ingenious solutions provide an exceptional improvement in acquisition speed, mass resolution and mass accuracy. In particular, the ICR offers the highest resolution and mass accuracy, compared to all modern analyzers, followed by Orbitrap- and ToF- based analyzers, despite the acquisition times

are longer for the higher number of ion recording. ToF mass analyzers have the highest scanning speed among all mass analyzers (Di Girolamo, *et al.*, 2013).
In the context of the present thesis, two types of mass analyzers have been used, namely Q and Q-(IMS)-ToF, and they will be discussed below.

Table V-1. *Common hybrid mass spectrometers and their technical specifications.*

Combined Mass Analyzers	Commercial Name of the Instrument	Mass Accuracy (ppm)	Resolution (m/z)	Acquisition Speed (Hz)
QqQ	LCMS-8030, Shimadzu	-	0.7	15
	6490, Agilent	-	0.4	10
	Triple Quad 5500, AB SCIEX	-	1	12
	TSQ Vantage, Thermo Scientific	5	0.07	5
	XEVO TQ-S, Waters	-	1	10
Q-Linear Ion Trap	QTRAP 5500, AB SCIEX	-	0.1	20
	QTRAP 6500, AB SCIEX	-	0.05	25
Q-TOF	maXis 4G, Bruker Daltonics	< 0.6	0.02	30 (MS), 10 (MS/MS)
	micrOTOF-Q II, Bruker Daltonics	<2	0.05	20
	XEVO G2 QTof, Waters	<1	0.04	30
	6550 QTOF, Agilent	<1	0.02	50
	TripleTOF 5600, AB SCIEX	0.5	0.03	50 (MS), 100(MS/MS)
Q-IMS-TOF	Synapt G2-S HDMS, Waters	<1	0.02	30
	MALDI Synapt G2-S HDMS, Waters	<1	0.1	-
Q-Orbitrap	Q Exactive, Thermo Scientific	<1	0.001	12

Q-ICR	SolariX 15T, Bruker Daltonics	< 0.25	0.0002	-
LIT-ICR	LTQ FT Ultra 7T, Thermo Scientific	<1	0.0005	2
LIT-Orbitrap	Orbitrap Elite, Thermo Scientific	<1	0.002	8
	MALDI LTQ Orbitrap XL, Thermo Scientific	<2	0.004	-
TOF/TOF	TOF/TOF 5800 System, AB SCIEX	<1	0.07	-
	UltrafleXtreme, Bruker Daltonics	< 1,5	0.08	-
	Axima Performance, Shimadzu	<5	0.2	-
Ion Trap-TOF	LCMS-IT-TOF, Shimadzu	3	0.1	10
	Axima Resonance, Shimadzu	3	0.3	-

The list contain only main manufacturers and may not be comprehensive (Di Girolamo, *et al.*, 2013).

5.3.2.1. Quadrupole (Q) and Q-based mass analyzers

Paul and Steinwegen first described the principle of the quadrupole mass analyzer in 1953 (Paul & Steinwegen, 1953). The quadrupole is the most broadly used analyzer due to its ease of use, mass range covered, good linearity, resolution, ruggedness and quality of mass spectra. It is a filter analyzer where only the ions with a specific *m/z* value reach the detector, depending on the electric fields applied. In detail, Q is made up of two pairs of metallic rods as shown in Figure V-2. One set of rod is at a positive electrical potential, and the other one at a negative potential. A combination of direct current (DC) and radio frequency (RF) voltages is applied on each set. The positive pair of rods is acting as a high mass filter; the other pair is acting as a low mass filter.

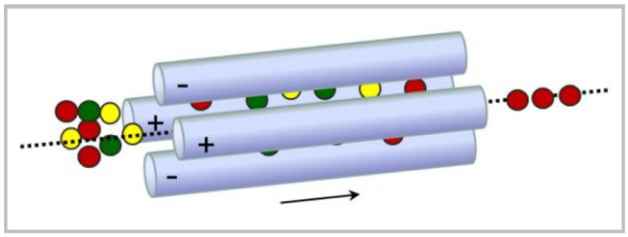

Figure V-2. *Schematic of the quadrupole analyzer*

The resolution depends on the DC value in relationship to the RF value. If the applied voltage is composed of a DC voltage (U) on which an oscillating RF voltage (Vcos(ωt)) is applied between one pair of rods, and the other, the field within the analyzer is created. A direct current voltage is then superimposed on the RF voltage (V) and the ions introduced into the quadrupole field undergo complex trajectories. The quads are operated at constant resolution, which means that the RF/DC ratio is maintained constant. For given amplitude of the DC and RF voltages, only the ions of a given *m/z* will resonate, have a stable path to pass the quadrupole and be detected. Other ions will be de-stabilized and hit the rods (March & Hughes, 1989). The performance (i.e. ability to

separate two adjacent masses across the applicable range) depends on the quad geometry, on the electronics, on the voltage settings and on the quality of the manufacturing. Increasing the resolution means that fewer ions will reach the detector, and consequently impacts the sensitivity. The Q analyzer has a relatively good dynamic range, which means that the quantification capabilities are generally very good. Recent quadrupole instrumentations allow for high-speed scanning (up to 10000 or even 15000 amu/s) and ultrafast polarity switching for ultrafast analyses.

During the years, the quadrupole mass filter has become an integral part of some of the most sophisticated mass spectrometers, such as Q-ToF and QqQ. The general goal in the design of a hybrid instrument is to combine different performance characteristics offered by the different analyzers into one mass spectrometer. In this regard, Q-ToF instrument is suitable for both quantitative and qualitative purposes by taking advantage from respectively the linearity of Q and the mass accuracy of ToF, beside the capability to accomplish tandem mass spectrometry experiments with high selectivity, by implementing a collision cell after the quadrupole.

The QqQ instruments represent the detectors of choice to carry out sensitive, fast and robust quantitative analysis for targeted compounds.

5.3.2.2. Time-of-flight

In the time-of-flight (ToF) analyzer, firstly proposed by Stephens in 1946 (Stephens, 1946), the ions expelled from the source are accelerated by a pulse of an electric field (from 10^3 to 10^4 V) and a frequency (from 10 to 50 kHz) into a field-free region, called flight tube. Ideally, all intact ions with the same charge will acquire the same kinetic energy, thus their velocities (v) vary inversely with their masses (m):

$$v = \sqrt{\frac{2eV}{m}} \qquad \textbf{(Eq. V-1)}$$

Provided that all the ions start their trip at the same time, or at least within a suitable short time interval, the lighter ones will arrive earlier at the detector than the heavier ones. The physical property that is measured during an analysis is the flight time of the ion *viz.* the time (*t*) that ions take to move through the flight tube (1-2 meters) between the source and the detector:

$$t = k\sqrt{\frac{m}{e}} \qquad \textbf{(Eq. V-2)}$$

where *k* is a constant of the instrument. Typically, the time of flight is ranging between 1 and 100 μs. Finally, this time is then converted into a mass value. The ToF is characterized by high transmission efficiency which leads to very high sensitivity compared to quadrupole, high scan speed (useful in fast chromatography application) and theoretically unlimited mass range (actually ca. 20000 *m/z*). The mass accuracy of ToF analyzers depends on the mode in which the instrument works. Specifically, in the reflectron mode, ToF instruments are able of attaining 5 ppm by means internal calibration. In many cases it is not possible to add internal calibrants, therefore the error in mass accuracy is frequently increased to 50-100 ppm. Operation of an instrument in a linear mode will typically decrease the mass accuracy. On the other hand, ToF analyzers suffer from poor mass resolution, which is mass dependent, and is also affected by the length of the flight path of the instrument. Clearly, the first effort was to extend the path of the flight tube. However, this ploy decreases the performance of the ToF analyzers because of the loss of ions by scattering after

collisions with gas molecules or by angular dispersion of the ion beam. Furthermore, the difference in the initial kinetic energy (kinetic energy distribution), due to the rate of proton transfer and time lag of reaction, and the length of the ion formation pulse (time distribution), are other critical factors that influence the mass resolution on ToF analyzers. The effects of such factors can be significantly decreased through the adoption of the reflectron or the delayed pulsed extraction (e.g. in MALDI sources).

- *Reflectron*

A reflectron consists of a series of electrode rings at increasing potential, which focus ions having the same *m/z* value but different kinetic energies in time. Ions having a higher kinetic energy (faster ions) will penetrate the reflectron to a greater depth and so spend slightly longer in the device than ions with lower kinetic energy (Gross, 2004; Hoffmann & Stroobant, 2007). In this way isobaric ions will reach the detector at the same time that provides the reduction of the distribution of flight times and the increase of the resolving power of the instrument. In Figure V-3 is illustrated the working principle of a single-stage reflectron. Although the reflectron increases the flight path, though without increasing the dimensions of the mass spectrometer, the beneficial increase in mass resolution comes at the expense of sensitivity and mass range limitation (especially for high mass ions). Consequently, the choice of operating ToF instruments in “linear” or “reflectron” mode is mainly dictated by the ions to be investigated. For instance, when carrying out analysis of high mass ions at very low concentrations, detection being performed in the linear mode.

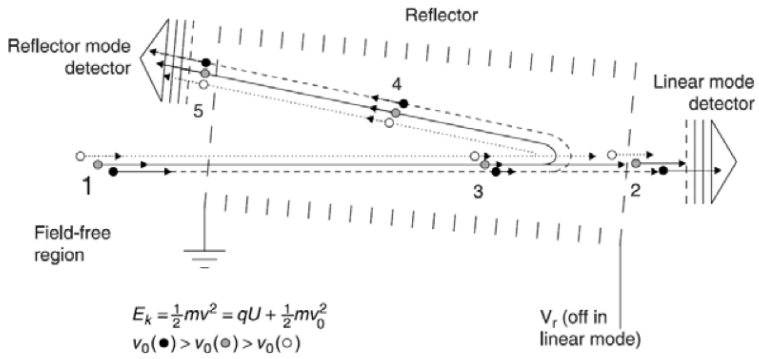

Figure V-3. *The working principle of a single-stage reflectron*

- Orthogonal acceleration

The design of the orthogonal acceleration ToF analyzer, (oa)ToF, has enormously contributed to the growth of applications involving time-of-flight mass spectrometry. Ideally, a ToF-MS experiment should begin with all ions with the same initial position and velocity. Orthogonal ion introduction, in which ions are accelerated in a direction perpendicular to the continuous ion beam axis of the ion source, well reached that condition, thus improving mass resolving power. At first, the ions fill the orthogonal acceleration region, then, to initiate a "push" an electric field is created at a frequency of several kilohertz, which forces ions to assume a direction orthogonal to their original trajectory, and thus they begin to fly towards the analyzer. The (oa)TOF analyzers provide high mass resolving power, as stated, and mass accuracy even up to or below 1 ppm.

5.3.3. Detectors

The ions, which have been separated according to their *m/z* in the mass analyzer, arrive at the detector where they are converted into an electrical signal, proportional to their abundance. There are various types of detectors that are employed in mass spectrometry; among these the simplest Faraday cup and

the most common electron multiplier (EM). The former is a metal conductive cup designed to catch charged particles in vacuum with suppressor electrode and then producing current, which can be measured and used to determine the number of ions striking the cup.

The latter operates according to the principle called secondary electron emission. Specifically, when a charged ion strikes on detector surface it provokes secondary electrons that are released from atoms in the surface layer. The number of secondary electrons produced depends on the type of incident primary particle, its energy and characteristic of the incident surface. The electron multipliers may be of either the discrete dynode or the continuous dynode type (channeltron, microchannel plate or microsphere plate).

5.4. Tandem mass spectrometry

The goals of any mass spectrometry analysis are to obtain more structural information on the analyte of interest, sometimes unattainable either (*i*) because the ionization technique used produces relatively few structurally diagnostic fragments (as for soft ionization), or (*ii*) because its fragmentation is suppressed by the presence of other compounds in the mixture introduced in the ion source, or (*iii*) because it is obscured by other ions generated from the matrix in the course of ionization.

For such a reason, the strong need for techniques able to bypass these problems and provide much valuable information about the molecular structure led to the introduction and instrumental development of tandem mass spectrometry. The term tandem mass spectrometry, or simply tandem MS, refers to any general methods where a given ion is subjected to a second mass spectrometric analysis, either in conjunction with a dissociation process or in a chemical reaction (Busch, *et al.*, 1988). Tandem MS is also defined as mass spectrometry/mass spectrometry (MS/MS). Several modern mass spectrometers

consist of two or more mass analyzers to perform the so-called *tandem-in-space* MS/MS, where different mass analyzers are involved "in different spaces". This MS/MS technology is based on the isolation of a specific precursor ion (*m/z*), and then undergone to dissociation and production of fragment or product ions. However, due to rapidly decreasing transmission and increased instrumental complexity and size, only MS/MS experiments are allowed, while MS^3 experiments and beyond are rarely performed in tandem-in-space instruments. Systems such as QqQ, Q-ToF, ToF/ToF belong to such a tandem MS technique. In all these combinations, the first and the final analyzers operate the ion isolation and scan, whereas the second analyzer is a collision cell that allows ion fragmentation.

There are four main MS/MS scan modes usually used: product ion scan, precursor ion scan, neutral loss scan, and selected reaction monitoring. In the product ion mode, the first analyzer selects a precursor ion of interest, which is fragmented into the collision cell, thus generating the product ions analyzed by the second analyzer. In the precursor ion scanning, the second analyzer is held static at the *m/z* of a specific product ion only after collision, whereas the first mass analyzer is scanned across the desired *m/z* range. This experiment results in a spectrum of precursor ions that produce that particular product ion during collision induced dissociation (CID) fragmentation. During the neutral loss scanning process, both the first and the second analyzer work in concert with a costant mass offset of "x". When a precursor ion is transmitted through the first mass analyzer, this ion is recorded if it produces a product ion corresponding to the loss of a neutral fragment of ''x'' from the precursor ion after collision cell. In the selected reaction monitoring scan mode, the first analyzer is set on the specific precursor mass, the collision energy is optimized to produce a diagnostic fragment of that precursor ion, and the second analyzer focuses on the specific mass of that fragment. Only ions with this exact transition will be

detected. This process is also known as multiple reaction monitoring (MRM) in the case of first or second or both mass analyzers are set to monitor for multiple reactions. This technique is broadly used for quantitative analysis of individual molecular species.

Along the tandem-in-space, the *tandem-in-time* is the other possible MS/MS method processing, which employs a single mass analyzer where ions are trapped, isolated, and subsequently fragmented "in the same space". This is only possible in trapping devices, such FT-ICR and IT-ToF. The time spent by the ions in the trap defines the number of MS^n measurements which can be performed. In fact, such a trapping device-based mass analyzers are well suited for multiple stage MS experiments.

5.5. Ion mobility spectrometry

Ion mobility spectrometry (IMS) arose in the 1970s as a modern analytical technique for the separation and subsequent detection of volatile and semi-volatile organic compounds based on the separation of their gaseous ions in a low or high electric field at ambient pressure. IMS techniques have received an increased interest as new instrumentation has become available to be equipped to mass spectrometry. The first coupling of ion mobility to MS is attributed to McDaniel who, between the 1950s and 1960s, developed drift cells coupled to a magnetic sector mass analyzer, with the objective of studying ion mobilities and ion-molecule reactions (McDaniel, *et al.*, 1962). Since then, a number of IMS-MS instruments have been used in different fields including environmental, explosive and chemical warfare, food, clinical and biological, forensic, and pharmaceutical applications. IMS enables the discrimination of ions by size, shape, charge as well as mass, thus providing additional information to the chromatographic separation of molecules and mass spectrometric separation of ions. Four methods of ion mobility separation can be combined with MS,

namely drift-time ion mobility spectrometry (DTIMS), aspiration ion mobility spectrometry (AIMS), differential-mobility spectrometry (DMS) also called field-asymmetric waveform ion mobility spectrometry (FAIMS) and traveling-wave ion mobility spectrometry (TWIMS). Only TWIMS and DMS/FAIMS are commercially available in the LC-MS coupling so far (Kanu, *et al.,* 2008). However, none employs the original drift tube (DT) IMS approach where axial field of constant intensity *E* pushes an ion through a gas-filled tube (drift tube) with velocity of:

$$v = KE \qquad \textbf{(Eq. V-3)}$$

where coefficient *K* is mobility (Shvartsburg & Smith, 2008). Hence, different species cross the tube in different times (Eiceman & Karpas, 2004; Hill, *et al.*, 1990; Hoaglund-Hyzer, *et al.*, 1999; Shvartsburg, *et al.*, 2001; Taraszka, *et al.*, 2005; Valentine, *et al.*, 2006). FAIMS/DMS uses periodic asymmetric electric field, orthogonal to the direction of travel. This device exploits the difference between mobilities at high and low fields with the opposite polarity. The different mobility of ions during the application of high and low voltages causes ions to drift towards one or the other electrode (Borsdorf, *et al.*, 2011; Kolakowski & Mester, 2007; O'Donnell, *et al.*, 2008), therefore, only those with a certain differential mobility will pass through the system. By applying an additional DC compensation field, the trajectory of particular ions along the radial axis can be corrected, avoiding ion discharge. DMS and FAIMS instruments work on the same ion separation principle, but they differ in the instrumental design. Electrodes are not segmented and the alternating electric field is placed between two electrodes (planar electrodes for DMS and cylindrical electrodes for FAIMS).

The design of the most recent TWIMS mobility cell is similar to that of the traditional segmented IMS. Unlike this one, in which a low electrical field is applied continuously to the cell, a high field is applied to one segment of the cell and swept sequentially through the series of segmented electrodes of the cell in the direction of ion migration, separating ions based on their mobility. Thus ions are moved through the mobility cell in pulses as waves of the electrical field pass through them (Kanu, *et al.*, 2008). In general, all types of mass analyzers can be employed after the ion mobility separation. The TWIMS is usually combined with ToF-MS, whereas FAIMS/DMS as integral to the source can be coupled to any mass analyzer.

The following sections provide a deep description of the TWIMS-MS employed in this thesis.

5.5.1. Separating ions according to differences in gas-phase structure

Ion mobility separations are based on differences in ion structures (or cross sections) and charge states (Mason & McDaniel, 1988). The latter is established by the excess charge on each species. Ion cross sections represents the effective area for the interaction between an individual ion and the neutral gas through which it is travelling (Mason & McDaniel, 1988). Two ions of equal mass and charge, but different three-dimensional conformation, will travel through an IMS device at velocity dependent on their mobilities, providing different drift times. Specifically, the ion with a more compact conformation will undergo fewer collisions with the neutral gas than do more open. Therefore, compact species with small collision cross sections (CCS, Ω) will have higher mobilities than do more open forms of the ion. The mobility can be used to derive a CCS for an ion according to the Mason-Schamp equation (Mason & Schamp, 1958):

$$\Omega = \frac{3ze}{16N} \cdot \left(\frac{2\pi}{\mu k_B T} \right)^{1/2} \cdot \frac{1}{K_0} \qquad \textbf{(Eq. V-4)}$$

where K_0 is the reduced mobility (measured mobility at standard temperature and pressure), z is the charge state of the ion, e is the elementary charge, N is the number density of the drift gas, μ is the reduced mass of the ion-neutral drift gas pair, k_B is the Boltzmann constant and T is the gas temperature. The proportional relationship between Ω and K_0 is only true at or below the "low-field limit", where the ratio between electric field strength and buffer gas density is small, ≤2 townsend (2×10^{-17} V cm^2) (Creaser, *et al.*, 2004). Despite the IMS devices previous discussed will all separate ions according to differences in their mobility through a buffer gas, only the time-based mobility devices (DTIMS, TWIMS) can be used to determine information about cross-sectional area. In contrast, FAIMS (and DMA) devices work as a scan filter, like quadrupoles in MS analysis. To deduce a structure from a mobility, molecular modeling is typically combined with a CCS estimating algorithm such as the trajectory method (Mesleh, *et al.*, 1996; Mesleh, *et al.*, 1997), projection superposition approximation (Bleiholder, *et al.*, 2011; Bleiholder, *et al.*, 2013a; Bleiholder, *et al.*, 2013b; Anderson, *et al.*, 2012), projection approximation (von Helden, *et al.*, 1993; Mack, 1925; Jarrold & Constant, 1991), exact hard-sphere scattering (Shvartsburg & Jarrold, 1996), or scattering on electron density isosurfaces (Shvartsburg , *et al.*, 2000a; Shvartsburg, *et al.*, 2000b; Alexeev, *et al.*, 2014). Taking into account that CCS values will change in different gases, it is important to measure ions in different buffer gases for the most accurate CCS values (Asbury & Hill, 2000; Beegle, *et al.*, 2002; Matz, *et al.*, 2002; Ruotolo, *et al.*, 2005; Bush, *et al.*, 2010; Bush, *et al.*, 2012; Larriba-Andaluz, *et al.*, 2015).

5.5.2. Traveling wave ion mobility spectrometry-mass spectrometry: introduction to Synapt G2-Si HDMS instrument

Many different instrument designs have been described that combine IMS with different types of MS analyzers. The TWIMS device was commercially introduced by Waters in 2006, in the Synapt line of instruments (Giles, *et al.*, 2004; Thalassinos, *et al.*, 2004; Giles, *et al.*, 2011). The traveling-wave IMS device comprises a series of ring electrodes called stacked ring ion guide (SRIG), to which a traveling voltage wave is applied. Radio frequency voltages of opposite phases are applied to adjacent electrodes; these voltages confine the ions radially. By applying a continuous train of DC pulses traveling along the stacked ring electrodes, ions are moved through the gas-filled guide. The ability of an ion to travel along with the DC pulse through the gas-filled T-wave ion guide is governed by the ion's size, charge, shape, and the interaction cross section between the ion and the neutral gas (N_2). Different parameters significantly influence the capability of an ion to move with the traveling wave, such as the height and velocity of the wave, and the type and pressure of the background gas. By optimizing these parameters, high mobility ions will travel with the wave and cross the ion guide faster than ions with low mobility, which roll over the top of the wave and as a result elapse more time in the device (Pringle, *et al.*, 2007).

In details, the TriWave region, implemented in the Synapt G2-Si HDMS (the hybrid Q-IMS-(oa)ToF MS), consists of three traveling-wave-enabled stacked ring ion guides, as shown in Figure V-4.

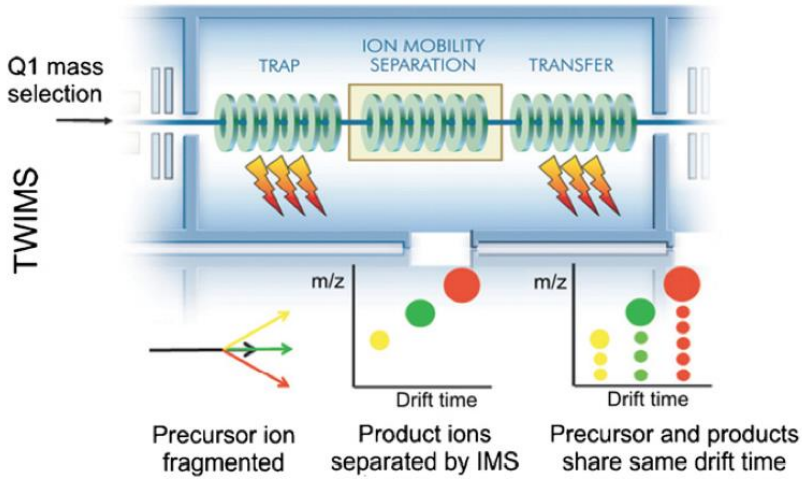

Figure V-4. *Schematic of traveling wave ion mobility.*

The trap ion guide (the first T-Wave) accumulates and releases the ions as packets into the ion mobility separation device (the second T-Wave), where it takes place the separation of the ions. The transfer ion guide (the third T-Wave) transfers the mobility-separated ions to the (oa)ToF analyzer. The trap and transfer assemblies allow for fragmentation to occur before and/or after mobility separation. In addition to the many advantages deriving by the use of IMS device, this TWIMS has a number of benefits due to the particular instrument arrangement. In this regard, the Synapt G2-Si HDMS combines exact mass and high resolution mass spectrometry with high efficiency ion mobility-based measurements and separation.

As shown in Figure V-5, the ions follow a specific path from ion generation (generally API source) to a stepwave ion guide, a selecting quadrupole, a triwave region, and finally a reflectron ToF mass analyzer.

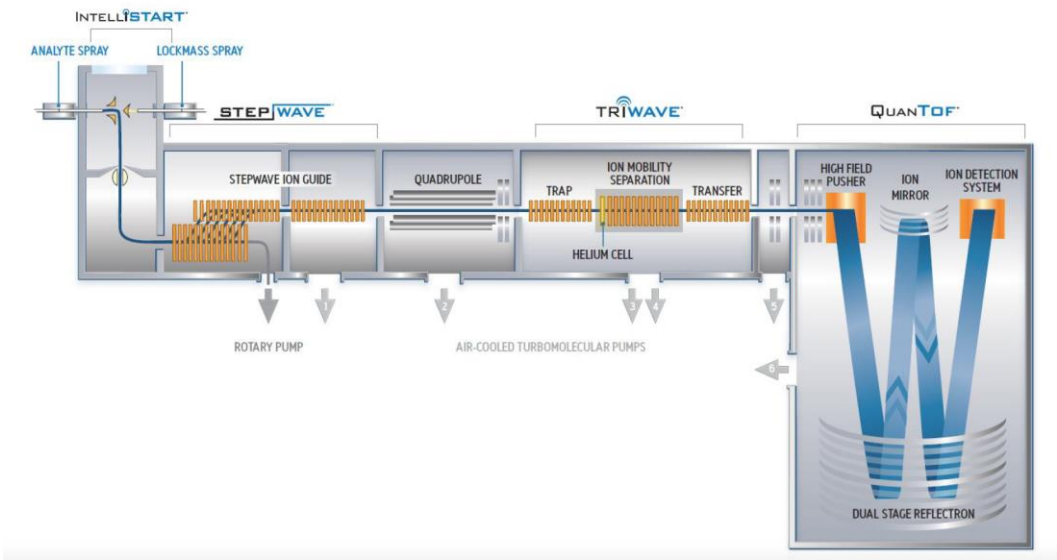

Figure V-5. *Schematic of a Synapt G2-Si HDMS instrument.*

The stepwave ion guide represents an innovative method of removing neutral contaminants from the ions beam by driving primary gas flow along a linear path and employing an effective electric field to lead ions into a parallel linear path and from there into the rest of the instrument. The selecting quadrupole can then be used as selector of specific masses prior to ion mobility separation, or directed to pass all ions through. As mentioned before, the trap assembly is primarily to accumulate ions before injection into the ion mobility cell, but can also be used to hold ions for CID prior to mobility separation. The chamber on the front of the IMS cell filled with helium reduces the fragmentation (lower centre of mass) and maintains transmission at higher pressures (where high pressure is desired for higher resolving power of ion mobility separation) (Giles, *et al.*, 2011; Pringle, *et al.*, 2007). After ion mobility separation, fragmentation can be also performed in the transfer cell. Finally the dual-stage reflectron ToF mass analyzer can be operated in "sensitivity", "resolution", "high resolution" and "enhanced resolution" modes where ions pass through a

reflectron either once for lower mass resolution but higher sensitivity or twice for higher mass resolution but lower sensitivity.

The Synapt has two main modes of operation consisting of: Q-ToF MS with IMS cell evacuated of background gas, and Q-IMS-ToF MS. The combination of IMS and MS with high-RP and MS/MS experiments represents a mighty tool for the structural determination. In addition to CID, new fragmentation approaches are possible with this instrument, namely energy dependent fragmentation (MS^E) and time-aligned parallel (TAP) fragmentation. The former provides parallel alternating scans, which are acquired at either low collision energy (CE) in the collision cell to obtain precursor ion information, and high CE to have full-scan accurate mass fragment, precursor ion and neutral loss information. All of these data are attained within a single analytical run. TAP methodology enables first and second generation product ions to be acquired. Specifically, the precursor ion is fragmented in the trap cell with subsequent separation of the first generation of product ions by IMS. The second generation of fragment ions is formed in the transfer, and they are associated to the first generation parent based on individual drift-times (Figure V-4) (Borsdorf, *et al.*, 2011; Sun, *et al.*, 2011).

A wide range of applications for LC-IMS-MS can be found in the literature, e.g. profiling of plasma proteome (Liu, *et al.*, 2007), study of isomeric transformation of phenolic compounds present in foodstuff (Xie, *et al.*, 2011), improvement of separation of drug-related materials (Eckers, *et al.*, 2007), drug metabolism study (Dear, *et al.*, 2010), etc.

REFERENCES

- Alexeev Y., Fedorov D.G., Shvartsburg A.A., J. Phys. Chem. A 2014, 118, 6763-6772.
- Anderson S.E., Bleiholder C., Brocker E.R., Stang P.J., Bowers M.T., Int. J.

Mass Spectrom. 2012, 330, 78-84.
- Asbury G.R., Hill H.H., Anal. Chem. 2000, 72, 580-584.
- Barber M., Bordoli R.S., Sedgwick R.D., Tyler A.N., Nature 1981, 293, 270-275.
- Beegle L.W., Kanik I., Matz L., Hill H.H., Int. J. Mass Spectrom. 2002, 216, 257-268.
- Bleakney W., Phys. Rev. 1929, 34, 157-160.
- Bleiholder C., Contreras S., Bowers M.T., Int. J. Mass Spectrom. 2013, 354, 275-280.
- Bleiholder C., Contreras S., Do T.D., Bowers M.T., Int. J. Mass Spectrom. 2013, 345, 89-96.
- Bleiholder C., Wyttenbach T., Bowers M.T., Int. J. Mass Spectrom. 2011, 308, 1-10.
- Borsdorf H., Mayer T., Zarejousheghani M., Eiceman G.A., Appl. Spectrosc. Rev. 2011, 46, 472-521.
- Busch K.L., Glish G.L., McLuckey S.A., Wiley VCH 1988.
- Bush M.F., Campuzano I.D.G., Robinson C.V., Anal. Chem. 2012, 84, 7124-7130.
- Bush M.F., Hall Z., Giles K., Hoyes J., Robinson C.V., Ruotolo B.T., Anal. Chem. 2010, 82, 9557-9565.
- Cooper H.J., Marshall A.G., J. Agric. Food Chem. 2001, 49, 5710-5718.
- Creaser C.S., Griffiths J.R., Bramwell C.J., Noreen S., Hill C.A, Thomas C.L. P., Analyst 2004, 129, 984-994.
- Dear G.J., Munoz-Muriedas J., Beaumont C., Roberts A., Kirk J., Williams J.P., Campuzano I., Rapid Commun. Mass Spectrom. 2010, 24, 3157-3162.
- Di Girolamo F., Lante I., Muraca M., Putignani L., Curr. Org. Chem. 2013, 17, 2891-2905.
- Eckers C., Laures A.M.F., Giles K., Major H., Pringle S., Rapid Commun. Mass Spectrom. 2007, 21, 1255-1263.
- Eiceman G.A., Karpas Z., CRC Press: Boca Raton, FL, 2004.
- Giles K., Pringle S.D., Worthington K.R., Little D., Wildgoose J.L., Bateman

R.H., Rapid Commun. Mass Spectrom. 2004, 18, 2401-2414.
- Giles K., Williams J. P., Campuzano I., Rapid Commun. Mass Spectrom. 2011, 25, 1559-1566.
- Gross J.H., Springer: Berlin Heidelberg New York 2004.
- Harris W.A., Reilly P.T.A., Whitten W.B., Anal. Chem. 2007, 79, 2354-2358.
- Hill H.H., Siems W.F., St. Louis R.H., McMinn D.G., Anal. Chem. 1990, 62, A1201-A1209.
- Hoaglund-Hyzer C.S., Counterman A.E., Clemmer D.E., Chem. Rev. 1999, 99, 3037-3079.
- Hoffmann E., Stroobant V., 3rd ed. John Wiley and Son: Chichester 2007.
- Holcapek M., Jirásko R., Lísa M., J. Chromatogr. A 2012,1259, 3-15.
- Horning E.C., Carroll I., Haegele K.D., Horning M.G., Stillwell R.N., J. Chromatogr. Sci. 1974, 12, 725-729.
- Hughey C.A., Rodgers R.P., Marshall A.G., Anal. Chem. 2002, 74, 4145-4149.
- Jarrold M.F., Constant V.A., Phys. Rev. Lett. 1991, 67, 2994-2997.
- Kanu A.B., Dwivedi P., Tam M., Matz L., Hill Jr. H.H., J. Mass Spectrom. 2008, 43, 1-22.
- Karas M., Glückmann M., Schäfer J.J., Mass Spectrom. 2000, 35, 1-12.
- Kolakowski B. M., Mester Z., Analyst 2007, 132, 842-864.
- Larriba-Andaluz C., Fernández-García J., Ewing M.A., Hogan C.J., Clemmer D.E., Phys. Chem. Chem. Phys. 2015, 17, 15019-15029.
- Liu X.Y., Valentine S.J., Plasencia M.D., Trimpin S., Naylor S.,. Clemmer D.E, J. Am. Soc. Mass Spectrom. 2007, 18, 1249-1264.
- Macfarlane R.D., Torgerson D. F., Science 1976, 191, 920-925.
- Mack E., J. Am. Chem. Soc. 1925, 47, 2468-2482.
- Mamyrin B.A., Int. J. Mass Spectrom. Ion Proc. 1994, 131, 1-19.
- March R.E., Hughes R.J., John Wiley and Son: New York 1989.
- Mason E.A., Schamp H.W. Jr., Ann. Phys. 1958, 4, 233-270.
- Mason E.A., McDaniel E.W., WILEY VCH Verlag GmbH& Co. KGaA, Weinheim, Federal Republic of Germany 1988.

- Matz L.M., Hill H.H., Beegle L.W., Kanik I., J. Am. Soc. Mass Spectrom. 2002, 13, 300-307.
- McDaniel E.W., Martin D.W., Barnes W.S., Rev. Sci. Instrum. 1962, 33, 2-7.
- Mesleh M.F., Hunter J.M., Shvartsburg A.A., Schatz G.C., Jarrold M.F., J. Phys. Chem. A 1997, 101, 968.
- Mesleh M.F., Hunter J.M., Shvartsburg A.A., Schatz G.C., Jarrold M.F., J. Phys. Chem. 1996, 100, 16082-16086.
- Morgan R.P., Benyon J.H., Bateman R.H., Green B.N., Int J. Mass Spectrom. Ion Phys. 1978, 28, 171-191.
- Naegele E., Agilent Technologies, Inc. 2011
- Nier A. O., Rev. Sci. Instrum. 1947, 18, 415-422.
- O'Donnell R.M., Sun X.B., Harrington P.D., Trends Anal. Chem. 2008, 27, 44-53.
- Paul W., Steinwedel H., Z. Naturforsch. A 1953,8, 448-450.
- Pringle S.D., Giles K., Wildgoose J.L., Williams J.P., Slade S.E., Thalassinos K., Bateman R.H., Bowers M.T., Scrivens J.H., Int. J. Mass Spectrom. 2007, 261, 1-12.
- Robb D.B., Covey T.R., Bruins A.P., Anal. Chem. 2000, 72, 3653-3659.
- Ruotolo B.T., McLean J.A., Gillig K.J., Russell D.H., J. Am. Soc. Mass Spectrom. 2005, 16, 158-165.
- Short L.C., Syage J.A., Rapid Commun. Mass Spectrom. 2008, 22, 541-548.
- Shvartsburg A.A., Hudgins R.R., Dugourd P., Jarrold M. F., Chem. Soc. Rev. 2001, 30, 26-35.
- Shvartsburg A.A., Jarrold M.F., Chem. Phys. Lett. 1996, 261, 86-91.
- Shvartsburg A.A., Liu B., Jarrold M.F., Ho K.M., J. Chem. Phys. 2000, 112, 4517-4526.
- Shvartsburg A.A., Smith R.D., Anal. Chem. 2008, 80, 9689-9699.
- Shvartsburgc A.A., Liu B., Siu K.W.M., Ho K.M., J. Phys. Chem. A 2000, 104, 6152-6157.
- Stephens W.E., Phys. Rev. 1946,69, 674-792.
- Sun J.H., Baker A., Chen P., Rapid Commun. Mass Spectrom. 2011, 25,

2591-2602.
- Tanaka K., Waki H., Ido Y., Akita S., Yoshida Y., Yoshida T., Rapid Commun. Mass Spectrom. 1988, 2, 151-153.
- Taraszka J.A., Gao X., Valentine S.J., Sowell R.A., Koeniger S.L., Miller D.F., Kaufman T.C., Clemmer D.E., J. Proteome Res. 2005, 4, 1238-1247.
- Thalassinos K., Slade S.E., Jennings K.R., Scrivens J.H., Giles K., Wildgoose J., Hoyes J., Bateman R.H., Bowers M.T., Int. J. Mass Spectrom. 2004, 236, 55-63.
- Valentine S.J., Plasencia M.D., Liu X., Krishnan M., Naylor S., Udseth H.R., Smith R.D., Clemmer D.E., J. Proteome Res. 2006, 5, 2977-2984.
- von Helden G., Hsu M.T., Gotts N., Bowers M.T., J. Phys. Chem. 1993, 97, 8182-8192.
- Whitehouse C.M., Dreyer R.N., Yamashita M., Fenn J. B., Anal. Chem. 1985, 57, 675-679.
- Wiley W.C., McLaren I.H., Rev. Sci. Instrum. 1955, 26, 1150-1157.
- Wollnik H., Academic Press, San Diego 1987.
- Xian F., Hendrickson C.L., Marshall A.G., Anal. Chem. 2012, 84, 708-719.
- Xie C., Yu K., Zhong D.F., Yuan T., Ye F., Jarrell J.A., Millar A., Chen X.Y., J. Agric. Food Chem. 2011, 59, 11078-11087.
- Zhou Y., Wang Y., Wang R.F., Guo F., Yan C., J. Sep. Sci. 2008, 31, 2388-2394.
- Zuccato E., Chiabrando C., Castiglioni S., Calamari D., Bagnati R., Schiarea S., Fanelli R., Environ. Health 2005, 4:14, 1-7.

CHAPTER VI
Lipidomics-type analysis by ultra-high pressure liquid chromatogragraphy – quadrupole mass spectrometry by using ESI and APCI interfaces

6.1. Introduction

Lipidomics is a branch of metabolomics, which investigates in detail the structures, functions and dynamic changes of lipids in cells, tissues or body fluids to correlate them to the health status of the human organism. In fact, some lipids can be involved in many diseases, such as cancer, diabetes, and cardiovascular disorders (Hannun, 2015). Cellular lipids are a complex of biological metabolites and can be divided into eight main categories: fatty acyls, glycerolipids, glycerophospholipids, sphingolipids, sterols, prenols, saccharolipids, and polyketides (Fahy, *et al.*, 2005). They play multiple and critical roles, for instance, non-polar lipids such as triacylglycerols (TAGs) are important storage components, amphiphilic glycerophospholipids (GPs) are the main building blocks of biological membranes, and some polar lipids act as signalling molecules between organelles or cells (Anjani, *et al.*, 2015).

The high structural diversity in lipid classes present in biological samples makes their characterization a very challenging task. Chromatographic techniques, and in particular LC-MS provides several advantages over direct infusion techniques (e.g. shotgun MS). The main advantages are: I) more reliable identification of individual lipid species, even at trace levels; II) separation of isomers and isobars; and III) reduced ion-suppression effects (Astarita, 2012; Cacciola, *et al.*, 2012; Aguennouz, *et al.*, 2016). The primary separation mechanism employed within lipidomics applications exploits hydrophobic interactions, which depends generally on the equivalent carbon number (ECN) related to the carbon-chain length (CN) and the number of

double bonds (DB) (ECN=CN-2DB). Thus, lipid species containing longer acyl chains are eluted from the LC column later than shorter chain lipids, and saturated acyl structures are eluted later than polyunsaturated analogs. LC-MS investigations can be carried out in untargeted or targeted mode. The former is usually performed using an MS capable of full mass spectra acquisition, usually in high-resolution mode to benefit from the capability to resolve partially or completely between ions having the same nominal mass (Chernushevich, *et al.*, 2001). Instead, targeted mode is devoted to monitor a specific compound (e.g. a biomarker) or a class of compounds with high sensitivity and selectivity, possibly for quantitative purposes. In this case, the MS system of choice is usually tandem MS or HR-MS, acquiring in MRM or SIM modes, respectively (Holčapek, *et al.*, 2012). The main limitation of MRM and SIM approaches is that monitoring only specific transitions or specific ions, respectively, excludes post-acquisition re-processing. According to a recent review on LC-MS in lipidomics, 80% of the applications relied on a MS capable of full mass spectra acquisition (Cajka & Fiehn, 2014). ToF based techniques dominate the scene with about 40 % of the total applications, followed by QLIT, QqQ, and ion trap; while the single Q MS is employed only in the 2% of the applications (Cajka & Fiehn, 2014). Regarding the MS ionization mode used in lipidomics, the most popular is ESI, which is mainly employed for the identification of polar lipids (e.g. phospholipids), while APCI, used in a much smaller number of applications, is preferred for non-polar lipids (e.g. TAGs and cholesterol esters, CEs), but it has been occasionally used also for polar lipids with success (Byrdwell & Borchman, 1997; Byrdwell, 1998; Imbert, *et al.*, 2012; Cai & Sayge, 2006). APCI, differently from ESI, produces some degree of fragmentation useful for structural characterization (Byrdwell, 2001). In 1997, Byrdwell and Borchman (Byrdwell & Borchman, 1997) reported LC-APCI-MS characterization of sphingolipids (SLs) and other phospholipids (PLs) of human

eye lens membrane extract. A year later, Byrdwell (Byrdwell, 1998) extended the previous LC-MS system by employing two MS detectors, namely a Q MS and a QqQ MS, equipped with APCI and ESI interfaces, respectively. Several classes of compounds, such as sphingomyelin (SM), glycerophospholipid, and plasmalogen molecular species in different biological samples were analyzed, pinpointing the complementarity of the two interfaces. In 2006, Cai & Sayge (Cai & Sayge, 2006) and successively, in 2012, Imbert and co-wokers (Imbert, *et al.*, 2012) compared API interfaces in lipids and lipidomics analysis, in term of sensitivity. Up-to-now, very few research groups have used the APCI interface to investigate a complete lipid profile in biological samples.

The aim of this work was to develop a simple, fast, and versatile UHPLC method suitable for both ESI and APCI interface coupled to MS, without any modification of the chromatographic conditions (mobile phase, flow, injection volume, gradient, etc.). The proposed method was tested for untargeted lipid profile characterization of human plasma. Furthermore, the capability of Q MS to work in positive- and negative-ion mode simultaneously was exploited to increase the information acquired in a single run. An extensive explanation of the mass patterns obtained under each different ionization condition was provided, highlighting the complementary information obtained and the presence of important diagnostic fragments.

6.2. Experimental section

6.2.1. Sample and chemicals

A plasma sample was supplied by a clinic laboratory located in Messina (Italy). The free fatty acid (FFA) standard compounds used were lauric acid (La: C12:0), myristic acid (M: C14:0), pentadecanoic acid (Pd: C15:0), palmitic acid (P: C16:0), palmitoleic acid (Po: C16:1), stearic acid (S: C18:0), oleic acid (O: C18:1n9), linoleic acid (L: C18:2n6), linolenic acid (Ln: C18:3n3), and

arachidonic acid (Ar: C20:4n6). TAG standards used were tripentadecanoin (C15:0C15:0C15:0), tripalmitolein (C16:1C16:1C16:1), triolein (C18:1C18:1C18:1), trilinolein (C18:2C18:2C18:2), trilinolenin (C18:3C18:3C18:3), triarachidonin (C20:4C20:4C20:4), trieicosapentaenoin (C20:5C20:5C20:5), and tridocosahexaenoin (C22:6C22:6C22:6). Sterol standards used were cholesterol (Chol), cholesteryl palmitate (Chol-C16:0), cholesteryl stearate (Chol-C18:0), cholesteryl oleate (Chol-C18:1) and cholesteryl linoleate (Chol-C18:2). All standards were obtained from Larodan (Solna, Sweden). L-α-phospatidyl-L-serine (PS) from Glycine max (soybean), L-α-phosphatidylethanolamine (PE) from Glycine max (soybean), L-α-phosphatidylcholine (PC) from egg yolk and sphyngomyelin (SM) from chicken egg yolk, L-α-phosphatidylinositol from Glycine max (soybean) and L-α-lysophosphatidylcholine (LPC) from Glycine max (soybean) were purchased from Sigma-Aldrich (Milan, Italy). MeOH, chloroform ($CHCl_3$) and water employed for the extraction procedure were obtained from Sigma-Aldrich (Milan, Italy). For LC-MS analyses, the solvents (all LC-MS grade) IPA and MeOH were supplied by Sigma-Aldrich (Milan, Italy), ACN and H_2O by Panreac Quimica S.L.U. (Barcelona, Spain). Powdered anhydrous sodium sulphate (Na_2SO_4) and formic acid (HCOOH) were purchased from Sigma-Aldrich (Milan, Italy); ammonium formate (NH_4COOH) was obtained from Alfa Aesar GmbH & Co KG (Karlsruhe, Germany).

Stock solutions of individual FFAs, PCs, LPCs, SMs, PSs, PEs, Chol, CEs, and TAGs in a mixture of MeOH/IPA (1:1, *v/v*), at concentrations in the 5 g/L - 25 g/L range, were prepared. Prior LC injection (1 μL) each stock solution was diluted at 50 mg/L.

6.2.2. Sample preparation

The lipid fraction was extracted according to a modified Folch method (Folch, *et al.*, 1957). Briefly, 1 mL of plasma was placed in a centrifuge Pyrex tube with 9 mL of a $CHCl_3$/MeOH (2:1, *v/v*) mixture, extracted for three times and centrifuged for ca. 20 minutes at 3000 rpm. To facilitate the separation between the phases, 500 µL of H_2O were added to the previous mixture. The lower lipid containing organic phases were gathered, dried with anhydrous Na_2SO_4, filtered on filter paper, and then dried with a rotating evaporator. Final extracts were dissolved in 500 µL of IPA/MeOH (1:1, *v/v*) mixture and injected into LC-MS.

6.2.3. Instrumentation and analytical conditions

The analyses were performed on a Shimadzu Ultra High Performance Liquid Chromatograph-Nexera system (Shimadzu, Milan, Italy), including a CBM-20A controller, two LC-30 AD dual-plunger parallel-flow pumps, a DGU-20A3R degasser, a CTO-20AC column oven, a SIL-30AC autosampler. The UHPLC system was coupled to an LCMS-2020 quadrupole mass spectrometer equipped with both ESI and APCI interfaces (Shimadzu). MS data acquisition was performed by the Shimadzu LabSolution software (ver. 5.60 SP2).

Chromatographic separation was achieved on a Titan C18, 100 mm × 2.1 mm I.D., 1.9 µm d_p (Supelco, Bellefonte, PA). The injection volume was 1 µL, mobile phase consisted of water with 20 mM NH_4COOH (solvent A) and IPA/ACN/H_2O with 0.1% HCOOH (60:36:4, *v/v*) (solvent B) and the linear gradient profile was as follows: 0 min, 80% B, 6 min, 100% B (hold for 16 min). Starting conditions were achieved in 0.01 min and the column was re-equilibrated for 3 min, resulting in a total run time of 25 min. Flow rate was 0.4 mL/min; oven temperature was 40 °C. MS acquisition was performed using alternatively ESI and APCI, in positive (+) and negative (-) ionization modes. The samples were analyzed in full scan mode and under SIM acquisition mode

simultaneously. Full-scan LC-MS chromatograms were obtained by scanning *m/z* 350-1250, with a scan speed of 5000 amu/s and an event time of 0.2 s, in positive mode both for APCI and ESI, and from *m/z* 150-1250 with a scan speed of 6000 amu/s and an event time of 0.2 s, in negative mode for APCI and ESI. Simultaneously, about 30 selected ions (reported in Table VI-1), which represent the most common FFAs in plasma sample (Quehenberger, *et al.*, 2010), were acquired in SIM(-) mode to obtain a more accurate identification.

Table VI-1. *m/z value used in SIM(+) and SIM(-) mode.*

SIM (+) *m/z*	**Sterol**
369	Chol
SIM (-) *m/z*	**FFA**
199	C12:0
227	C14:0
225	C14:1
255	C16:0
253	C16:1
251	C16:2
283	C18:0
281	C18:1
279	C18:2
277	C18:3
275	C18:4
311	C20:0
309	C20:1
307	C20:2
305	C20:3
303	C20:4
301	C20:5
331	C22:4
329	C22:5
327	C22:6

ESI parameters were as follows: nebulizing gas (N_2) flow rate: 2 L/min; drying gas (N_2) flow: 15 L/min; detector voltage: 1.5 kV; interface voltage: 4.5 kV; desolvation line (DL) temperature: 250 °C; heat block temperature: 200 °C.
APCI parameters were as follows: nebulizing gas (N_2) flow rate: 3 L/min; drying gas (N_2) flow: 15 L/min; detector voltage: 1.5 kV; interface voltage: 4.5 kV; interface temperature: 450 °C; DL temperature: 250 °C; heat block temperature: 200 °C.

6.3. Results and discussion

ESI-MS has arguably become the most employed method for lipid analysis, especially for polar lipid. ESI-Q MS normally produces no fragmentation; therefore HR-MS, MS/MS or MS^n experiments are often necessary for a complete structural elucidation. MS/MS experiments (over HR) allow identification of isobaric species, through a different fragmentation related to the specific structure. However, a drawback of applying ESI in MS/MS mode consists in the fact that some instruments (e.g. QqQ) are not able to operate in non-selective tandem MS mode. On the other hand, instruments able to work in non-selective tandem MS mode (e.g. IT-ToF) may consider only the most representative ions (in terms of ion abundance) at the expense of the less abundant ones; for this reason, it may need of several analyses to select the proper parent ion (e.g. in the case of coelutions) in order to not neglect the less expressed ions, thus requiring more effort for the optimization. On the other hand, APCI-MS can present low molecular ion intensity for some compounds, thus loosing important information whilst provided by ESI. For instance, some phospholipids produce such small abundances of related-molecular ions under APCI conditions, that information on molecular weight provided by ESI can be invaluable. Thus, combining the complementary information provided by ESI and APCI interfaces, an in-depth characterization of lipids can be carried out,

even without the necessity of very expensive MS analyzers.

An RP-UHPLC method, suitable to be performed using both ESI and APCI interfaces coupled to a Q MS, is herein proposed. The capability to work simultaneously in both (+) and (-) ion mode was exploited for a more comprehensive characterization.

6.3.1. UHPLC-Q MS method

When a large number of samples is analyzed, as in clinical cohorts, the total run time for each analysis plays an important role. Therefore, a compromise is needed to maximize the sample throughput and the lipidome coverage, maintaining high quality MS information. The most suitable choice to achieve this compromise is the employment of a UHPLC system equipped with a sub-2 μm particles, thus reducing the analysis time, without loss of resolution under optimized conditions. In RP-LC the amount of water in the mobile phase is particularly critical, especially at the beginning of the gradient, affecting the chromatographic resolution of polar lipids. Higher concentration of water significantly improves not only the elution profile, but also the signal-to-noise ratio (Sandra, *et al.*, 2010; Lísa, *et al.*, 2011). Different organic solvents (MeOH or ACN) in combination with water were tested to optimize the UHPLC method, but a rather long separation time (> 30 min) to elute TAGs and CEs was required. Better results were achieved using water containing ammonium formate (20mM) as solvent A and a mixture of IPA/ACN/water (water with 20mM of ammonium formate) (60:36:4, *v/v/v*) containing formic acid 0.1% as solvent B. The relative low pH, obtained by using formic acid, allowed to minimize the tailing of FFAs caused by the interaction of the ionized carboxyl function with free silanol sites on the LC column packing. The chromatographic pattern obtained partially fitted to the well-known model where the retention of lipids increases proportionally to their ECN (Lísa, *et al.*, 2011; Dugo, *et al.*,

2013; Beccaria, *et al.*, 2014; Beccaria, *et al.*, 2015; Ovčačíková, *et al.*, 2016). Some exceptions from this rule can be observed for lipids containing the combination of highly polyunsaturated and saturated fatty acyls, which can be retained more strongly and elute in higher ECN groups (Beccaria, *et al.*, 2015; Ovčačíková, *et al.*, 2016). The chromatographic LC method proposed was suitable, without any adjustment, to be used in combination with both ESI and APCI interfaces. In such a way, two chromatographic profiles, perfectly equivalent in terms of retention times were obtained, from which complementary MS information can be extrapolated for a comprehensive and detailed characterization.

6.3.2. Standard lipids analyzed by UHPLC-Q MS

All standard lipids (reported in Section 6.2.1) were analyzed and identified using the RP-UHPLC-Q MS method proposed, coupled with both ESI and APCI interface and acquired simultaneously in (+) and (-) mode. The retention times, ECN value and CN and DB (CN:DB) of the 54 standards are reported in Table VI-2. In general, ESI using mobile phase modifiers (i.e. ammonium formate) is more sensitive than APCI, but typical adducts generated are less stable and either non-linear or with dramatically reduced linear dynamic range (Imbert, *et al.*, 2012). However, the fragmentation produced by the APCI interface in a single MS event can provide similar information as ESI-MS/MS to elucidate the lipid structure (Byrdwell & Borchman, 1997; Byrdwell, 1998; Byrdwell, 2001).

Table VI-2. *List of the reference materials and related retention times, ECN value, CN and DB (CN:DB).*

N.	ECN	Rt	Standard-CN:DB	FA(s)
1	12	0.84	LCP-C18:3	18:3
2	14	0.88	LCP-C16:1	16:1
3	14	1.02	LPC-C18:2	18:2
4	16	1.18	LPC-C16:0	16:0
5	16	1.22	LCP-C18:1	18:1
6	12	1.32	FFA-C12:0	12:0
7	18	1.55	LPC-C18:0	18:0
8	12	1.64	FFA-C18:3	18:3
9	14	1.78	FFA-C14:0	14:0
10	12	1.90	FFA-C20:4	20:4
11	14	2.01	FFA-C18:2	18:2
12	16	2.43	FFA-C16:0	16:0
13	16	2.52	FFA-C18:1	18:1
14	26	2.55	PS-C36:5	18:3_18:2
15	28	2.61	PI-C34:3	16:0_18:3
16	28	2.83	PI-C36:4	18:2_18:2
17	28	2.84	PS-C34:3	16:0_18:3
18	28	2.93	PS-C36:4	18:2_18:2
19	30	3.01	PI-C34:2	16:0_18:2
20	30	3.13	PI-C36:3	18:1_18:2
21	18	3.24	FFA-C18:0	18:0
22	30	3.26	PS-C34:2	16:0_18:2
23	30	3.38	PS-C36:3	18:2_18:1
24	32	3.55	PI-C34:1	16:0_18:1

25	32	3.67	PI-C36:2	18:0_18:2
26	26	3.87	PE-C36:5	18:3_18:2
27	28	4.28	PE-C34:3	16:0_18:3
28	28	4.41	PE-C36:4	18:2_18:2
29	32	4.54	SM-C34:1	
30	30	4.86	PE-C34:2	16:0_18:2
31	30	4.98	PE-C36:3	18:2_18:1
32	30	5.04	SM-C34:2	
33		5.02	Chol	
34	30	5.16	PC-C34:2	16:0_18:2
35	32	5.31	PE-C34:1	16:0_C18:1
36	30	5.38	PC-C36:3	18:1_18:2
37	32	5.55	PE-C34:1	16:0_C18:1
38	34	5.66	SM-C36:1	
39	32	5.71	PE-C36:2	18:2_18:0
40	32	5.97	PC-C34:1	16:0_18:1
41	30	6.07	PC-C38:4	18:0_20:4
42	32	6.13	PC-C36:2	18:1_18:1
43	30	7.38	TAG-C60:15	20:5_20:5_20:5
44	30	7.81	TAG-C66:18	22:6_22:6_22:6
45	36	7.93	TAG-C54:9	18:3_18:3_18:3
46	36	8.72	TAG-C60:12	20:4_20:4_20:4
47	42	9.57	TAG-C48:3	16:1_16:1_16:1
48	42	9.78	TAG-C54:6	18:2_18:2_18:2
49	45	11.39	TAG-C45:0	15:0_15:0_15:0
50	14	13.27	CE-C18:2	18:2

51	48	13.43	TAG-C54:3	18:1_18:1_18:1
52	16	15.44	CE-C18:1	18:1
53	16	15.81	CE-C16:0	16:0
54	18	18.79	CE-C18:0	18:0

In the following section, APCI mass spectra were reported and discussed in more details, since the mass spectra obtained by ESI have been widely investigated and reported in previous works (Imbert, *et al.*, 2012; Dugo, *et al.*, 2013; Beccaria, *et al.*, 2014; Lytle, *et al.*, 2000; Hsu & Turk, 2003; Kerwin, *et al.*, 1994; Uran, *et al.*, 2001; Karlsson, *et al.*, 1996; Qiu & Xiao, 1999). Table X-3 summarizes the main ions present in the mass spectra of the different lipid classes (along with their relative intensities calculated on the standards). No investigation about regioisomeric species was carried out.

Table VI-3. *All ions generated from the analysis of lipid standards by APCI interface.*

$LIPID_{CN:DB}$	**APCI(+)**	**% int. Average (min/max)**	**APCI(-)**	**% int. Average (min/max)**
FFA	-		$[M-H]^-$	100 (100/100)
($FA_{18:2}$; $FA_{16:0}$; $FA_{18:1}$; $FA_{18:0}$)			$[M+HCOO]^-=[M+45]^-$	50 (40/60)
LPC	$[M+H-C_5H_{13}N]^+=[M+H-87]^+$	100 (100/100)	$[M-C_5H_{12}N-H_2O]^-=[M-104]^-$	100 (100/100)
($LPC_{18:2}$; $LPC_{16:0}$; $LPC_{18:1}$; $LPC_{18:0}$)	$[M+H-C_4H_{11}N]^+=[M+H-73]^+$	77 (73/80)	$[M-CH_3]^-=[M-15]^-$	30 (15/45)
	$[M+H-C_4H_{11}N-H_2O]^+=[M+H-91]^+$	75 (65/85)	$[M-C_5H_{12}N]^-=[M-86]^-$	n.q. (n.d/10)
	$[M+H]^+$	60 (10/85)	$[M-R_{sn\text{-}1/2}COOH-C_5H_{12}N]^-=[M-FA_{sn\text{-}1/2}\text{-}86]^-$	n.d.
	$[M+H-CH_2-H_2O]^+=[M+H-32]^+$	57 (40/74)	$[M-(R_{sn\text{-}1/2}=C=O)-C_5H_{12}N]^-=[M-Ketene_{sn\text{-}1/2}\text{-}86]^-$	n.d.
	$[M+H-(CH_2)_3]^+=[M+H-42]^+$	50 (20/65)	$[R_{sn\text{-}1/2}COOH-H]^-=[FA_{sn\text{-}1/2}-H]^-$	n.d.
	$[M+H-C_5H_{13}N-H_2O]^+=[M+H-105]^+$	52 (49/58)		
	$[M+H-C_3H_9N]^+=[M+H-59]^+$	35 (25/45)		
	$[M+H-C_3H_9N-H_2O]^+=[M+H-77]^+$	23 (18/27)		
	$[M+H-CH_2]^+=[M+H-14]^+$	n.q. (n.d./12)		
PC	$[M+H-C_5H_{14}NO_4P]^+=[M+H-183]^+$	100 (100/100)	$[M-CH_3]^-=[M-15]^-$	100 (100/100)
($PC_{34:2}$; $PC_{34:1}$; $PC_{36:2}$; $PC_{38:4}$)	$[M+H]^+$	71(60/86)	$[M-C_4H_{10}N]^-=[M-72]^-$	76 (46/87)
	$[M+H-CH_2]^+=[M+H-14]^+$	43 (36/55)	$[M-H-C_3H_9N]^-=[M-60]^-$	13 (7/21)
	$[M+K-CH_2]^+=[M+K-14]^+$	42 (39/47)	$[M-C_5H_{12}N]^-=[M-86]^-$	7 (4/9)
	$[M+H-(CH_2)_3]^+[M+H-42]^+$	40 (27/56)	$[M-R_{sn\text{-}1/2}COOH-C_5H_{12}N]^-=$	n.q.

			$[M\text{-}FA_{sn\text{-}1/2}\text{-}86]^-$	
	$[M+Na\text{-}CH_2]^+=[M+Na\text{-}14]^+$	12 (4/24)	$[M\text{-}(R_{sn\text{-}1/2}\text{=}C\text{=}O)\text{-}C_5H_{12}N]^-=$ $[M\text{-}Ketene_{sn\text{-}1/2}\text{-}86]^-$	n.q.
	$[M+H\text{-}C_5H_{13}N]^+=[M+H\text{-}87]^+$	n.d.	$[R_{sn\text{-}1/2}COOH\text{-}H]^-=[FA_{sn\text{-}1/2}\text{-}H]^-$	n.q.
	$[M+H\text{-}R_{sn\text{-}1/2}COOH]^+=$ $[M+H\text{-}FA_{sn1/2}]^+$	n.d.		.
SM	$[M+H\text{-}C_5H_{14}NO_4P]^+ = [M+H\text{-}183]^+$	100 (100/100)	$[M\text{-}C_5H_{12}NO_3\text{+}HCOO]^-=[M\text{-}120]^+$	100 (100/100)
($SM_{34:1}$; $SM_{34:0}$; $SM_{36:1}$)	$[M+H\text{-}C_5H_{12}NO_3P]^+=[M+H\text{-}165]^+$	16 (12/28)	$[M\text{-}CH_3]^-=[M\text{-}15]^-$	55 (36/84)
	$[M+H\text{-}C_3H_9N\text{-}H_2O]^+=[M+H\text{-}77]^+$	16 (11/24)	$[M\text{-}C_4H_{10}N]^-=[M\text{-}72]^-$	45 (30/60)
	$[M+H]^+$	10 (8/13)	$[M\text{-}C_5H_{12}N\text{-}H_2O]^-=[M\text{-}104]^-$	27 (19/35)
	$[M+H\text{-}C_3H_9N]^+=[M+H\text{-}59]^+$	9 (6/12)	$[M\text{-}H\text{-}C_3H_9N]^-=[M\text{-}60]^-$	22 (18/25)
	$[M+H\text{-}CH_2]^+=[M+H\text{-}14]^+$	6 (5/7)	$[M+HCOO]^-=[M+45]^-$	13 (7/23)
	$[M+H\text{-}CH_2\text{-}H_2O]^+=[M+H\text{-}32]^+$	n.q. (n.d./10)	$[M\text{-}C_5H_{12}N]^-=[M\text{-}86]^-$	11 (8/15)
	$[M+H\text{-}C_5H_{13}N]^+=[M+H\text{-}87]^+$	n.d.		
PE	$[M+H\text{-}C_2H_8NO_4P]^+=[M+H\text{-}141]^+$	95 (80/100)	$[M\text{-}H]^-$	100 (100/100)
($PE_{36:5}$; $PE_{36:4}$; $PE_{34:2}$; $PE_{34:1}$)	$[M+H]^+$	94 (85/100)	$[M\text{-}H+Na+HCOO]^-=[M+77]^-$	12 (6/22)
	$[M+H+Na+C_3H_8O]^+=[M+H\text{-}83]^+$	52 (47/62)	$[M\text{-}H\text{-}R_{1/2}COOH\text{-}C_2H_6N]^-=$ $[M\text{-}H\text{-}FA_{1/2}\text{-}44]^-$	n.q.
	$[M+Na]^+$	37 (16/55)	$[M\text{-}H\text{-}R_{sn\text{-}1/2}COOH]^-=[M\text{-}H\text{-}FA_{sn\text{-}1/2}]^-$	n.q.
	$[M+H\text{-}R_{sn\text{-}1/2}COOH]^+=$ $[M+H\text{-}FA_{sn\text{-}1/2}]^+$	n.q.	$[M\text{-}H\text{-}(R_{sn1/2}\text{=}C\text{=}O)]^-=$ $[M\text{-}H\text{-}Ketene_{sn\text{-}1/2}]^-$	n.q.
			$[M\text{-}H\text{-}(R_{sn1/2}\text{=}C\text{=}O)\text{-}C_2H_6N]^-=$ $[M\text{-}H\text{-}Ketene_{sn\text{-}1/2}\text{-}44]^-$	n.d.
			$[R_{1/2}COOH\text{-}H]^-=[FA_{sn\text{-}1/2}\text{-}H]^-$	n.d.

PS	$[M+H-C_3H_8NO_6P]^+=[M+H-185]^+$	100 (100/100)	$[M-H-C_3H_5NO_2]^-=[M-H-87]^-$	100 (100/100)
($PS_{36:5}$; $PS_{36:4}$; $PS_{36:3}$; $PS_{34:2}$)	$[M+H]^+$	55 (50/61)	$[M-H]^-$	43 (41/46)
	$[M+H+C_3H_8O+Na-C_3H_5NO_2]^+=[M+H-4]^+$	52 (40/75)	$[M-H-NH_2]^-=[M-17]^-$	38 (32/45)
	$[M+NH_4-C_3H_5NO_2]^+=[M+NH_4-87]^+$	48 (47/50)	$[M-R_{sn\text{-}1/2}COOH]^-=[M-H-FA_{sn\text{-}1/2}]^-$	n.q.
	$[M+H+Na+C_3H_8O]^+=[M+H-83]^+$	37 (32/45)	$[M-R_{sn\text{-}1/2}COOH-C_3H_5NO_2]^-=[M-FA_{sn\text{-}1/2}-87]^-$	n.q.
	$[M+NH_4-C_3H_7NO_5P]^+=[M+NH_4-167]^+$	23 (18/26)	$[M-(R_{sn1/2}=C=O)-C_3H_5NO_2]^-=[M-Ketene_{sn\text{-}1/2}-87]^-$	n.q.
	$[M+H-C_3H_5NO_2]^+=[M+H-87]^+$	n.q. (n.d./12)	$[M-(R_{sn1/2}=C=O)]^-=[M-H-Ketene_{sn\text{-}1/2}]^-$	n.d.
	$[M+H-R_{sn\text{-}1/2}COOH]^+=[M+H-FA_{sn\text{-}1/2}]^+$	n.d.		
PI	$[M+NH_4-C_6H_{11}O_8P]^+=[M+NH_4-242]^+$	100 (100/100)	$[M-H]^-$	100 (100/100)
($PI_{34:3}$; $PI_{36:4}$; $PI_{34:2}$; $PI_{36:2}$)	$[M+H-C_6H_{13}O_9P]^+=[M+H-260]^+$	72 (64/83)	$[C_6H_9O_7P]^-=[241]^-$	35 (20/50)
	$[M+H+C_3H_8O+Na]^+=[M+H-83]^+$	63 (57/65)	$[C_6H_{11}O_8P]^-=[259]^-$	20 (10/25)
	$[M+H-C_6H_{11}O_8P]^+=[M+H-242]^+$	36 (20/44)	$[C_6H_7O_8P]^-=[273]^-$	10 (7/13)
	$[M+NH_4]^+$	20 (15/25)	$[C_6H_7O_6P]^-=[223]^-$	n.q.
	$[M+Na]^+$	15 (7/20)	$[M-R_{sn\text{-}1/2}COOH-C_6H_{10}O_5]^-=[M-FA_{sn\text{-}1/2}-162]^-$	n.q.
	$[M+H]^+$	n.q. (n.d/10)	$[M-R_{sn\text{-}1/2}COOH]^-=[M-FA_{sn\text{-}1/2}]^-$	n.q.
	$[M+H-R_{sn\text{-}1/2}COOH]^+=[M+H-FA_{sn\text{-}1/2}]^+$	n.q	$[M-(R_{sn1/2}=C=O)]^-=[M-Ketene_{sn\text{-}1/2}]^-$	n.d.
			$[M-(R_{sn\text{-}1/2}=C=O)-C_6H_{10}O_5]^-=[M-Ketene_{sn\text{-}1/2}-162]^-$	n.d.

Chol (free cholesterol)	$[M+H-H_2O]^+=[C_{27}H_{44}+H]^+=[369]^+$	100 (100/100)	-	
CE ($CE_{18:2}$; $CE_{18:1}$; $CE_{16:0}$; $CE_{18:0}$)	$[M+H-FA]^+=[C_{27}H_{44}+H]^+=[369]^+$	100 (100/100)	$[M-H-C_{27}H_{45}]^-=[FA-H]^-$ $[M+HCOO-C_{27}H_{45}]^-=[FA+HCOO]=[FA+45]^-$	100 (100/100) 40 (27/58)
TAG	$[M+H]^+$ $[M-R_{1/2/3}COOH]^+=[M+H-FA_{1/2/3}]^+$	n.q n.q.	$[R_{sn\text{-}1/2/3}COOH-H]^-=[FA_{sn\text{-}1/2/3}-H]^-$ $[R_{sn\text{-}1/2/3}COOH+HCOO]^-=[FA_{sn\text{-}1/2/3}+45]^{--}$ $[M-H]^-$	n.q. n.q. n.q.

n.q: ion intensity non-quantifiable, where the ion intensity can depend by the combination of different factors (e.g. number of unsaturations, carbon chain length, and/or position of FA on glycerol backbone). **n.d:** expected ions but non detected.

6.3.2.1. Polar standards lipids

- Free fatty acid (FFAs)

FFAs can be analyzed in both (+) and (-) ion mode with API interfaces, although the ionization of choice is always the negative one (both in scan and SIM mode). The base peak was the deprotonated molecular ion $[M-H]^-$, followed, in some case, by formate adduct $[M+HCOO]^-=[M+45]^-$ ion, while no fragmentation at all was observed. The SIM(-) values used to detect FFA are reported in Table VI-1.

- Phosphatydilcholine (PC) and Lysophosphatydilcholine (LPC)

All the combination, both ESI and APCI under positive and negative mode were applied. The use of ESI(+), leads to the protonated molecular $[M+H]^+$ ion as base peak, followed by sodiate adduct $[M+Na]^+$. No fragmentation was observed. The use of ESI(-) in PC analysis generally gave mass spectra containing different PC molecule-related ions. However, if formic acid is used as mobile phase additive (as in the proposed method), the PC species form an adduct $[M+45]^-$ ion as base peak, as also observed by other authors (Kerwin, *et al.*, 1994; Karlsson, *et al.*, 1996).

By using APCI(+) interface, the fragmentation of protonated molecules of PC, which occurs in-source, is dominated by a prominent $[M+H-C_5H_{14}NO_4P]^+=[M+H-183]^+$ ion (loss of the head polar group $C_5H_{14}NO_4P$) (Byrdwell, 1998; Imbert, *et al.*, 2012; Cai & Sayge, 2006). The protonated molecular ion $[M+H]^+$ is also present. Other characteristic fragments were $[M+H-CH_2]^+=[M+H-14]^+$, $[M+H-N(CH_3)_3]^+=[M+H-59]^+$ and a particular fragment ion $[M+H-42]^+$ that was identified as $[M+H-(CH_2)_3]^+$. The latter fragment can be confounding since can lead to a misinterpretation of the lipid class. The loss of three methyl groups of choline and substitution with H^+ ions convert choline in ethanolamine (i.e. $[PC\_34:2+H-(CH_2)_3]^+ = [PE\_34:2+H]^+$ in

term of *m/z*). This misinterpretation can be resolved considering the ions generated by APCI(-), where the presence of the $[M-H]^-$ ion is needed for confirming the belonging to the PE class (i.e. $[PE\_34:2-H]^-$, see also Phosphatidylethanolamine (PE) section).

When subjected to APCI(-), PC showed no ion from the intact molecule, such as a deprotonated molecule ion. The ion $[M-H]^-$ was reported only once by Qiu et al. (Qiu & Xiao, 1999). PC does not contain any acid protons and the authors did not discuss about this remarkable phenomenon. Instead, PC forms mainly a set of four ion species: $[M-CH_3]^- = [M-15]^-$ (loss of methyl group), $[M-H-C_3H_9N]^- = [M-60]^-$ (loss of trimethylamine group), $[M-C_5H_{12}N]^- = [M-86]^-$ (loss of choline residue), and $[M-C_4H_{10}N]^- = [M-72]^-$ fragment ion. Some of these fragments generated by APCI(-) have been observed before, but never considered (Imbert, *et al.*, 2012; Qiu & Xiao, 1999; Karlsson, *et al.*, 1998). Additional characteristic fragments, as $[M-R_{sn-1/2}COOH-C_5H_{12}N]^- = [M-FA_{sn-1/2}-86]^-$ (loss of the fatty acyl substituents as FFA and choline residue), $[M-(R_{sn-1/2}=C=O)-C_5H_{12}N]^- = [M-Ketene_{sn-1/2}-86]^-$ (loss of the fatty acyl substituent as ketene and choline residue) and $[R_{sn-1/2}COOH-H]^- = [FA_{sn-1/2}-H]^-$ (fatty carboxylate anions) were observed. Mass spectra of PC-16:0_18:2 from egg yolk, in both APCI(+) and (-) are reported in Figure VI-1, while in Figure VI-2 the hypothesized structures related to a fragmentation of choline group are shown. LPC in ESI(+) leaded to the protonated molecular ion $[M+H]^+$ as base peak, while in the ESI(-) showed the adduct $[M+HCOO]^-$ and the fragment $[M-CH_3]^- = [M-15]^-$. APCI(+) generated $[M+H-C_5H_{13}N]^+ = [M+H-87]^+$ (loss of choline residue) as base peak ion, followed by $[M+H-C_4H_{11}N]^+ = [M+H-73]^+$, $[M+H-C_4H_{11}N-H_2O]^+ = [M+H-91]^+$, the protonated molecular $[M+H]^+$ ion, $[M+H-CH_2-H_2O]^+ = [M+H-32]^+$, $[M+H-(CH_2)_3]^+ = [M+H-42]^+$, $[M+H-C_5H_{13}N-H_2O]^+ = [M+H-105]^+$ (loss of $C_5H_{13}N$ choline residue + loss of H_2O from the glycerol backbone), $[M+H-C_3H_9N]^+ = [M+H-59]^+$, $[M+H-C_3H_9N-H_2O]^+ = [M+H-$

77]$^+$, and [M+H-CH_2]$^+$=[M+H-14]$^+$ ions. Moreover, APCI(+) generates a multitude of additional fragment ions, some of which difficult to be identified. Important structural information was obtained in APCI(-). The [M-$C_5H_{12}N$-H_2O]$^-$=[M-104]$^-$ ion (loss of $C_5H_{12}N$ choline residue + loss of H_2O from the glycerol backbone) was the main ion, followed by [M-CH_3]$^-$=[M-15]$^-$, and [M-$C_4H_{10}N$]$^-$ =[M-72]$^-$, the same fragment-ion found for each choline-related lipid (see Figure VI-2b). [$R_{sn\text{-}1/2}$COOH-H]$^-$=[$FA_{sn\text{-}1/2}$-H]$^-$ ions may also be present.

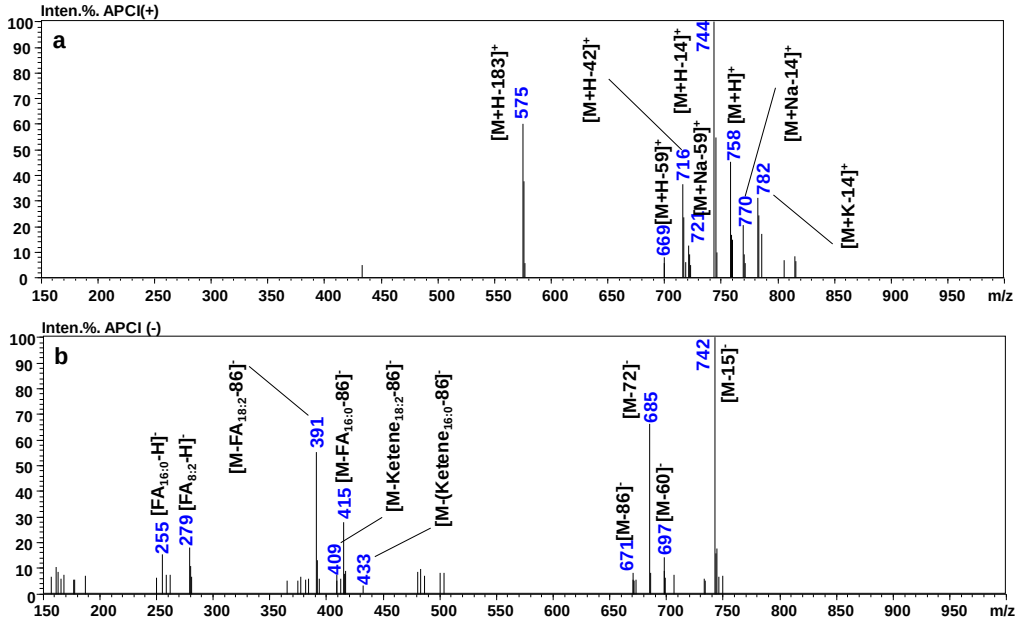

Figure VI-1. *Full mass spectra of PC-34:2 standard (PC-16:0_18:2) by APCI(+) (a) and APCI(-) (b).*

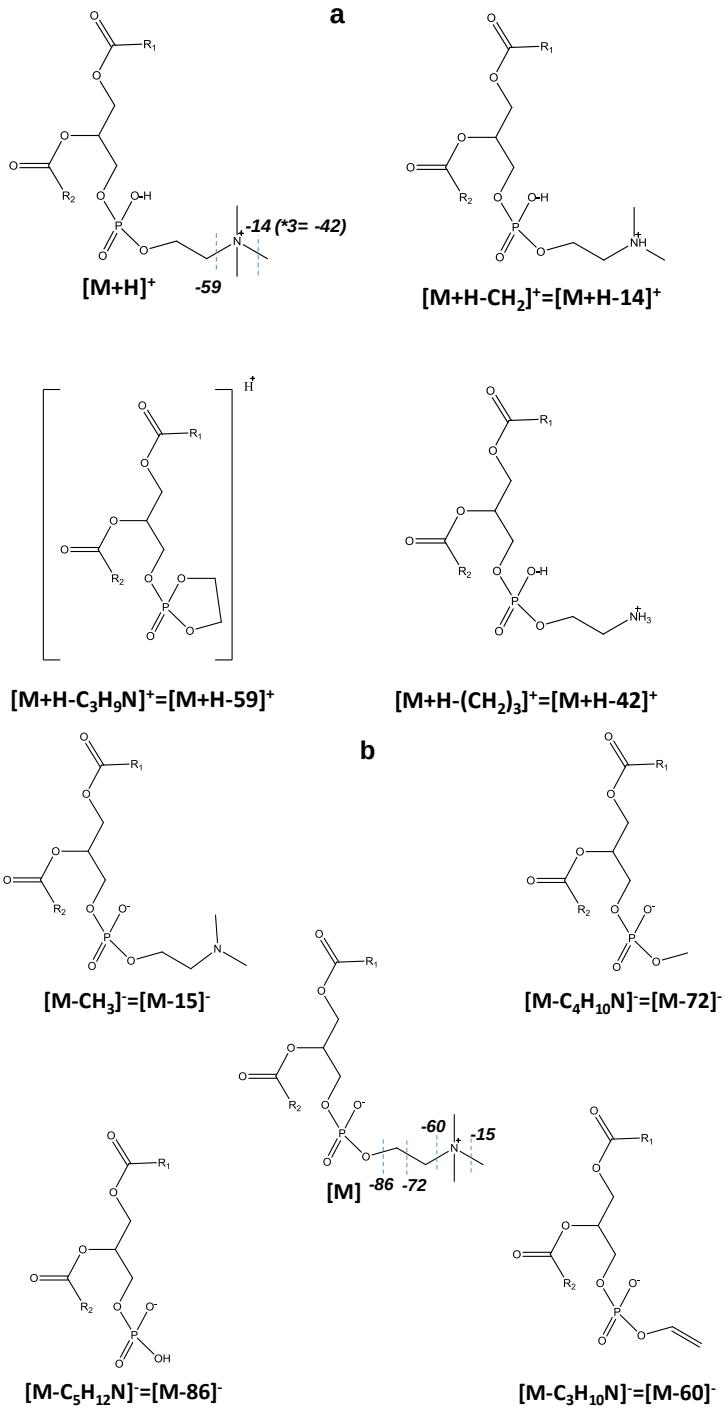

Figure VI-2. *Hypothesized structures related to a fragmentation of choline group in PC lipid class by APCI(+) (a) and APCI(-) (b).*

- *Sphingomyelin (SM)*

The base peaks in the mass spectra of SMs, analyzed using ESI(+), were the protonated molecular ion $[M+H]^+$ and the sodiate adduct $[M+Na]^+$. With ESI(-) the $[M+HCOO]^-$ ion was the major fragment observed. Poor structure information was obtained from these fragments, even when ESI-MS/MS was employed, as reported by other research groups (Karlsson, *et al.*, 1998). APCI(+) due to more extensive in-source fragmentation, gave mainly ceramide (Cer)-like product ions $[M+H-C_5H_{14}NO_4P]^+=[M+H-183]^+$ ion (loss of head polar group $C_5H_{14}NO_4P$, corresponding to $[Cer-H_2O]^+$ ion), but also $[M+H]^+$ and $[M+H-C_5H_{12}NO_3P]^+=[M+H-165]^+$ (corresponding to $[Cer+H]^+$ ion) were present. Other characteristic fragments were $[M+H-C_3H_9N-H_2O]^+=[M+H-59-18]^+=[M+H-77]^+$, $[M+H-CH_2]^+=[M+H-14]^+$, $[M+H-C_3H_9N]^+=[M+H-59]^+$, and $[M+H-CH_2-H_2O]^+=[M+H-14-18]^+=[M+H-32]^+$. APCI(+) has been already reported to be more useful than ESI(+) for structural characterization of these compounds (Byrdwell & Borchman, 1997; Byrdwell, 1998; Karlsson, *et al.*, 1998), while very little information about SMs' fragments, obtained using APCI(-) mode have been reported. The same set of four ion species, obtained from PCs were observed, plus two additional diagnostic fragments, namely $[M-C_5H_{12}N-H_2O]^-=[M-86-18]^-=[M-104]^-$ and $[M-C_5H_{12}NO_3P+HCOO]^-=[M-165+45]^-=[M-120]^-$. The first fragment, observed also in LPC class, was most probably generated from the simultaneous loss of a choline residue (86 *m/z*) and H_2O (18 *m/z*) from the sphingosin, while the latter, present only for SMs class, is a fragment that was conferred as $[Cer+HCOO]^-$ formate adduct ion (loss of $C_5H_{12}NO_3P$ residue from head polar group, corresponding to ceramide, + formate adduct). In Figure VI-3, mass spectra of SM-34:0 from chicken egg yolk, by APCI(+) and (-), are shown. Also in this case, the hypothesized structures related to a fragmentation of choline group are reported (Figure VI-4).

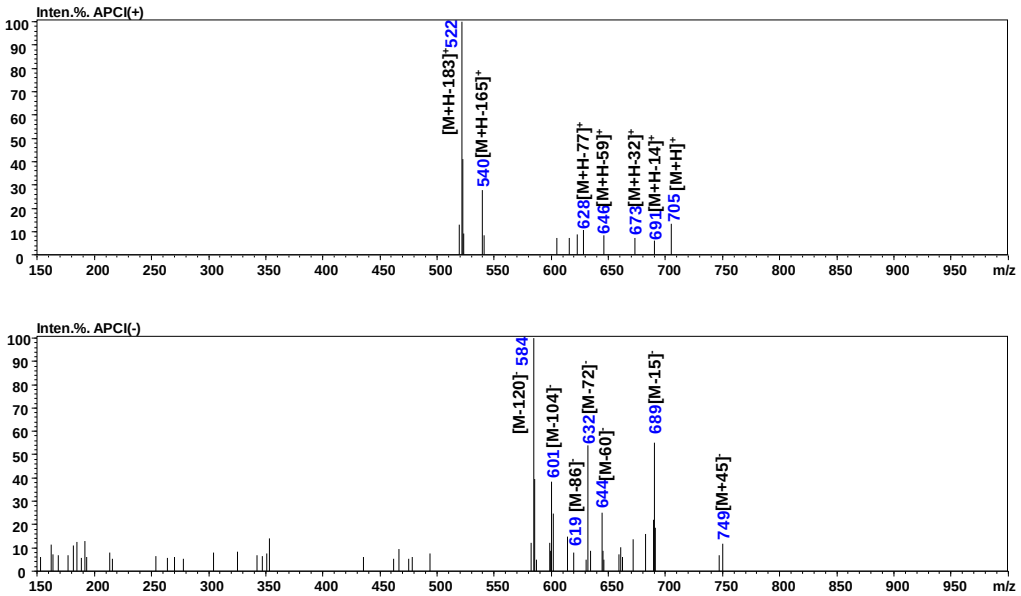

Figure VI-3. *Full mass spectra of SM-34:0 standard by APCI(+) (a) and APCI(-) (b).*

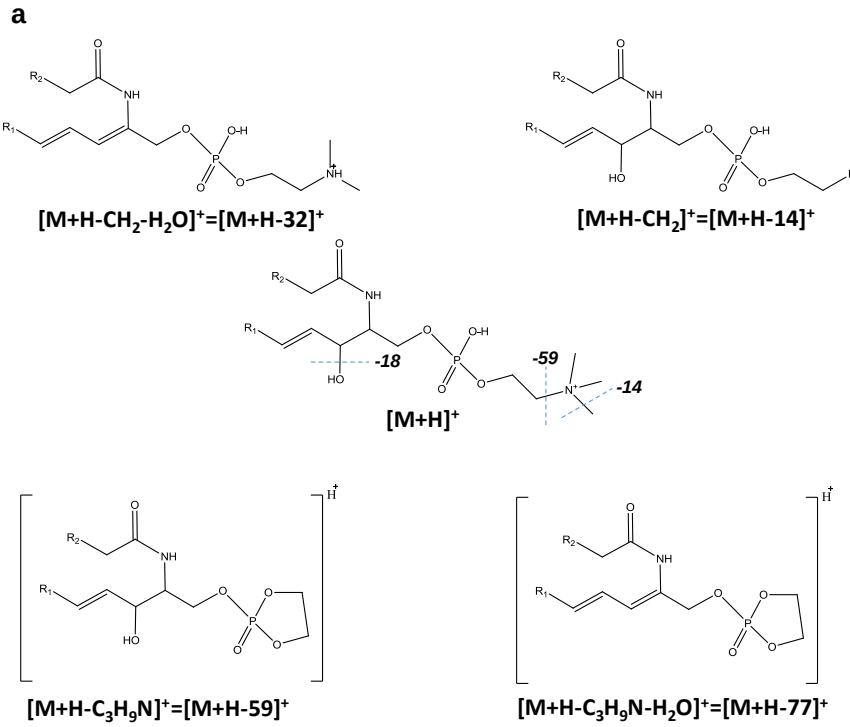

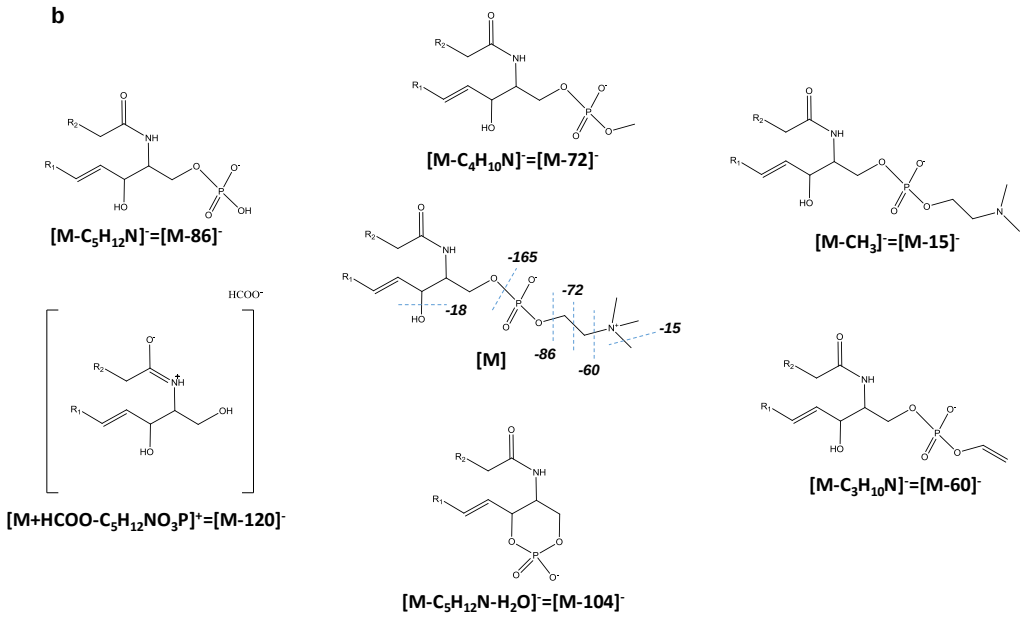

Figure VI-4. *Hypothesized structures related to a fragmentation of choline residue in SM lipid class by APCI(+) (a) and APCI(-) (b).*

- *Phosphatidylethanolamine (PE)*

The main molecule-related ion of PE by using ESI(+) was $[M+H]^+$ ion and its sodiate adduct $[M+Na]^+$. PE was the only phospholipid where $[M+H-C_2H_8NO_4P]^+=[M+H-141]^+$ ion (loss of head polar group) was observed in ESI(+). ESI(-) generated mainly the $[M-H]^-$ ion and no adducts was observed. By using APCI(+), the main protonated molecules were the fragment ions of $[M+H-C_2H_8NO_4P]^+=[M+H-141]^+$ and protonated molecular ion $[M+H]^+$, followed by sodiate adduct $[M+Na]^+$ and a protonated adduct $[M+H-83]^+$ ion that was attributed as $[M+H+Na+C_3H_8O]^+$ (C_3H_8O: isopropanol) (Metabolomics Fiehn Lab, 2010). The latter adduct-ion was also generated from PS and PI in APCI(+) mode. In APCI(-), $[M-H]^-$ ion was the base peak for each PE investigated, followed by a $[M-H+Na+HCOO]^-=[M-H+Na+45]^-=[M+67]^-$. Other fragments, as $[M-H-R_{sn-1/2}COOH]^-=[M-H-FA_{sn-1/2}]^-$ (loss of fatty acid), $[M-H-(R_{sn1/2}=C=O)]^-=[M-H-Ketene_{sn-1/2}]^-$ (loss of the fatty acyl

substituent as ketenes) and $[M\text{-}_{Rsn\text{-}1/2}COOH\text{-}C_2H_6N]^-$=$[M\text{-}FA_{sn\text{-}1/2}\text{-}44]^-$ (loss of the fatty acyl substituents + ethanolamine residue) ions were also observed. In Figure VI-5, mass spectra of PE-C34:6 (PE-C18:2_C18:2) obtained by using both APCI(+) and APCI(-), are shown.

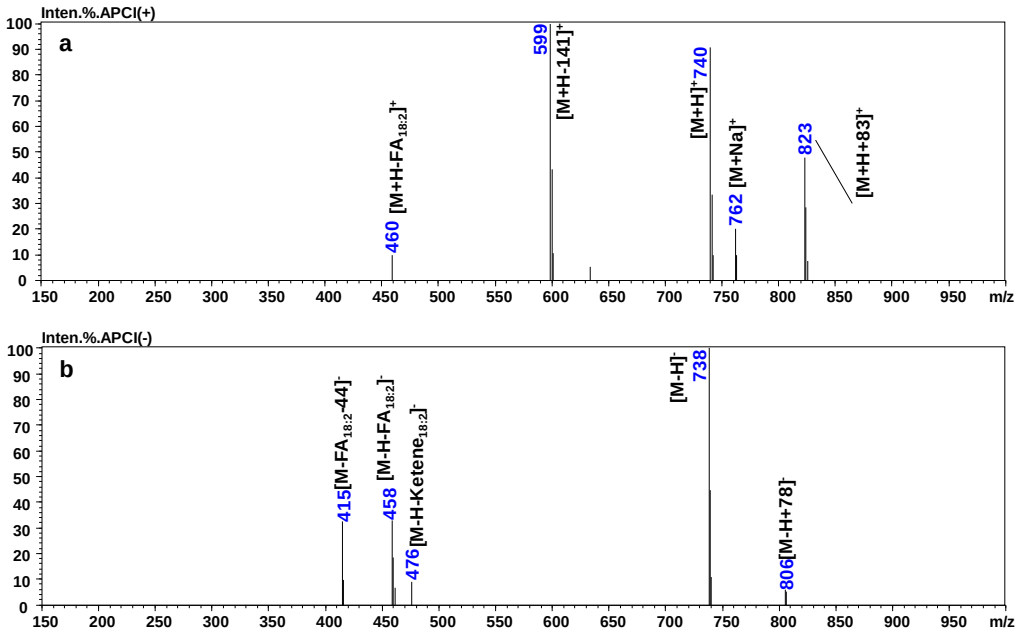

Figure VI-5. *Full mass spectra of PE-36:4 standard from Glycine max (soybean) (PE-18:2_18:2) by APCI(+) (a) and APCI(-) (b).*

- *Phosphatidylserin (PS)*

In ESI(+), PS yielded related molecular ion as $[M+H]^+$ ion and sodiate adduct $[M+Na]^+$ ion. When subjected to ESI(-), PS generated mainly $[M-H]^-$ ion. APCI(+) generated $[M+H\text{-}C_3H_8NO_6P]^+$=$[M+H\text{-}185]^+$ (loss of the head polar group, corresponding to $[DAG\text{-}H_2O]^+$) as the base peak followed by $[M+H]^+$ ion. As PE, PS in APCI(+) showed the formation of $[M+H+Na+C_3H_8O]^+$=$[M+H+83]^+$ adduct ion. Furthermore, a series of related serine fragmentation ions from the loss of serine residue (87 *m/z*) were observed: $[M+H\text{-}C_3H_5NO_2]^+$=$[M+H\text{-}87]^+$, $[M+NH_4\text{-}C_3H_5NO_2]^+$=$[M+NH_4\text{-}87]^+$, and

$[M+H+Na+C_3H_8O\text{-}C_3H_5NO_2]^+=[M+H+23+60\text{-}87]^+=[M+H\text{-}4]^+$, and $[M+NH_4\text{-}C_3H_7NO_5P]^+=[M+NH_4\text{-}167]^+$ ion (loss of $C_3H_6NO_5P$ head polar group residue). Even if APCI(+) was very informative, APCI(-) gave more structure information in this class of phospholipid and resulted very similar to ESI-MS/MS(-) (Hsu & Turk, 2005). $[M\text{-}H\text{-}C_3H_5NO_2]^-=[M\text{-}H\text{-}87]^-$ ion (arisen from neutral loss of the serine group) was the base peak, followed by $[M\text{-}H]^-$ ion and an undefined $[M\text{-}17]^-$ ion. The latter ion was attributed as $[M\text{-}H\text{-}NH_2]^-$ ion (loss of amino group). As for the PE, $[M\text{-}(R_{sn1/2}\text{=}C\text{=}O)\text{-}C_3H_5NO_2]^-=[M\text{-}Ketene_{sn\text{-}1/2}\text{-}87]^-$ ion (neutral loss of the serine group and the acyl ketene), $[M\text{-}R_{sn\text{-}1/2}COOH\text{-}C_3H_5NO_2]^-=[M\text{-}FA_{sn\text{-}1/2}\text{-}87]^-$ ion (neutral losses of serine group and the FA) and, $[M\text{-}R_{sn\text{-}1/2}COOH]^-=[M\text{-}FA_{sn\text{-}1/2}]^-$ (loss of FA) ions were present. Figure VI-6 shows the APCI(+/-) mass spectra of two co-eluted PSs (PS-C16:0_C18:2; PS-C18:2_C18:1), where all fragment ions aforementioned are present.

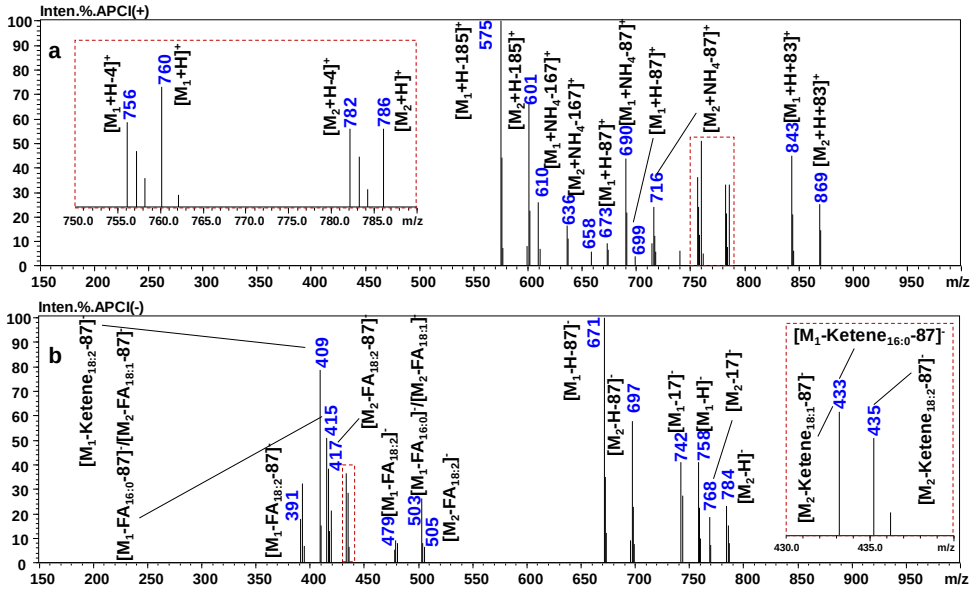

Figure VI-6. *Full mass spectra of co-eluted PS-34:2 (M_1) and PS-36:3 (M_2) standards from Glycine max (soybean) (M_1: PS-16:0_18:2; M_2: PS-18:1_18:2) by APCI(+) (a) and APCI(-) (b).*

- Phosphatidylinositol (PI)

In ESI(+), $[M+Na]^+$ and low intensity of protonated $[M+H]^+$ ion were observed, while ESI(-) formed an abundant $[M-H]^-$ ions of PI species, followed by $[M+45]^-$. In APCI(+) a series of related molecular ion as [M+H]+, $[M+NH_4]^+$, $[M+Na]^+$, and the same $[M+H+C_3H_8O+Na]^+=[M+84]^+$ adduct ion observed for PE and PS, was observed. The base peak was $[M+NH_4\text{-}C_6H_{11}O_8P]^+=[M+NH_4\text{-}242]^+=[M-224]^+$ ion, corresponding to $[DAG+NH_4]^+$ ion (where 242 corresponds to the loss of $C_6H_{11}O_8P$ head polar group residue of monophosphate inositol), followed by ion $[M+H\text{-}C_6H_{13}O_9P]^+=[M+H-260]^+$ and the $[M+H\text{-}C_6H_{11}O_8P]^+=[M+H-242]^+$ ion, corresponding to $[DAG+H]^+$ ion (loss of head polar residue). $[M\text{-}R_{sn\text{-}1/2}COOH]^+=[M\text{-}FA_{sn\text{-}1/2}]^+$ can also be observed. APCI(-) leaded to the formation of a different ions related to phosphoinositol molecule: mainly 241 *m/z* $[C_6H_9O_7P]^-$, 259 *m/z* $[C_6H_{11}O_8P]^-$ (corresponding to inositol monophosphate), 273 *m/z* $[C_7H_{13}O_8P]^-$, and 223 *m/z* $[C_6H_7O_6P]^-$ (Hsu & Turk, 2000). As for PE in APCI(-) conditions, deprotonated molecular ion $[M\text{-}H]^-$ (as base peak), followed by $[M\text{-}R_{sn\text{-}1/2}COOH\text{-}C_6H_{10}O_5]^-=[M\text{-}FA_{sn\text{-}1/2}\text{-}162]^-$ (162 is a residue of inositol) were observed.

6.3.2.2. Non-polar lipids

- Triacylglycerol (TAG)

By using ESI(+) a series of protonated ions $[M+X]^+$ ($X=NH4^+$; Na^+) were generated, but less or no fragmentation was observed. No information was obtained by ESI(-). APCI(+) is the most applied TAGs ionization mode and the fragmentation pattern is widely known (Byrdwell, 2001; Baiocchi, *et al.*, 2015; Řezanka & Sigler, 2007). Briefly, APCI(+) was able to produce protonated molecular ion $[M+H]^+$ and fragments (corresponding to $[DAG\text{-}H_2O]^+$ ion) generated for the loss a fatty acid forming the $[M+H\text{-}_{Rsn\text{-}1/2/3}COOH]^+=[M+H\text{-}FA_{sn\text{-}1/2/3}]^+$ ion. In APCI(-) the base peak was represented by the loss of a fatty

acids from TAG, but in general poor fragmentation was observed. Only the ESI(+) and APCI(+) were considered for further identification.

- *Cholesterol (Chol) and cholesterol-ester (CE)*

The ESI(+) generated protonated molecular ions $[M+X]^+$ (X= $NH4^+$, Na^+) and fragment ions $[M+H-RCOOH]^+=[M+H-FA]^+$ for the CEs, and $[M+H-H_2O]^+$ for the free cholesterol (Chol); while APCI(+) generated $[M+H-H_2O]^+$ and $[M+H-FA]^+$ as base peak, for Chol and CEs, respectively, giving in both cases 369 *m/z*. Using only APCI(+) it would have been not possible to determine any structure information from different CEs, due to the absence of fragments related to the loss of the fatty acid bonded on the cholesterol backbone. Therefore, identification could rely only on the chromatographic behaviour related to the ECN value and the use of pure standards. APCI(-) generated the fragment deriving by the loss of a fatty acid from CE $[M-H-C_{27}H_{45}]^-=[FA-H]^-$ ion, followed by the respective formate adduct $[M+HCOO-C_{27}H_{45}]^-=[FA+HCOO]^-=[FA+45]^-$ ion. Thus, combining the information obtained by APCI spectra acquired using both (+) and (-) mode, the complete identification of CEs was possible. A comparison of ESI and APCI mass spectra of a CE standard (Chol-C18:2) is shown in Figure VI-7.

6.3.3. Lipidomics analysis of plasma sample by UHPLC-Q MS

The blood lipidome is a complicated mixture of different lipid classes, which vary in FAs composition (Lísa, *et al.*, 2011). Most of the FAs are bound as esters, with only small amounts occurring as non-esterified fatty acids. Retention times and pattern fragmentations of each lipid standard, in (+) and (-) ion mode, by using both interfaces, were considered for accurate lipid identification in plasma sample.

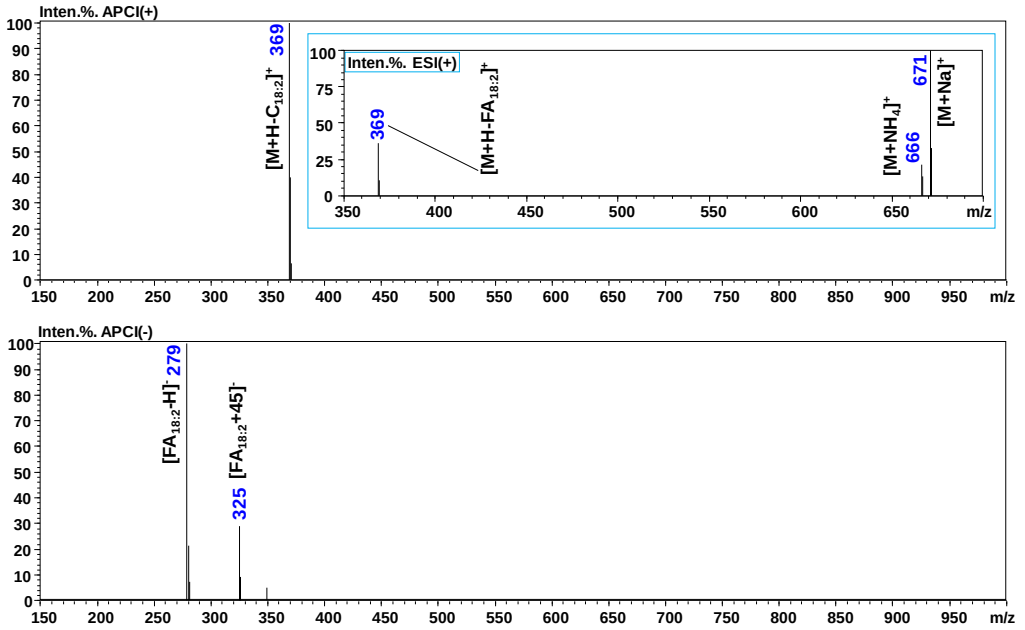

Figure VI-7. *Full mass spectra of CE-18:2 standard by using APCI(+) (a) and APCI(-) (b). The ESI(+) spectrum of the same CE-18:2 standard is reported as insert in Figure 7a.*

The lipid extract from human plasma was analyzed by using the described UHPLC-Q MS method. Total ion chromatograms acquired using both APCI(+) and APCI(-) are shown in Figure VI-8. A list of all the identified lipids is reported in Table VI-4.

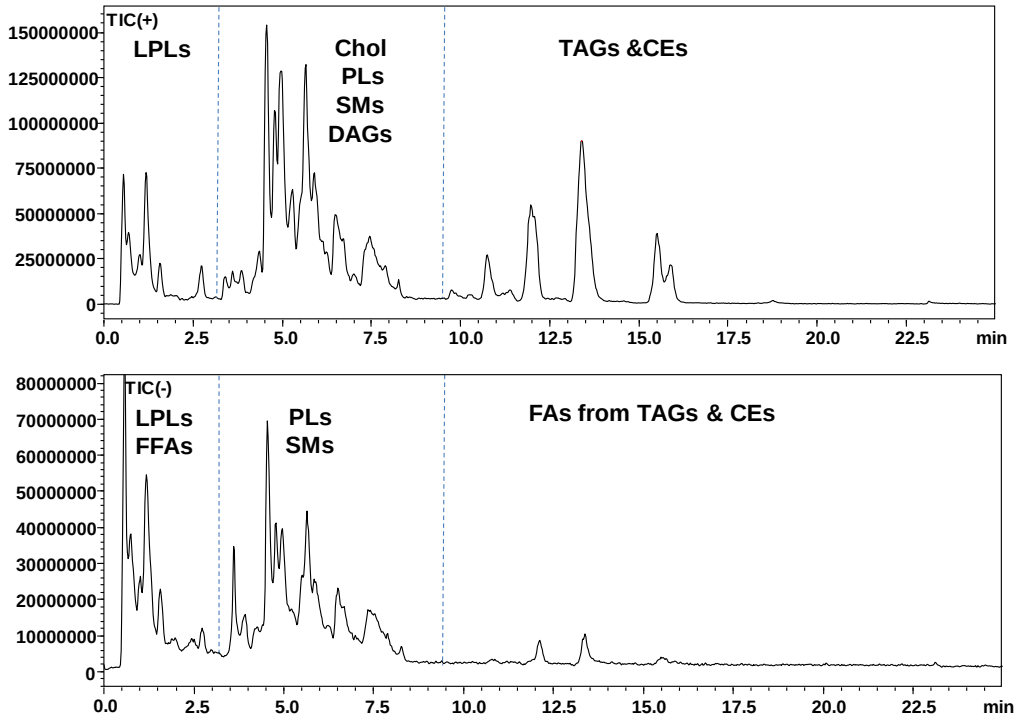

Figure VI-8. *Total ion chromatograms of both APCI(+) (a) and APCI(-) (b).*

Table VI-4. *Lipids indentified in human plasma extract by RP-UHPLC-Q MS.*

No.	ECN	r_T	Lipid	$[M+H]^+$	$[M+X]^+$	$[M+H-H_2O]^+$	$[M-H]^-$	$[M+X]^-$
1	12	0.95	LPC-20:4	544	566[a]			588[c]
2	14	1.02	LPC-18:2	520	542[a]			564[c]
3	16	1.21	LPC-16:0	496	518[a]			540[c]
4	16	1.28	LPC-18:1	522	544[a]			566[c]
5	18	1.56	LPC-18:0	524	546[a]			568[c]
6	10	1.73	FFA-22:6				327	372[c]
7	10	1.75	FFA-20:5				301	346[c]
8	14	1.87	FFA-16:1				253	298[c]
9	12	1.91	FFA-20:4				303	348[c]
10	14	2.01	FFA-18:2				279	324[c]
11	16	2.39	FFA-16:0				255	300[c]
12	16	2.52	FFA-18:1				281	326[c]
13	18	3.26	FFA-18:0				283	328[c]
14	30	3.59	PI-18:0_20:4	887	909[a]/970[b]/904[d]		885	930[c]
15	30	3.85	SM-34:2	701	723[a]			745[c]
16	28	4.27	PE-18:1_20:4	766	788[a]/849[b]		764	
17	26	4.32	PC-16:0_20:5	738	760[a]/821[b]		736	

18	26	4.35	PC-18:1_20:5					
19	28	4.43	PE-18:2_18:2	740	762[a]/823[b]		738	
20	30	4.47	PE-18:0_20:4	768	790[a]/851[b]		766	
21	32	4.51	SM-34:1	703	725[a]			747[c]
22	26	4.60	PC-16:0_22:6					
23	26	4.63	PC-18:1_22:6					
24	32	4.73	SM-36:2	729	751[a]			773[c]
25	28	4.78	PC-16:0_20:4	782	804[a]			826[c]
26	28	4.82	PC-18:1_20:4	808	830[a]			
27	30	4.86	PE-16:0_18:2	716	738[a]/799[b]		714	
28	30	4.98	PE-18:1_18:2	742	764[a]/825[b]		740	
29		5.02	Chol			369		
30	28	5.05	PC-18:0_20:5					
31	30	5.15	PC-16:0_18:2	758	780[a]			802[c]
32	30	5.18	PC-18:1_18:2					
33	30	5.27	PC-16:0_20:3	784	806[a]			828[c]
34	28	5.38	PC-18:0_22:6					
35	30	5.66	PC-18:0_20:4	810	832[a]			854[c]
36	32	5.78	PC-18:2_18:0	786	808[a]			830[c]
37	32	5.90	PC-16:0_16:0	734	756[a]			778[c]
38	32	5.97	PC-18:1_16:0	760	782[a]			804[c]

39	30	6.10	PC-20:4_18:0	810	832[a]			854[c]
40	32	6.13	PC-18:1_18:1	786	808[a]			830[c]
42	32	6.34	PC-20:3_18:0	812	834[a]			856[c]
41	34	6.40	PC-18:0_18:1	788	810[a]			832[c]
	36	6.59	SM-38:1	759	781[a]			803[c]
43	36	6.59	SM-42:3	811	833[a]			855[c]
44	36	6.63	SM-40:2	785	807[a]			829[c]
45	32	6.71	DAG-16:0_16:0		591[a]	551		
46	32	6.71	DAG-18:1_16:0		617[a]	577		
47	34	7.01	DAG-18:0_16:0		619[a]	579		
		7.31	SM-39:1	773	795[a]			817[c]
48	37	7.31	SM-41:2	799	821[a]			843[c]
49	38	7.51	SM-42:2	813	835[a]			857[c]
		7.80	PC-18:0_18:0	790	812[a]			
50	38	7.97	SM-40:1	787	899[a]			831[c]
51	39	8.26	SM-41:1	801	823[a]			845[c]
52	40	8.32	SM-42:1	815	837[a]			859[c]
53	42	9.61	TAG-18:2_18:1_12:0	801	823[a]/818[d]			
54	42	9.61	TAG-18:1_14:0_12:0	749	771[a]/766[d]			
55	42	9.75	TAG-18:2_18:2_18:2	879	901[a]/896[d]			

56	42	9.75	TAG-18:2_16:1_16:1	827	849[a]/844[d]
57	42	9.75	TAG-18:2_18:2_16:1	853	875[a]/870[d]
58	42	9.89	TAG-20:4_16:0_14:0	827	849[a]/844[d]
59	42	10.27	TAG-20:4_18:2_16:0	879	901[a]/896[d]
60	42	10.27	TAG-20:4_18:1_18:2	905	927[a]/922[d]
61	44	10.45	TAG-18:1_18:1_12:0	803	825[a]/820[d]
62	44	10.45	TAG-18:1_16:0_14:1	803	825[a]/820[d]
63	44	10.78	TAG-18:1_18:2_14:0	829	851[a]/846[d]
64	44	10.78	TAG-18:1_18:1_14:1	829	851[a]/846[d]
65	44	10.78	TAG-18:1_16:1_16:1	829	851[a]/846[d]
66	44	10.78	TAG-18:2_16:0_16:1	829	851[a]/846[d]
67	44	10.78	TAG-20:2_16:1_14:0	829	851[a]/846[d]
68	44	10.78	TAG-20:2_16:1_16:1	855	877[a]/872[d]
69	44	10.78	TAG-20:3_16:0_16:1	855	877[a]/872[d]
70	44	10.78	TAG-18:1_18:2_16:1	855	877[a]/872[d]
71	44	10.78	TAG-18:1_18:3_16:0	855	877[a]/872[d]
72	44	10.78	TAG-20:2_16:1_16:1	855	877[a]/872[d]
73	44	10.78	TAG-18:1_18:1_18:3	881	903[a]/898[d]
74	10	10.96	CE-20:5		693[a]/688[d]
75	10	11.17	CE-22:6		719[a]/714[d]

76	44	11.43	TAG-20:4_18:1_16:0	881	903[a]/898[d]
77	44	11.43	TAG-20:4_18:1_18:1	907	929[a]/924[d]
78	46	11.85	TAG-18:1_16:0_14:0	805	827[a]/822[d]
79	46	11.85	TAG-18:1_18:1_14:0	831	853[a]/848[d]
80	46	11.85	TAG-18:1_16:0_16:1	831	853[a]/848[d]
81	46	11.85	TAG-20:2_16:0_16:1	857	879[a]/874[d]
82	46	11.85	TAG-18:1_18:2_16:0	857	879[a]/874[d]
83	46	11.85	TAG-18:1_18:1_16:1	857	879[a]/874[d]
84	46	11.85	TAG-18:1_18:1_18:2	883	905[a]/900[d]
85	12	11.99	CE-18:3		669[a]/664[d]
86	12	12.23	CE-20:4		695[a]/690[d]
87	47	12.60	TAG-18:1_18:1_15:0	845	867[a]/862[d]
88	47	12.60	TAG-18:1_16:0_15:0	819	841[a]/836[d]
89	47	12.82	TAG-16:0_16:0_15:0	793	815[a]/810[d]
90	14	13.24	CE-18:2		671[a]/666[d]
91	48	13.43	TAG-18:1_18:1_16:0	859	881[a]/876[d]
92	48	13.46	TAG-18:1_18:1_18:1	885	907[a]/902[d]
93	48	13.66	TAG-18:1_16:0_16:0	833	855[a]/850[d]
94	48	13.87	TAG-16:0_16:0_16:0	807	829[a]/824[d]
95	48	13.87	TAG-18:0_16:0_14:0	807	829[a]/824[d]

96	49	14.38	TAG-18:1_17:0_16:0	821	843[a]/838[d]
97	16	15.39	CE-18:1		673[a]/668[d]
98	16	15.81	CE-16:0		647[a]/642[d]
99	18	18.79	CE-18:0		675[a]/670[d]

[a][M+Na]$^+$; [b][M+H+Na+C_3H_8O]$^+$; [c][M+HCOO]$^-$; [d][M+NH4]$^+$.

APCI interface allowed the formation of diagnostic fragment ions for all classes of lipid in both (+) and (-) ion modes (except for FFAs where the only $[M-H]^-$ was observed by using both interfaces), reducing the number of misidentification that can occur considering only related molecular ions. On the top of Figure VI-9, a mass scan spectrum at 11.86 min of RP-UHPLC-ESI(+)-MS analysis of plasma sample is reported. It is evident the coelution of several TAGs with the same ECN=46. In fact, four different pairs of *m/z* $[M+X]^+$ (where X = NH_4^+; Na^+) values, namely, 822/827 (C48:1), 848/853 (C50:2), 874/879 (C52:3), 900/905 (C54:4) were present. From these, according to the combination of most common FAs present in human plasma sample into glycerol backbone (Salivo, *et al.*, 2015), 30 different TAGs could be tentatively identified, not considering the occurrence of positional isomers (on the right of Figure VI-9). On the bottom of the same figure, the same mass scan spectrum at 11.86 min obtained using the APCI(+) interface is reported. The presence of fragment $[M+H-R_{sn\text{-}1/2/3}COOH]^+=[M+H-FA_{sn\text{-}1/2/3}]^+$ ions (corresponding to different $[DAG_{(s)}-H_2O]^+$ species) and the combination with their protonated molecular $[M+H]^+$ ions (corresponding to different TAG species), allowed to confirm the identity of only 7 TAGs out of 30 previously hypothesized (marked in red on the right of Figure VI-9). APCI(+) provided informative spectra, with a protonated molecular ion and fragment ions, which allowed structural elucidation (bottom of Figure VI-9).

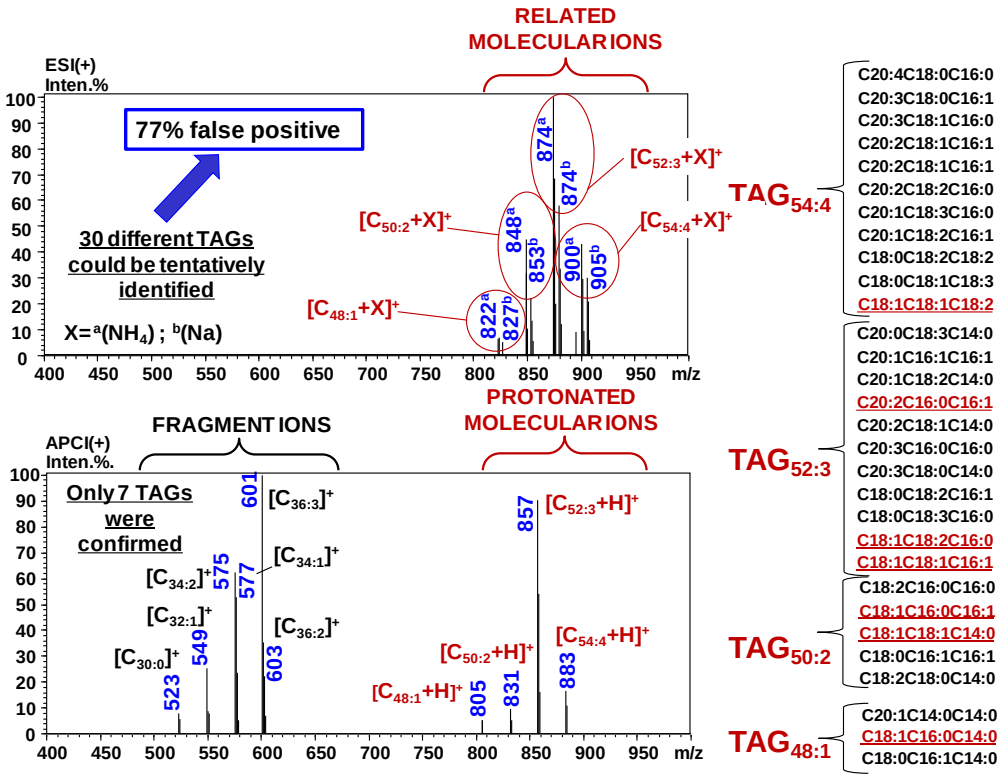

Figure VI-9. *On the top, a mass scan spectrum at 11.86 min of RP-UHPLC-ESI-Q MS analysis of human plasma extract. On the bottom, a mass scan spectrum at the same time analysis by RP-UHPLC-APCI-Q MS of human plasma extract. On the right, the list of 30 different TAGs tentatively identified by ESI(+) and, marked in red, the 7 TAGs confirmed by APCI(+) out of 30 previously hypothesized.*

In (-) mode, less used in this research field, APCI generated important structural information, in particular in cholesterol esters and glycerophospholipids, eliminating some potential ambiguity in identification of possible isobaric fragment ions, generated by positive-ion mode. In Figure VI-10 the mass spectra by APCI(+/-) of PI compound (PI-18:0_20:4) identified in human plasma is reported. As for other PLs, the use of two polarities (+/-) was needed to obtain unambiguous information on the structure. Although, all ions generated from the analysis of phospholipids standards with APCI interface

were previously discussed, only the ions with a ratio greater than or equal to 30% compared to the base peak were considered for the identification (with some exceptions, such as the fragment ions related to the loss of FA and/or FA as ketene, or in the case where all fragment ions are below 30%).

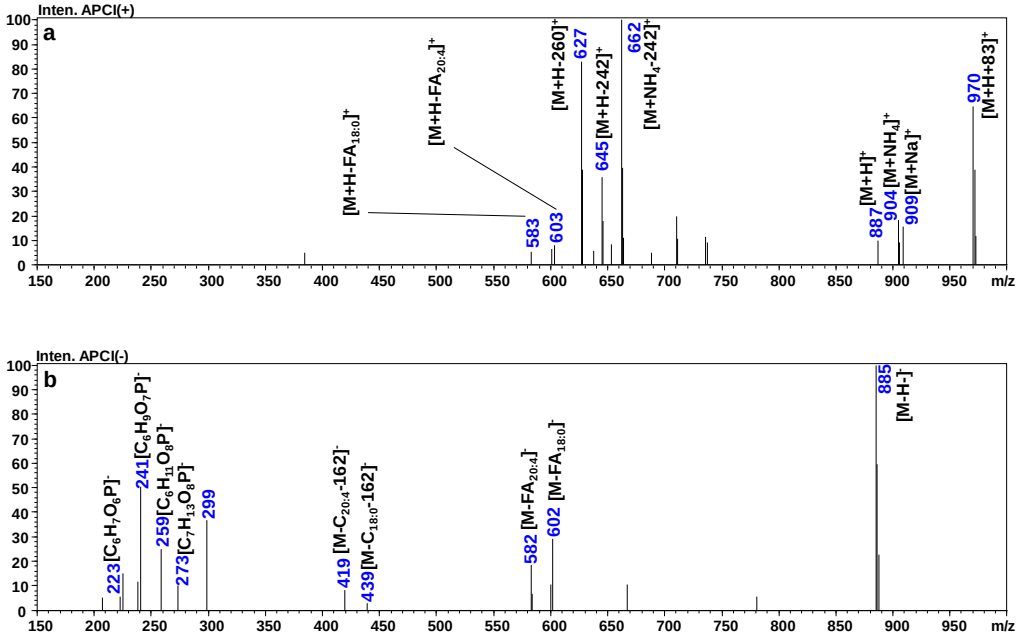

Figure VI-10. *Full mass spectra of PI-38:4 from human plasma extract (PI-18:0_20:4) by APCI(+) (a) and APCI(-) (b) are reported.*

About 100 lipid species from 10 lipid classes, namely FFA, LPC, SM, PI, PE, PC, DG, Chol, CE, and TAG have been positively identified in total lipid extracts of human plasma in 25 min analysis time. The propose method proved to be very powerful. For instance, considering the PL profile, no loss of information (in terms of number of compounds identified) was observed, compared to a multidimensional approach (Dugo, *et al.*, 2013). Moreover, the analysis time was 14 times faster, including re-equilibration time (25 min *vs* 360 min).

6.4. Conclusions

The proposed method can be considered a comprehensive platform for lipidomics studies. A flow rate compatible with both ESI and APCI interfaces was used without any chromatographic conditions modification (i.e. mobile phase composition and/or flow-rate). Although the sensitivity of APCI-MS is usually less than ESI-MS when a buffer is added in the mobile phase, the structural information to be gleaned from the fragmentation is well worth the trade off in sensitivity. However, in some case, ESI is an indispensable complement to APCI when lipids containing oxygen functional group are investigated or for confirming related molecular ions, generally less expressed by APCI. LC-APCI-Q MS can be a valid, simple, and cheaper technique easily reproducible elsewhere for lipidomics studies, which can provide almost similar information compared to more sophisticated techniques, as LC-ESI-HRMS and/or multidimensional LC-ESI-MS.

Moreover, at the best of our knowledge, this is the first time that mass spectra of PS and PI were reported and discussed by using APCI interface.

REFERENCES

- Aguennouz M., Beccaria M., Purcaro G., Oteri M., Micalizzi G., Musumesci O., Ciranni A., Di Giorgio R.M., Toscano A., Dugo P., Mondello L., J. Chromatogr. B 2016, 1029, 157-168.

- Anjani K., Lhomme M., Sokolovska N., Poitou C., Wisnewsky J.A., Bouillot J.L., Lesnik P., Bedossa P., Kontush A., Clement K., Dugail I., Tordjman J., J. Hepatology 2015, 62, 905-912.

- Astarita G., LC-GC North Am. 2012, 30, 482-487.

- Baiocchi C., Medana C., Dal Bello F., Giancotti V., Aigotti R., Gastaldi D., Food Chem. 2015, 166, 551-560.

- Beccaria M., Costa R., Sullini G., Grasso E., Cacciola F., Dugo P., Mondello L., Anal. Bioanal. Chem. 2015, 407, 5211-5225.

- Beccaria M., Sullini G., Cacciola F., Donato P., Dugo P., Mondello L., J. Chromatogr. A 2014, 1360, 172-187.
- Byrdwell W.C., Borchman D., Ophthalmic Res. 1997, 29, 191-206.
- Byrdwell W.C., Lipids 2001, 36, 327-346.
- Byrdwell W.C., Rapid Comm. Mass Spectrom. 1998, 12, 256-272.
- Cacciola F., Donato P., Beccaria M., Dugo P., Mondello L., LC-GC Europe 2012, 25, 15-24.
- Cai S.S., Sayge J.A., Anal. Chem. 2006, 78, 1191-1199.
- Cajka T., Fiehn O., Trends in Anal. Chem. 2014, 61, 192-206.
- Chernushevich I.V., Loboda A.V., Thomson B.A., J. Mass Spectrom. 2001, 36, 849-865.
- Dugo P., Fawzy N., Cichello F., Cacciola F., Donato P., Mondello L., J. Chromatogr. A 2013, 1278, 46-53.
- Fahy E., Subramaniam S., Brown H.A., Glass C.K., Merrill A.H., Murphy R.C., Raetz C.R., Russell D.W., Seyama Y., Shaw W., Shimizu T., Spener F., van Meer G., VanNieuwenhze M.S., White S.H., Witztum J.L., Dennis E.A., J Lipid Res. 2005, 46, 839-861.
- Folch J., Lees M., Sloane Stanley G.H, J. Biol. Chem. 1957, 226, 497-509.
- Hannun Y.A., Eur. J. Lipid Sci., 2015, 117, 1814-1821.
- Holčapek M., Jirasko R., Lisa M., J. Chromatogr. A 2012, 1259, 3-15.
- Hsu F.F., Turk J., J. Am. Soc. Mass Spectrom. 2000, 11, 986-999.
- Hsu F.F., Turk J., J. Am. Soc. Mass Spectrom. 2003, 14: 352-363.
- Hsu F.F., Turk J., J. Am. Soc. Mass Spectrom. 2005, 16, 1510-1522.
- Imbert L., Gaudin M., Libong D., Touboul D., Abreu S., Loiseau P.M., Laprevote O., Chaminade P., J. Chromatogr. A 2012, 1242, 75-83.
- Karlsson A.A., Michelsen P., Larsen A., Odham G., Rapid Commun. Mass Spectrom. 1996, 10, 775-780.
- Karlsson A.A., Michelsen P., Odham G., J. Mass Spectrom. 1998, 11, 437-449.
- Kerwin J.L., Tuiniga A.R., Ericsson L.H., J. Lipid Research 1994, 35, 1102-1114.

- Lisa M., Cifkova E., Holčapek M., J. Chromatogr. A 2011, 1218, 5146-5156.
- Lytle C.A., Gan Y.D., White D.C., J. Microbiol. Methods 2000, 41, 227-234.
- Metabolomics Fiehn Lab:
http://fiehnlab.ucdavis.edu/staff/kind/Metabolomics/MS-Adduct-Calculator/,
Edited by T. Kind (2010).
- Ovčačíková M., Lísa M., Cífková E., Holčapek M., J. Chromatogr. A 2016, 1450, 76-85.
- Qiu D.F., Xiao X.Y., Eur. Mass Spectrom. 1999, 5, 151-156.
- Quehenberger O., Armando A.M., Brown A.H., Milne S.B., Myers D.S., Merrill A.H., Bandyopadhyay S., Jones K.N., Kelly S., Shaner R.L., Sullards C.M., Wang E., Murphy R.C., Barkley R.M., Leiker T.J., Raetz C.R.H., Guan Z., Laird G.M., Six D.A., Russell D.W., McDonald J.G., Subramaniam S., Fahy E., Dennis E.A., J. Lipid Res. 2010, 51, 3299-3305.
- Řezanka T., Sigler K., Curr. Anal. Chem. 2007, 3, 252-271.
- Salivo S., Beccaria M., Sullini G., Tranchida P., Dugo P., Mondello L., J. Sep. Sci. 2015, 38, 267-275.
- Sandra K., dos Santos Pereira A., Vanhoenacker G., David F., Sandra P., J. Chromatogr. A 2010, 1217, 4087-4099.
- Uran S., Larsen A., Jacobsen P.B., Skotland T., J. Chromatogr. B 2001, 758, 265-275.

CHAPTER VII
Impact of ultra performance convergence chromatography coupled to time-of-flight mass spectrometry on lipid analysis: applications to triacylglycerol fingerprinting in edible oils

7.1. Introduction

Triacylglycerols are the main constituents of vegetable oils, determining the functionalities of these food ingredients and also the physiological effects exerted from the dietary intake of essential fatty acids. For these reasons, the analysis of intact triglyceride fraction in oils without pre-saponification is able to provide typical fingerprints for their characterization, and furthermore may be used to assess the quality and the authenticity of different oils. However, the wide variety of TAGs makes their analysis difficult, because of the complexity of FAs. Differing in the carbon numbers, numbers of double bonds, and *cis-/trans*-configuration, hundreds of natural FAs have been identified so far in nature. Moreover, various positional isomers of TAGs are formed when natural FAs esterify the glycerol backbone in different stereo chemical positions, namely *sn*-1, *sn*-2 or *sn*-3 position. The task of TAG profiling has been reviewed widely in the literature (Buchgraber, *et al.*, 2004; Laakso, 1996). Various chromatographic techniques have been used for TAG separation, including HPLC, TLC, GC and SFC. Due to low volatility of TAGs, they are not generally analyzed by GC; furthermore the high temperatures required (about 360 °C) may cause the degradation of long-chain polyunsaturated fatty acids (PUFAs) and reduce the lifetime of the capillary GC column. In contrast, the chromatographic separation of intact TAGs performed by HPLC is operated at mild temperatures, alleviating degradation issues. At present, two HPLC methods have been successfully employed to attain detailed information on

TAG and FA composition of natural samples, namely NARP-LC and silver ion LC (Ag^+-LC) (Acheampong, *et al.*, 2011; Dobson, *et al.*, 1995; Holčapek, *et al.*, 2005). NARP-LC employs silica based stationary phases linked to C18 chains, whereas silver ion chromatography (SIC) uses the cation-exchange stationary phases impregnated with Ag^+ ions. Taking into account that TAGs are not soluble in water, the use of organic solvents is indispensable in both techniques. In NARP-LC mode, TAGs are separated according to acyl chain lengths and the degree of unsaturation. The separation is governed by the so-called partition number (PN), which is calculated from the total carbon number of the fatty acid chain, minus twice the total double bond number (ΣCN – 2 DB). This approach can be applied even for very complex samples containing tens to hundreds of TAGs species (Baiocchi, *et al.*, 2015; Beccaria, *et al.*, 2014; Dugo, *et al.*, 2012; Holčapek, *et al.*, 2003). Ag^+-LC is widely used for the separation of TAGs containing DBs due to the formation of week reversible charged-transfer complexes between the π electrons of DBs and Ag^+ immobilized of the stationary phase (Nikolova-Damyanova, 2009). In this case, TAGs are separated according to the number (Christie, 1988; Schuyl, *et al.*, 1998), position (Laakso & Voutilainen, 1996) and geometry (Adlof, *et al.*, 2002; Adlof & List, 2004) of DBs. The retention of TAGs increases with the increasing number of DBs, and TAG regioisomers can also be separated under optimized chromatographic conditions (Adlof & List, 2004; Adlof, 1995; Février, *et al.*, 2001; Macher & Holmqvist, 2001; Kalo, *et al.*, 2003). However, it should be noted that, generally, Ag^+-LC has a poorer reproducibility and a lower selectivity of saturated TAGs compared with NARP-LC. Besides, both HPLC methods share some drawbacks such as the use of toxic solvents and the relatively long run times (typically from 50 min to 200 min). Recently, SFC has received extensive attention for its excellent performance in analysing TAGs in oil samples (Lee, *et al.*, 2012; Bernal, *et al.*, 2013; Lesellier & Tchapla, 1999;

Sandra, *et al.*, 2002; Lee, *et al.*, 2014), thanks to its unique selectivity, faster separations, low consumption of organic solvents and the improvements in instrumentation. When addressing the task of lipid analysis, main benefits of SFC over other chromatographic approaches consist in the absence of a derivatization step (often used before GC analyses), the potential coupling to universal detectors (such as FID, ELSD, and MS), a high resolution per unit of time (compared to HPLC). Furthermore, this technique is well suited for the analysis of such compounds that are highly soluble in organic solvents. UPC^2 represents an evolution of SFC, combining the use of CO_2 with (sub)-2 μm particle columns, is complementary and may be a preferred technique to GC and LC, in terms of speed and reproducibility of analysis.

The main purpose of this study is to develop a high-throughput method to get the profiling of TAGs in different vegetable oils, in which the hyphenation to mass spectrometry (UPC^2-MS) enables new ways of separating non-polar lipids with substantial advantages over conventional LC methods. In the context of this research, the potentiality of ion mobility spectrometry was also investigated. The technique delivers an additional dimension of separation, based on molecular size, shape and *m/z*. Mobility separation is orthogonal to both chromatography and mass spectrometry, and permits to improve the peak capacity and selectivity of an analytical method.

7.2. Experimental section

7.2.1. Samples and chemicals

This research was carried out on 5 different vegetable oils, varying in their TAG composition and complexity, i.e. extra virgin olive oil, peanut oil, corn oil, soybean oil, and borage oil. All samples were diluted to ca. 100 ppm in 2-propanol. Acetonitrile, and methanol, both Optima LC/MS grade, were purchased from Thermo Fisher Scientific (Milan, Italy); LC grade ethanol and

LC-MS grade 2-propanol were obtained from Sigma-Aldrich (Milan, Italy). CO_2, 99.99% purity, was a product of the Tirino Gas Vari di Di Carlo Roberto (Messina, Italy).

7.2.2. Instrumentation and analytical conditions

Separations were performed on an Acquity UPC^2 instrument (Waters Corp., Manchester, England), consisting of a convergence manager with an automatic backpressure regulator, a sample manager fixed-loop, a binary solvent manager and a column manager. The final method for TAGs analyses used the following conditions: Ascentis Express C18 column (100 mm × 3 mm I.D., 2 μm d_p, (Supelco, Bellefonte, PA); flow rate, 1.5 mL/min; injection volume, 2 μL; column temperature, 20 °C; active back pressure regulator (ABPR) pressure, 1500 psi; the mobile phase consisted of pure CO_2 (solvent A) and acetonitrile (solvent B). The elution gradient was: 0 min, 5% B, 20 min, 30% B, 23 min, 30% B. The UPC^2 instrument was connected with the mass spectrometer via the APCI interface, in positive ion mode. The hybrid quadrupole-traveling wave ion mobility-time of flight mass spectrometer Synapt G2-Si HDMS (Waters Corp., Manchester, England), in high resolution mode, was used in the mass range *m/z* 100-1200 with the following setting of tuning parameters: source temperature, 120 °C; probe temperature, 400 °C; desolvation gas flow (N_2), 400 L/h; corona current, 4 μA; sampling cone, 40 V. Leucine enkephaline was used as the lock mass for all experiments.

Conditions for ion mobility experiments were as follows: IMS gas flow rate (N_2), 90 mL/min, IMS wave velocity, 501 m/s, and wave height, 40 V. Typical acquisition of an ion mobility experiment consisted of 200 bins with each bin having a mobility drift time of 50 μs (10 ms for a complete ion mobility experiment). ToF MS data were acquired and analyzed with MassLynx V4.1 SCN916 software, while IMS data were processed with DriftScope 2.7 (Waters)

7.3. Results and discussion

7.3.1. Optimization of chromatographic conditions

The chromatographic conditions were optimized to separate each individual TAG compound with good resolution within a reasonable analysis time. Different modifiers including 2-propanol, ethanol, methanol, acetonitrile, and acetonitrile/methanol (1:1, *v/v*) were evaluated. The best results were obtained using the solvent mixture CO_2/ACN, with a linear gradient elution mode. It is well known that pressure is an important factor on the density of supercritical CO_2. The setting of backpressure obviously influences the eluotropic strength of supercritical fluid. An optimal backpressure of 1500 psi was selected for the UPC^2 analysis. In order to improve the separation, two different chromatographic columns were tested, including Acquity UPC^2 HSS C18 SB (100 mm × 3 mm I.D., 1.8 μm d_p, Waters) and Ascentis Express C18 (100 mm × 3 mm I.D., 2 μm d_p, Supelco). The latter resulted in a better resolution, especially for some critical pairs (e.g., OOO+POO PN 48, OLO+PLO PN 46), and in a shorter analysis time (reduced by 50%), as shown in Figure VII-1. Furthermore, it is possible to note changes of elution order for some TAGs and in particular for the more polar diacylglycerols (DAGs); these compounds are eluted after the TAGs (NP-like) on the Acquity column, while on the Ascentis they are the first to elute (RP-like). This difference could be linked to the different carbon load, and then to the residual silanol activity of the two stationary phases, which is greater for the Acquity column. The latter has a non end-capped phase, in contrast to the first one.

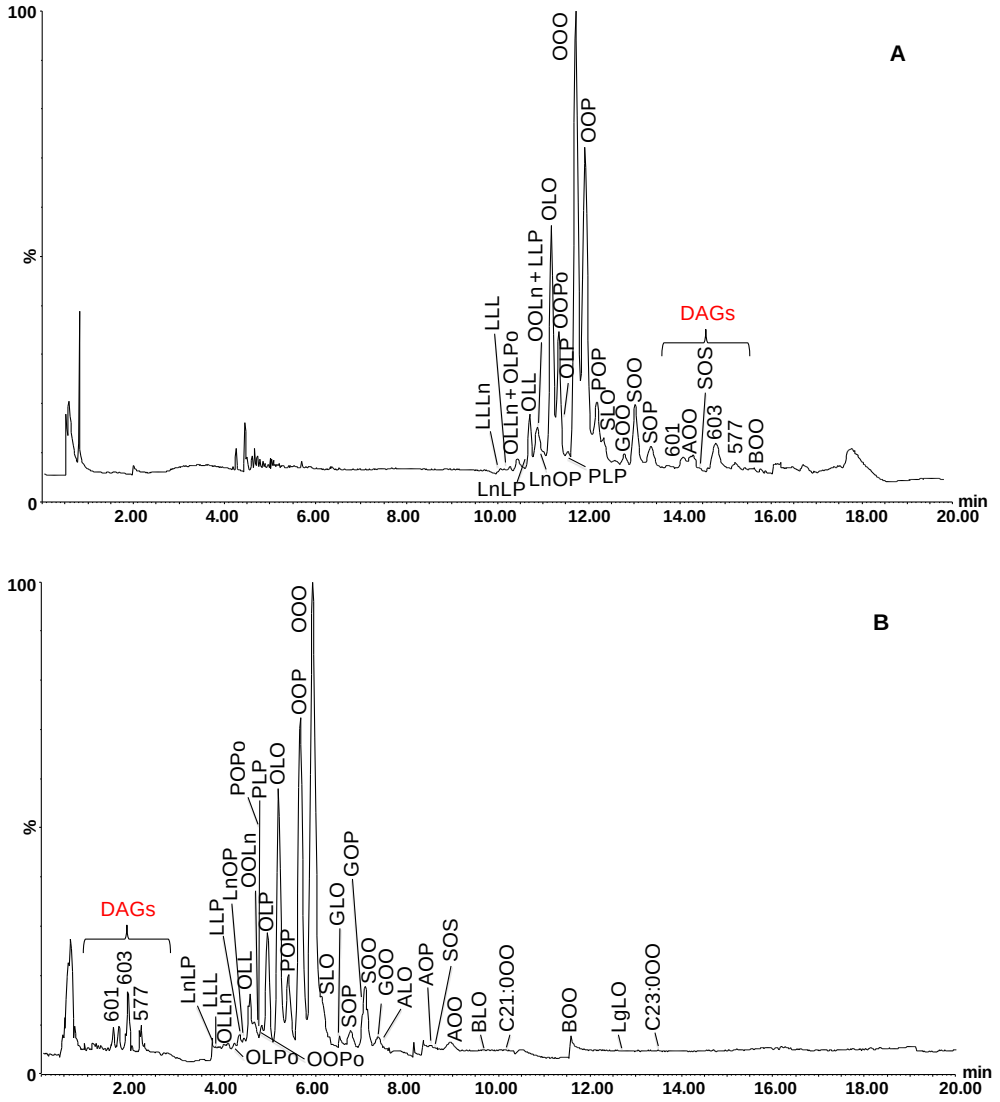

Figure VII-1. *UHPSFC-APCI-MS chromatograms of TAGs in extra virgin olive oil on Acquity UPC² HSS C18 SB column, 100 mm ×3.0 mm, 1.8 µm (A), and Ascentis Express C18 column, 100 mm ×3.0 mm, 2 µm (B).*

7.3.2. Chromatographic separation and identification of triacylglycerols

As shown in Figure VII-2 and Table VII-1, 79 individual TAGs were separated under the optimized UPC²-ToF MS conditions. The elution order of such compounds follows the increasing PN, reflecting the relation between CNs and

DBs in acyl chains, like in NARP-LC. As can be seen, TAGs are eluted within 10 min gradient, according to their increasing hydrophobicity, with a calculated PN number ranging from 36 to 56 for the more complex borage oil sample. The retention behaviour of TAGs within one single PN group is strongly influenced by the FA composition in individual TAGs, mainly by the unsaturation degree and acyl chain lengths. TAG retention, within one PN group, increases with increasing DB number in the acyl chains. Despite the short analysis time, the separation for all the samples was satisfactory, except for the borage oil where some co-elutions still occur. However the identification of the co-eluted peaks was mainly based on the accurate mass data.

In the samples analyzed, TAGs have been identified using positive ion APCI-MS based on protonated molecules $[M+H]^+$ and sodium/lithium adducts $[M+Na+Li]^+$, used for the molecular weight assignment, and fragment ions $[M+H-R_iCOOH]^+$, formed by cleavage of FAs from the glycerol backbone, used for the identification of individual FAs. The standard notation of TAGs uses initials of FA trivial names, listed in the order of *sn*-1, *sn*-2, and *sn*-3. Since an achiral approach cannot differentiate *sn*-1 and *sn*-3 enantiomers, we regarded them as equivalent and arranged them in the order of decreasing molecular weight (Lísa & Holčapek, 2008). The FA in *sn*-2 position, instead, can be determined because the neutral loss of FA from the inner position is less favoured compared to *sn*-1 and *sn*-3 positions and thus it produces fragment ions of lower intensity. Considering that in nature regioisomers are present in mixtures and relative abundances of fragment ions resulted from fragment ions of all isomers, only predominant FAs in the *sn*-2 position are defined. According to literature data, unsaturated FAs, mainly linoleic acid, preferentially occupy the *sn*-2 position in plant oils (Lísa & Holčapek, 2008).

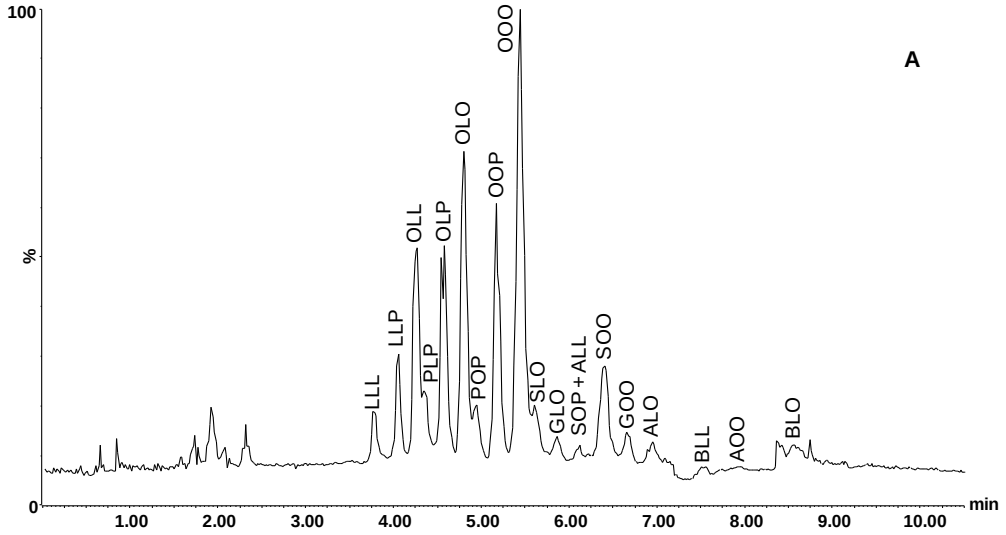
100
%
0
A
LLL
LLP
PLP
OLL
OLP
OLO
POP
OOP
OOO
SLO
GLO
SOP + ALL
SOO
GOO
ALO
BLL
AOO
BLO
1.00
2.00
3.00
4.00
5.00
6.00
7.00
8.00
9.00
10.00
min

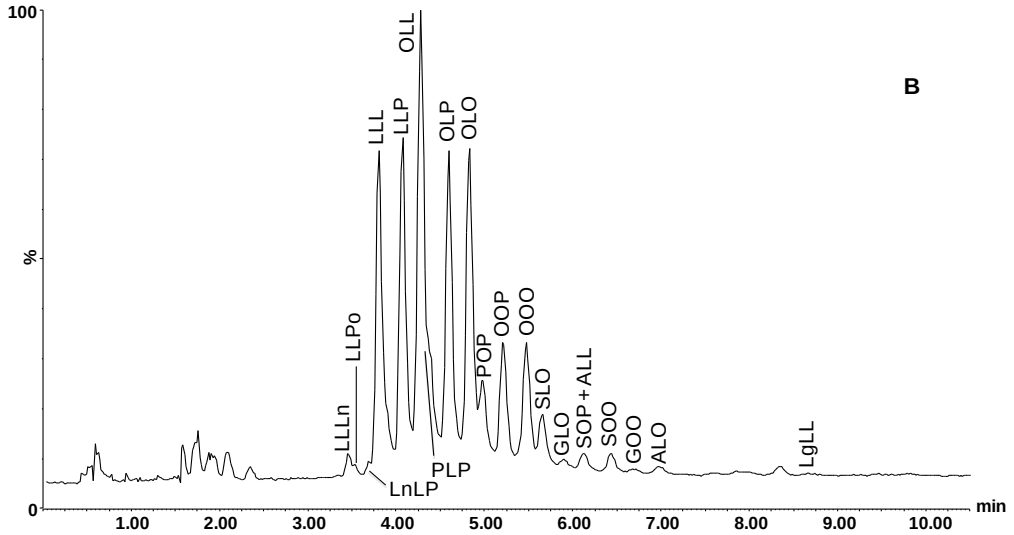
100
%
0
B
LLLn
LLPo
LnLP
PLP
LLL
LLP
OLL
OLP
OLO
POP
OOP
OOO
SLO
GLO
SOP + ALL
SOO
GOO
ALO
LgLL
1.00
2.00
3.00
4.00
5.00
6.00
7.00
8.00
9.00
10.00
min

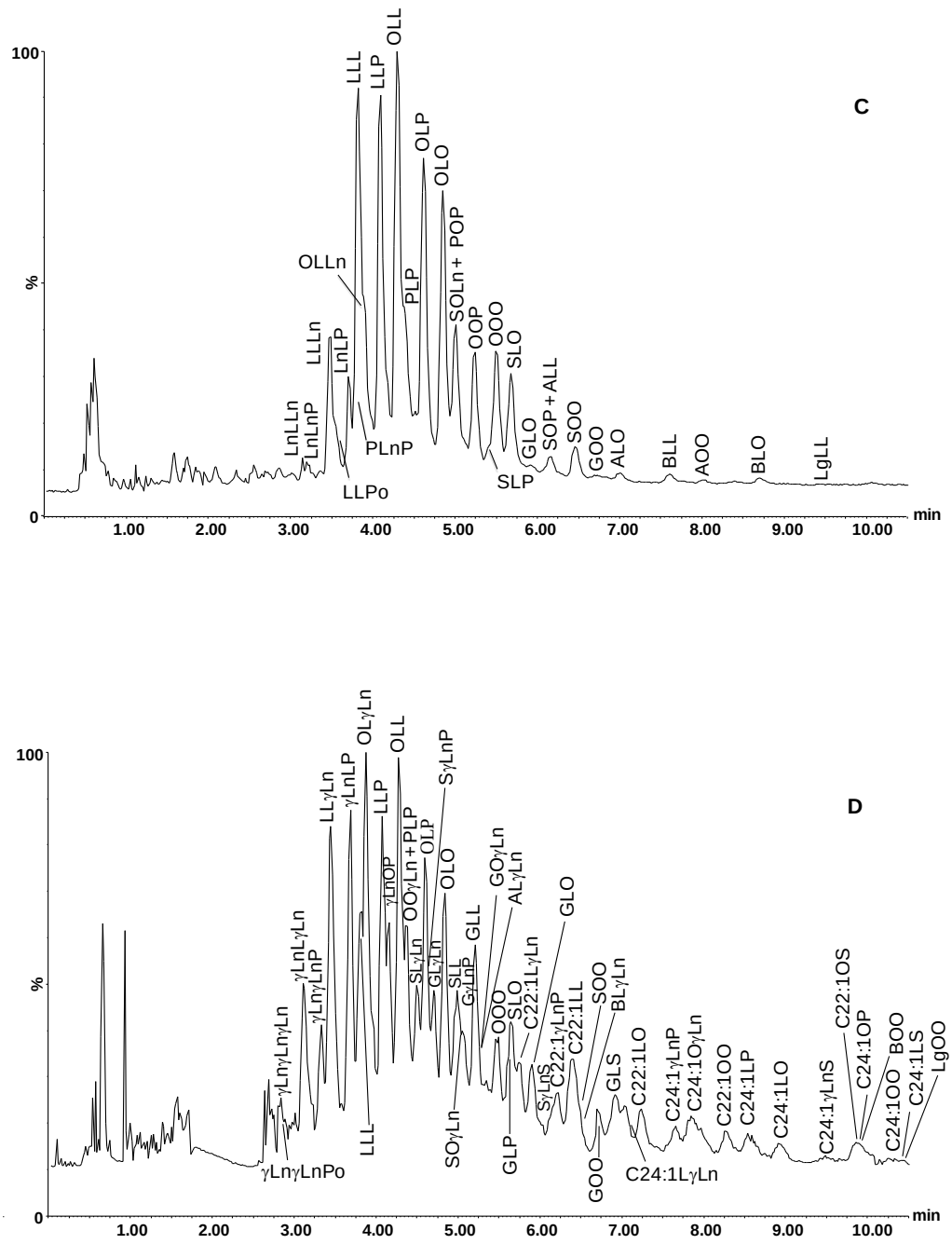

Figure VII-2. *UHPSFC-APCI-MS analysis of peanut oil (A), corn oil (B), soybean oil (C), and borage oil (D).*

Table VII-1. *TAGs identified in the vegetable oils analyzed. The PN value, DB and experimental m/z are also reported.*

N°	TAGs	PN	DB	$[M+H]^+_{exp}$	Peanut	Corn	EVOO	Soybean	Borage
1	γLnγLnγLn	36	9	873.6983					*
2	γLnγLnPo	38	7	849.6981					*
3	LnLLn	38	8	875.7129				*	
4	γLnLγLn	38	8	875.7130					*
5	LnLnP	40	6	851.7136				*	
6	γLnγLnP	40	6	851.7138					*
7	LLLn	40	7	877.7291		*		*	
8	LLγLn	40	7	877.7294					*
9	LLPo	42	5	853.7295		*		*	
10	LnLP	42	5	853.7293		*	*	*	
11	γLnLP	42	5	853.7294					*
12	PLnP	44	3	829.7292				*	
13	LLL	42	6	879.7441	*	*	*	*	*
14	OLLn	42	6	879.7450			*	*	
15	OLγLn	42	6	879.7451					*
16	OLPo	44	4	855.7445			*		
17	LLP	44	4	855.7453	*	*	*	*	*
18	LnOP	44	4	855.7448			*		
19	γLnOP	44	4	855.7450					*
20	OLL	44	5	881.7599	*	*	*	*	*

21	OOLn	44	5	881.7598			*		
22	OOγLn	44	5	881.7599					*
23	POPo	46	2	831.7442			*		
24	PLP	46	2	831.7446	*	*	*	*	*
25	OOPo	46	3	857.7599			*		
26	SLγLn	44	5	881.7598					*
27	OLP	46	3	857.7599	*	*	*	*	*
28	SγLnP	46	3	857.7599					*
29	GLγLn	44	6	907.7762					*
30	OLO	46	4	883.7765	*	*	*	*	*
31	SLL	46	4	883.7757					*
32	SOLn	46	4	883.7758				*	
33	SOγLn	46	4	883.7759					*
34	POP	48	1	833.7599	*	*	*	*	
35	GγLnP	46	4	883.7749					*
36	GLL	46	5	909.7916					*
37	GOγLn	46	5	909.7915					*
38	ALγLn	46	5	909.7917					*
39	OOP	48	2	859.7758	*	*	*	*	
40	SLP	48	2	859.7760				*	
41	OOO	48	3	885.7920	*	*	*	*	*
42	GLP	48	3	885.7918					*

43	SLO	48	3	885.7923	*	*	*	*	*
44	C22:1LγLn	46	6	935.8071					*
45	GLO	48	4	911.8072	*	*	*	*	*
46	SγLnS	48	3	885.7916					*
47	C22:1γLnP	48	4	911.8069					*
48	ALL	48	4	911.8070	*	*		*	
49	SOP	50	1	861.7913	*	*	*	*	
50	C22:1LL	48	5	937.8229					*
51	GOP	50	2	887.8069			*		
52	SOO	50	2	887.8073	*	*	*	*	*
53	BLγLn	48	5	937.8227					*
54	GOO	50	3	913.8230	*	*	*	*	*
55	GLS	50	3	913.8227					*
56	ALO	50	3	913.8227	*	*	*	*	
57	C24:1LγLn	48	5	963.8384					*
58	C22:1LO	50	4	939.8383					*
59	BLL	50	4	939.8389	*	*		*	
60	C24:1γLnP	50	4	939.8385					*
61	C24:1OγLn	50	5	965.8539					*
62	AOP	52	1	889.8230			*		
63	SOS	52	1	889.8232			*		
64	AOO	52	2	915.8382	*	*	*	*	

65	C22:1OO	52	3	941.8539					*
66	C24:1LP	52	3	941.8538					*
67	BLO	52	3	941.8540	*	*	*	*	
68	LgLL	54	3	969.8857		*		*	
69	C24:1LO	52	4	967.8695					*
70	C24:1γLnS	52	4	967.8697					*
71	C21:0OO	53	2	929.8539			*		
72	C22:1OS	54	2	943.8699					*
73	C24:1OP	54	2	943.8697					*
74	BOO	54	2	943.8699			*		*
75	C24:1OO	54	3	969.8862					*
76	C24:1LS	54	3	969.8858					*
77	LgLO	54	3	969.8859			*		
78	C23:0OO	55	2	957.8861			*		
79	LgOO	56	2	971.9009					*

7.3.3. IMS separation of triacylglycerols

The combination of retention times, MS and MS/MS spectra allows to identify the sample components, except than in the presence of co-eluting, isobaric compounds which would also render indistinguishable MS/MS spectra obtained upon collision. On the other hand, the mobility of an ion passing through the IMS assembly and governed by the size, shape and *m/z* can afford further separation. In Figure V-3 is reported the UPC^2-IM-MS analysis of an extra virgin olive oil sample. In the case presented, two TAGs, *viz.* OLP and OOPo with the same PN and the same protonated molecular ion, are chromatographically co-eluted.

With additional selectivity provided by IMS drift time, we were able to assign fragment ion spectra, at a given drift time and a chromatographic retention time, to the precursor ion. This resulted in much cleaner fragment ion spectra making structural elucidation possible, as illustrated in Figure V-3.

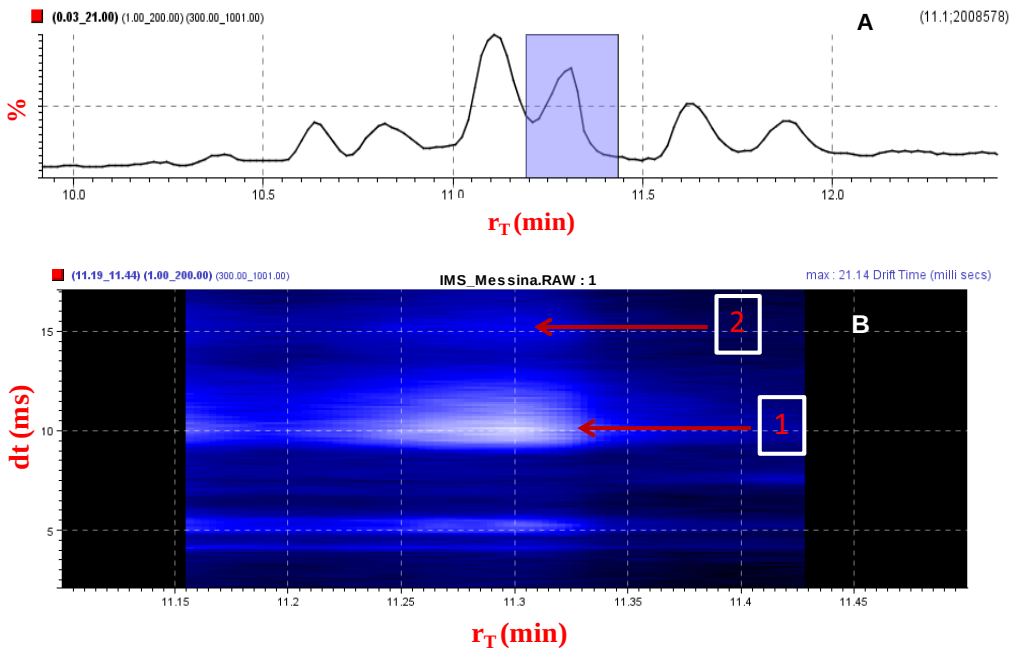

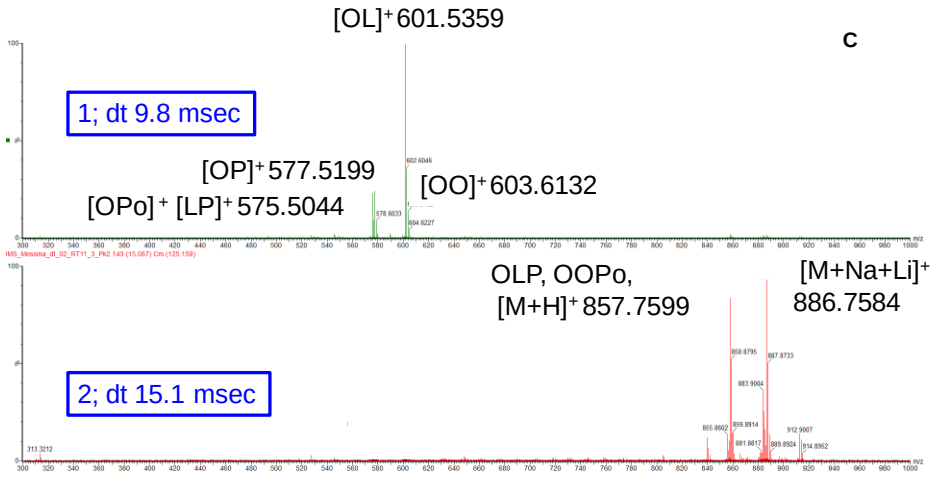

Figure VII-3. *UPC^2-IM-MS analysis of an extra virgin olive oil: (A) enlargement of the chromatogram with ion mobility separation turned on; (B) corresponding driftogram (drift time vs.r_T); (C) spectra of co-eluting TAGs.*

Figure V-4 shows the UPC^2-IM-MS analysis of borage oil. As can be noted, for TAGs species IMS distribution is very similar, and it is critical to obtain structural insight without any preliminar chromatographic separation. However, the combination of the retention times, MS spectra, together with the additional drift times, gives supplementary insight into the identity of the compounds of interest.

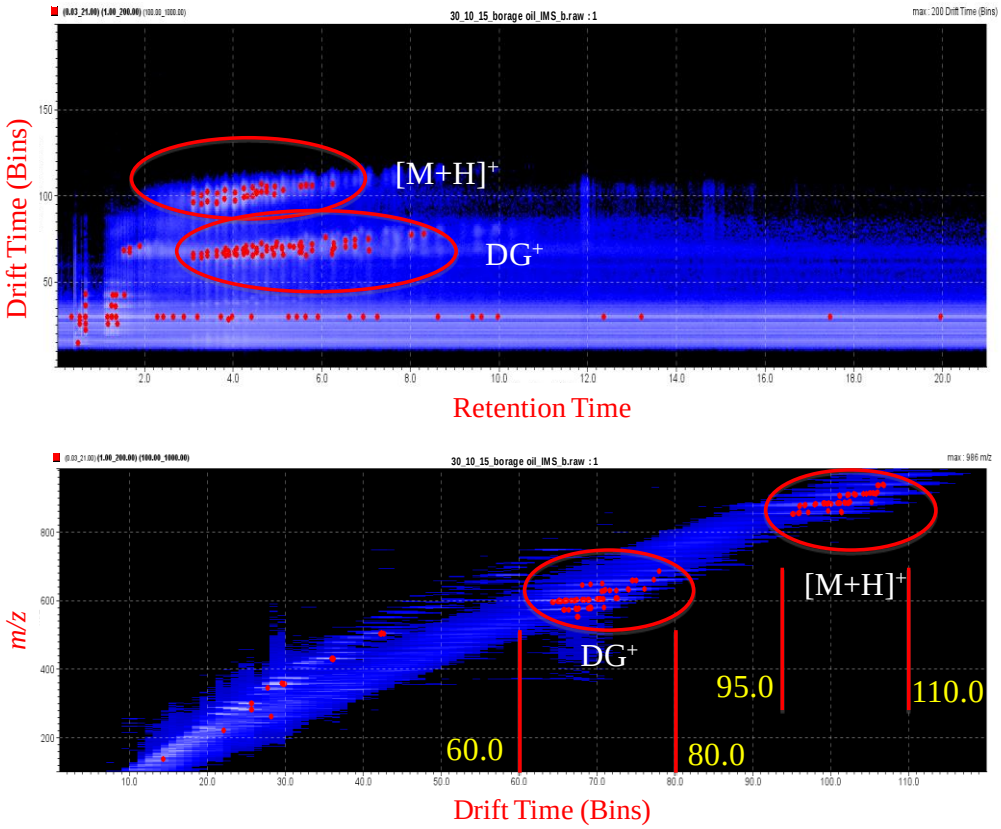

Figure VII-4. *UPC^2-IM-MS plots of borage oil: (A) drift time vs.r_T; (B) m/z vs. drift time.*

7.4. Conclusions

From the perspective of current applied lipid research, UPC^2 enabling new ways of separating non-polar lipids. Good resolution was achieved on a single end-capped C18 column, in as little as 10 min analysis time, for the separation of TAGs in a variety of vegetable oils with excellent repeatability (average retention time CV 0.21%). While the number of positive identifications was comparable to what reported in the literature, run time was drastically reduced (up to >10 times) and also the organic solvent consumption (up to >30). Remarkably, the use of APCI interface alleviates the need for a post-column make-up solvent/pump, retaining the advantages of less toxic, environmental-

friendly technique.

REFERENCES

- Acheampong A., Leveque N., Tchapla A., Heron S., J. Chromatogr. A 2011, 1218(31), 5087-5100.
- Adlof R., List G., J. Chromatogr. A 2004, 1046, 109-113.
- Adlof R.O., J. High Resolut. Chromatogr. 1995, 18, 105-107,
- Adlof R.O., Menzel A., Dorovska-Taran V., J. Chromatogr. A 2002, 953, 293-297.
- Baiocchi C., Medana C., Dal Bello F., Giancotti V., Aigotti R., Gastaldi D., Food Chem. 2015, 166, 551-560.
- Beccaria M., Sullini G., Cacciola F., Donato P., Dugo P., Mondello L., J. Chromatogr. A 2014, 1360, 172-187.
- Bernal J.L., Martìn M.T., Toribio L., J. Chromatogr. A 2013, 1313, 24-36.
- Buchgraber M., Ulberth F., Emons H., Anklam E., Eur. J. Lipid Sci. Technol. 2004, 106, 621-648.
- Christie W.W., J. Chromatogr. 1988, 454, 273-284.
- Dobson G., Christie W.W., Nikolova-Damyanova B., J. Chromatogr. B 1995, 671, 197-222.
- Dugo P., Beccaria M., Fawzy N., Donato P., Cacciola F., Mondello L., J. Chromatogr. A 2012, 1259, 227-236.
- Février P., Binet A., Dufossé L., Grée R., Yvergnaux F., J. Chromatogr. A 2001, 923, 53-57.
- Holčapek M., Jandera P., Zderadička P., Hrubá L., J. Chromatogr. A 2003, 1010, 195-215.
- Holčapek M., Lísa M., Jandera P., Kabátová N., J. Sep. Sci. 2005, 28, 1315-1333.
- Kalo P., Kemppinen A., Ollilainen V., Kuksis A., Int. J. Mass Spectrom. 2003, 229, 167-180.
- Laakso P., Food Rev. Int. 1996, 12, 199-250.

- Laakso P., Voutilainen P., Lipids 1996, 31, 1311-1322.
- Lee J. W., Uchikata T., Matsubara A., Nakamura T., Fukusaki E., Bamba T., J. Biosci. Bioeng. 2012, 113, 262-268.
- Lee J.W., Nagai T., Gotoh N., Fukusaki E., Bamba T., J. Chromatogr. B: Anal. Technol. Biomed. Life Sci. 2014, 966, 193-199.
- Lesellier E., Tchapla A., Anal. Chem. 1999, 71, 5372-5378.
- Lísa M., Holčapek M., J. Chromatogr. A 2008, 1198-1199, 115-130.
- Macher M.B., Holmqvist A., J. Sep. Sci. 2001, 24, 179-185.
- Nikolova-Damyanova B., J. Chromatogr. A 2009, 1216, 1815-1824.
- Sandra P., Medvedovici A., Zhao Y., David F., J. Chromatogr. A 2002, 974, 231-241.
- Schuyl P.J.W., de Joode T., Vasconcellos M.A., Duchateau G., J. Chromatogr. A 1998, 810, 53-61.

CHAPTER VIII
Off-line multidimensional convergence chromatography/liquid chromatography-mass spectrometry for characterization of the pigment fraction in sweet bell peppers (*Capsicum annuum* L.)

8.1. Introduction

Carotenoids are an important class of naturally occurring pigments that are widely distributed in plant-derived foods and products. Although these compounds have been traditionally used in the food industry as colorants, nowadays, they attract great attention since they have been described to possess several important functional properties, mainly antioxidant activity (Beutner, *et al.*, 2001), as well as prevention of cardiovascular diseases (Arab & Steck, 2000; Rao & Rao, 2007), cancer (Nishino, *et al.*, 1999), and macular degeneration (Snodderly, 1995). Carotenoids are usually based on a C_{40}-tetraterpenoid skeleton and an extended conjugated double-bond system, which constitutes the light-absorbing chromophore, responsible for the functions mentioned above. This basic structure can undergo a number of modifications, such as cyclization in one or both ends, hydrogenation, dehydrogenation, addition of lateral groups, among others, resulting in an extremely wide group of compounds. Usually, these compounds are divided into two groups: hydrocarbons, generally known as carotenes (such as β-carotene, lycopene), and oxygenated compounds, named xanthophylls (e.g. β–cryptoxanthin, lutein) (Herrero, *et al.*, 2008; Cacciola, *et al.*, 2012). Carotenoids can be found in nature in their free form or in a more stable fatty acid esterified form, in the case of the oxygenated compounds. To simplify to some extent their analysis, a saponification procedure has been traditionally employed prior to the

carotenoid analysis, so that all the compounds could be transformed in their free form. Although this saponification step also acts as a clean-up procedure, some drawbacks are found, mainly related to the formation of artifacts as well as to the carotenoid degradation (isomerization and other reactions can occur). Furthermore, as a result of the saponification step, information on the native carotenoids' composition of the studied samples is therefore lost. Thus, a better approach to carotenoid content is through classifying plant materials depending on a free or esterified xanthophylls profile. *Capsicum annuum* is a carotenogenic fruit: during ripening the transformation of the chloroplast into chromoplast occurs. Chlorophylls disappear and more and new carotenoids are formed. *Capsicum* species have capsanthin-capsorubin synthase that synthesizes two red pigments, capsanthin and capsorubin. During the fruits ripening process, esterification dramatically increases. *Capsicum* is one of the most popular vegetables and spices in the world (Mokhtar, *et al.*, 2015; Mokhtar, *et al.*, 2016). The native carotenoid composition in spicy chilli peppers has been extensively investigated (Minguez-Mosquera & Hornero-Mendez, 1994; Markus, *et al.*, 1999; Hornero-Mendez & Minguez-Mosquera, 2000; Schweiggert, *et al.*, 2005; Giuffrida, *et al.*, 2013; Cacciola, *et al.*, 2012) compared with the not spicy sweet bell peppers cultivars (Giuffrida, *et al.*, 2011).

The aim of this research was to further examine the chlorophyll and the native carotenoid composition in sweet bell peppers by developing an off-line multidimensional chromatographic approach comprised of a UPC^2 system, combined with an RP-LC-PDA-MS system for direct identification of the carotenoids and chlorophylls in green, overripe yellow, and overripe red bell peppers' samples.

The separation of carotenoids has long been the subject of SFC (Giddings, *et al.*, 1968; Aubert, *et al.*, 1991; Lesellier, *et al.*, 1991; Lesellier, *et al.*, 1993; O'Neil & Schwartz, 1992; Sakaki, *et al.*, 1994; Tee & Lim, 1991) studies since its inception. The primary component of the mobile phase in SFC, CO_2, offers superior solubility for carotenoids and promotes non-polar interactions between carotenoids and the mobile phase, thereby reducing the retention time (Sakaki, *et al.*, 1994). In addition to high chromatographic efficiency rendered by the high diffusivity of CO_2, the mild temperatures used in SFC are advantageous by avoiding thermal degradation of carotenoids. The advantages of using such technique have been extensively described in chapter III. UPC^2 system, while adhering to the basic principles of SFC and considering a fast and green chromatographic technique, brings in the added advantage of a reduced system volume and better pressure control, resulting in greatly reduced run time, improved resolution, and increased detection sensitivity.

Coupling of UPC^2 and LC for a multidimensional separation of complex samples, a larger fraction of the separation space is produced. Moreover, the present study, also aimed to investigate and to compare the carotenoid stability and composition in overripe yellow and red bell peppers collected directly from the plant, thus also evaluating whether biochemical changes are linked to carotenoid degradation in the nonclimacteric investigated fruits, for the first time.

8.2. Experimental section

8.2.1. Chemicals

Carotenoid standards were all above 98% of purity, namely, β-carotene, lutein, β-cryptoxanthin, zeaxanthin, capsanthin, and were purchased from Extrasynthese (Genay, France), and violaxanthin, neoxanthin, antheraxanthin,

phytoene, and phytofluene were purchased from Sigma-Aldrich/Supelco (Milan, Italy). Chlorophyll a and b were purchased from Sigma-Aldrich/Supelco. The pheophytins were obtained by acid hydrolysis of the parent chlorophylls. All the carotenoid standards were stored protected from light at –18 °C. All the solvents used, namely, *n*-hexane (Hex), ethyl acetate (EtAc), EtOH, methyl *tert*-butyl ether (MTBE), and H_2O, were of HPLC grade and purchased from Sigma-Aldrich. The employed reagents and BHT (butylated-hydroxy-toluene) were obtained from Sigma-Aldrich. Carbon dioxide of N45 quality was from Air Liquide (Luik, Belgium).

8.2.2. Samples and sample preparation

Fresh samples of green, overripe yellow, green, and overripe red sweet bell peppers were supplied by a local producer, just after harvesting, which occurred the same day in the same field from plants of two different varieties producing yellow and red bell peppers. The samples were classified in four groups: G-Y (green bell peppers that after maturation would become yellow), Y (yellow bell peppers), G-R (green bell peppers that after maturation would become red), and R (red bell peppers).

The raw material was homogenized with a hand blender and 200-300 g of each sample was put into aluminum plates and frozen at –20 °C. Lyophilization of the samples was performed by an ING Brizio Basi BVF 6/R freeze-drier equipped with a BH814 vacuum pump at 0.05 Pa using a temperature program from –40 to 42 °C overnight. Carotenoid and chlorophyll extraction was performed using an aliquot of 0.5 g lyophilized sample extracted with 4 × 5 mL Hex (0.1% BHT) and 4 × 5 mL EtAc (0.1% BHT) consecutively. At every extraction step, the mixture was sonicated for 15 min at room temperature in dark room; after every extraction step the extract was centrifuged for 15 min at

3000 × *g* and the supernatant was filtered through a 0.45 μm syringe filter (Pall Life Sciences, Ann Arbor, MI, USA) and collected. Afterward, the collected supernatant was subjected to evaporation under vacuum until dryness and then re-suspended in a given volume of MTBE/MeOH (1:1, *v/v*).

8.2.3. Instrumentation and software

One-dimensional LC analyses were carried out on a Shimadzu Prominence LC-20A (Shimadzu, Milan, Italy), consisting of a CBM-20A controller, two LC-20AD dual-plunger parallel-flow pumps, a DGU-20 A5 degasser, an SPD-M20A photo diode array detector, a CTO-20AC column oven, a SIL-20A autosampler, and an LC-2010 mass spectrometer equipped with an APCI interface. Data acquisition was performed by Shimadzu LCMS solution software (v. 3.50 SP2).

Off-line multidimensional UPC^2/LC-MS analyses were performed on two different instruments. For ^{1}D analyses, an Acquity UPC^2 (Waters, Manchester, England) equipped with convergence manager with an automatic backpressure regulator, sample manager-FL, binary solvent manager, column manager, auxiliary column manager, and evaporative light scattering detector. Data acquisition was performed by Waters MassLynx V4.1 SCN916 software. For the ^{2}D analyses, the same system employed for 1D-LC analysis was used.

8.2.4. Analytical conditions

For LC-PDA-MS analyses, an YMC C30 column, 250 × 4.6 mm I.D. packed with 3 μm particles (YMC Europe, Dinslaken, Germany) was employed. The mobile phases consisted of MeOH/MTBE/H_2O (86:12:2, *v/v/v*; solvent A) and MeOH/MTBE/H_2O, (8:90:2, *v/v/v*; solvent B) with the following gradient: 0-60 min, 0-60% B; 60-70 min, 60-90% B; 70-100 min, 90% B; 100 min, 0% B. The

flow rate was 1.0 mL/min and the injection volume was 20 μL. The PDA spectra were acquired in the range of 250-700 nm, while the chromatograms were extracted at 450 nm (time constant: 0.025 s; sampling frequency: 40 Hz).
MS parameters (APCI both positive and negative) were as follows: *m/z* range, 350-1200; scan speed, 6000 u/s; nebulizing gas (N_2) flow rate, 2.5 L/min; event time: 600 ms; detector voltage, 1.6 kV; interface voltage, 1.6 kV (–), 1.35 (+); interface temperature, 450 °C; CDL (curved desolvation line) temperature, 350 °C; heat block temperature, 350 °C.
External standards quantitative determination of each compound was performed using all reference materials listed in Section 8.2.1, in the concentration range from 1 to 200 ppm at six concentrations levels. The results were obtained from the average of three determinations and are expressed as micrograms per gram raw material (dry weight), and the CV% was below 8% in all the LC measurements as reported in Table VIII-1. For those compounds where the standard was not available the quantitative analysis was performed by assuming valid the calibration curve determined by the standard of the most similar compound in terms of structure and chromophores, thus using when possible the reference standard of the same class of compound as indicated in Table VIII-2.
For off-line UHPSFC × RP-LC analyses, an Acquity HSS C18 SB (100 × 3 mm I.D., 1.8 μm d_p, Waters) column was employed as the ^{1}D with the mobile phase consisting of CO_2 (solvent A) and EtOH (solvent B). The flow rate was 1 mL/min with a working pressure of 150 bar. The injection volume was 2 μL. The gradient was as follows: 0 min, 2% B; 9 min, 20% B; and 10 min, 20% B. ELS detector conditions were as follows: nebulizer heating, drift tube 55 °C, gas pressure 2.8 bar.

For the ^{2}D separations, the same column and analytical conditions employed for LC-PDA-MS analyses were used. Fractions from the ^{1}D were collected in 1 mL of MTBE/Hex (50:50, *v/v*, 0.1% BHT); the solvent was evaporated by nitrogen stream then the dry sample was re-dissolved in MTBE/MeOH (50:50, *v/v*, 0.1% BHT) and transferred to the ^{2}D for the analyses.

Table VIII-1. *Parameters for the quantitative analysis based on external standards.*

Compound	Equation	R^2	LOD	LOQ	CV%
lutein	y=2233x-42.22	0.9962	0.06	0.18	7.5
capsantin	y=1807x+1242	0.9970	0.05	0.17	6.9
zeaxanthin	y=2355x+78.82	0.9994	0.09	0.30	7.7
β-cryptoxanthin	y=2297x-406.64	0.9995	0.10	0.33	4.2
β-carotene	y=3406x+125.7	0.9990	0.07	0.22	6.8
phytofluene	y=1524x-399.40	0.9969	0.16	0.54	7.6
violaxanthin	y=1522x+203.27	0.9974	0.02	0.07	6.9
neoxanthin	y=1201x+205.21	0.9926	0.03	0.11	6.1
antheraxanthin	y=1756x-131.95	0.9995	0.04	0.13	5.8
phytoene	y=2086x+270.92	0.9998	0.05	0.15	7.9
chlorophyll a	y=3160x+1487	0.9995	0.03	0.10	4.8
pheophorbide a	y=2932x+870.67	0.9998	0.06	0.20	6.3
pheophytin a	y=2578x+16876	0.9992	0.05	0.17	7.5

8.2.5. Statistical analysis

All analyses were performed in triplicate and the results were expressed as means ± SD. Precision expressed as coefficient of variation percentage (CV%) is reported in Table VIII-1. The results were analyzed using statistical software and means were accepted as significantly different at 95% confidence interval ($P < 0.05$).

8.3. Results and discussion

In this work, an off-line multidimensional UPC^2-LC-MS separation was developed for the pigments separation in extracts obtained from different sweet bell pepper samples, for the first time. The choice of such instrumentation is due to the high complexity of the extracts, which give several overlapping and co-eluting peaks in the conventional 1D RP-LC analysis. Figures VIII-1 shows the RP-HPLC profiles of the G-Y and G-R samples, while in Figure VIII-2 is reported the comparison of the proposed off-line 2D chromatographic analysis and the conventional RP-LC analysis for red bell pepper.

The eluted fractions from UPC^2 were collected and further analyzed by RP-LC with PDA and MS detection. Fractions from the ^{1}D were collected at three different times, I (4-6 min), II (6-7.75 min), and III (7.75-10 min), selected in function of the chromatographic profile, and transferred to the ^{2}D for the RP-LC analyses. Thanks to the very high reproducibility of the retention times on UPC^2 (RSD usually below 2%), it was possible to perform the collection of the fractions in blindness, without simultaneous detection. The general retention rules during SFC analysis, according to increasing polarity, are opposite to those observed in RP-LC. Despite the similarity of the stationary phases, the separation mechanisms provided by the two techniques employed in the off-line multidimensional approach resulted almost orthogonal.

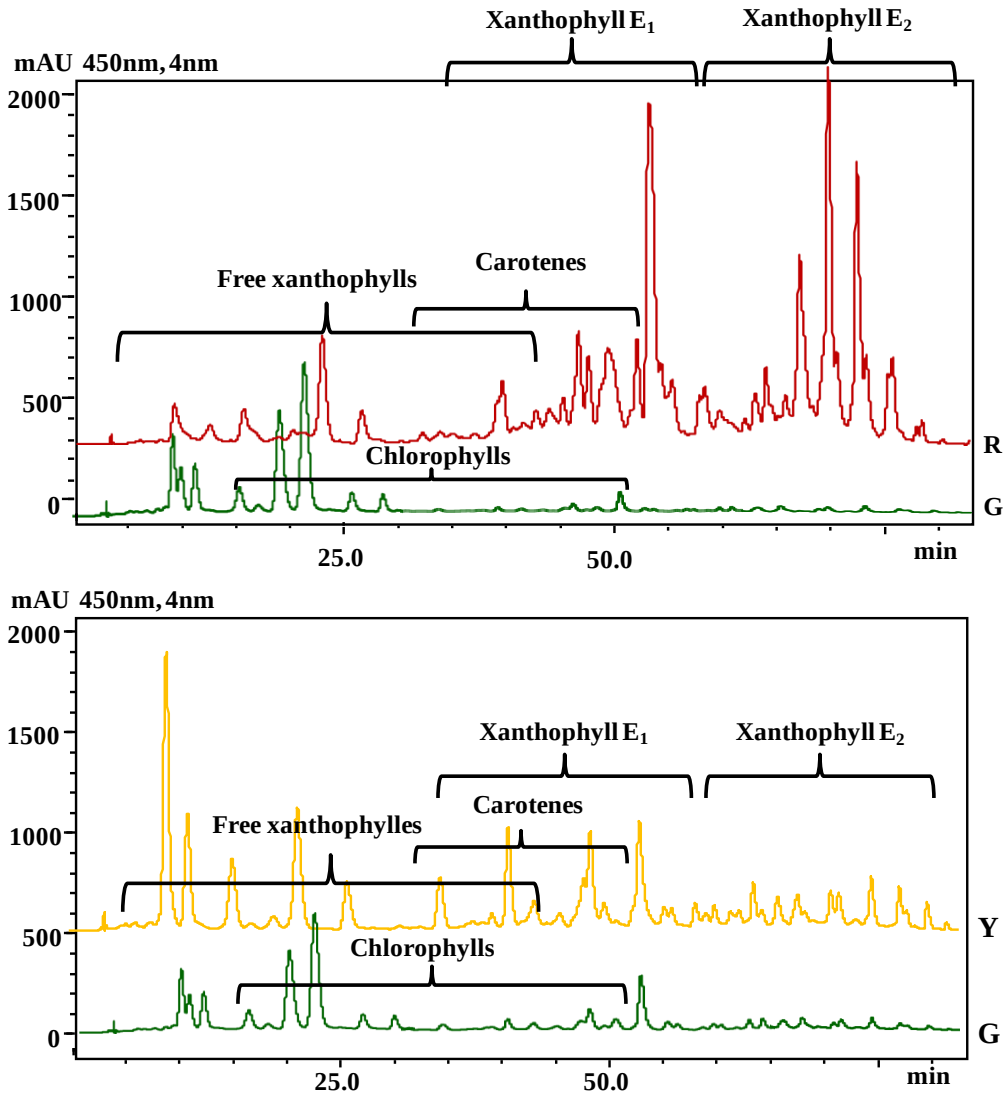

Figure VIII-1. *C30 HPLC chromatograms (450 nm) showing the pigments profile of: the green (G-Y) and yellow (Y) sweet bell pepper extracts (A); the green (G-R) and red (R) sweet bell pepper extracts (B).*
(E_1, xanthophylls monoesters; E_2, xanthophylls diesters).

As can be seen at the top of the Figure VIII-2, the analysis time in UPC^2 was dramatically reduced, with the first peak eluting at 4.65 min and the last peak at 9.05 min, and with average peak width measured as 0.16 min. In the same

Figure (middle: ^{2}D HPLC), the three respective second dimension C30 HPLC separations of the three selected transferred fractions, are shown; it is possible to note an increased peaks' resolution in the different ^{2}D analyses compared to the corresponding ^{1}D UPC^{2} insets, thanks to the overall much higher peak capacity of the multidimensional system. The off-line coupling UPC^{2}-RP-LC here reported allowed the determination of 115 pigment compounds, and 101 of them were positively identified by comparison of elution order, PDA, and MS data. In particular, five different classes were observed, namely, 24 xanthophylls, 9 chlorophylls and derivatives, 10 carotenes and derivatives, 22 xanthophyll monoesters, and 36 xanthophyll diesters. Tables VIII-2 and VIII-3 report the list of the pigments identified and quantified respectively in the four different sweet bell pepper samples. As indicated in Table VIII-3, the amount of the different classes of components greatly differs among the four samples.

Concerning the red variety, the green unripe G-R peppers were characterized by a very complex and abundant fraction of free xanthophylls (294 ppm), low amount of carotenes, and the total absence of xanthophylls esters, while the green pigments were really high (808 ppm). When the peppers become overripe the composition changes dramatically: carotenes increase to more than 100 ppm, free xanthophylls reduce to almost half of the initial amount (117 ppm), while mono- and diesters appear during ripening reaching extremely high values (more than 1000 ppm in total). On the other hand, the unripe G-Y sample presented about 170 ppm of free xanthophylls, 34 ppm of carotenes, and about 40 ppm of xanthophylls esters equally divided between mono- and diesters, while the amount of green pigments (chlorophylls and derivatives) was 380 ppm; the ripe yellow pepper showed significant variation in composition of all the classes of compounds with a total amount of free xanthophylls almost doubled (273 ppm), carotenes more than four times higher (135 ppm), the

monoesters doubled (47 ppm), and the diesters almost five times higher (125 ppm) than the green one, while as predictable chlorophylls decreased almost eightfold (46 ppm). Compared to previous work (Giuffrida, *et al.*, 2011), more than 30 pigments were identified in green peppers and almost 50 in yellow peppers.

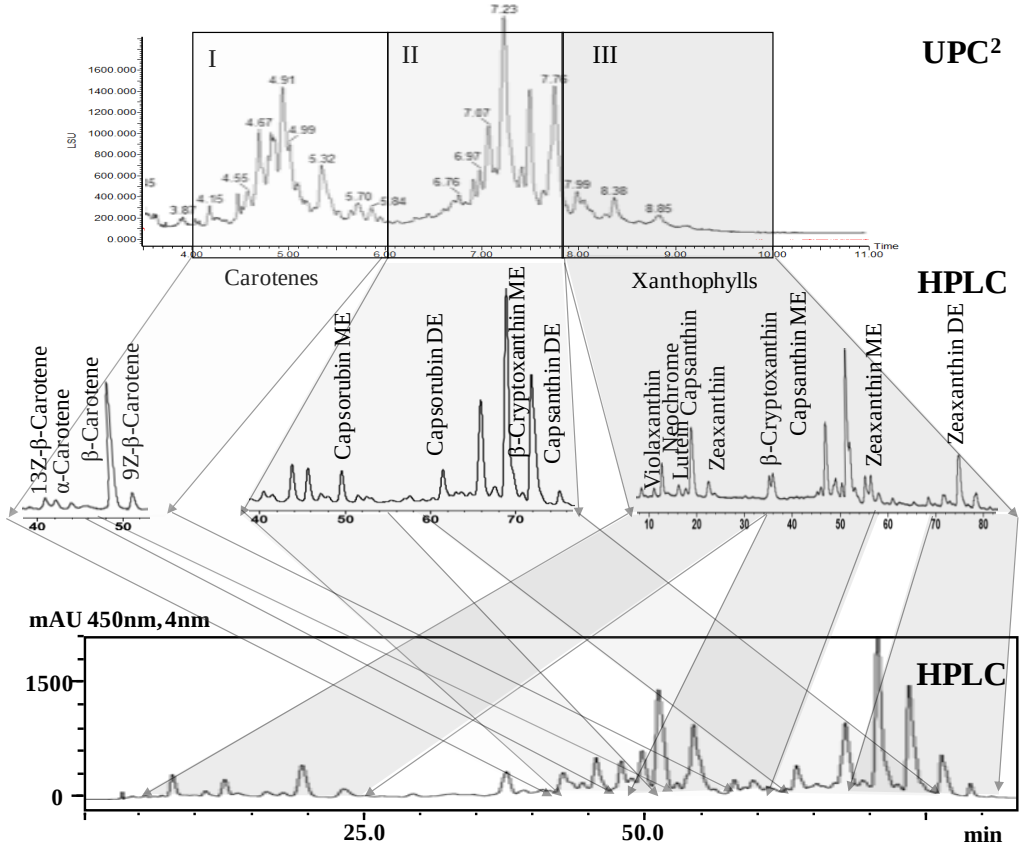

Figure VIII-2. *Off-line multidimensional UPC²/RP-LC of the red bell pepper extract. Top: ¹D UPC² chromatogram, with the insets showing the three selected fractions transferred to the ²D; middle: snapshot ²D RP-LC chromatograms of the transferred fractions; bottom: RP-LC chromatogram of the whole red bell pepper extract.*

Table VIII-2. *List of pigments identified in the four sweet bell peppers investigated.*

Peak	Pigment compound	t_r	λ_{max} (nm)	$[M-H]^-$	Y-G	Y	R-G	R
1	Neochrome	7.40	400 421 448	601 565				
2	Violaxanthin	7.94	417 441 470	601 583 565	X	X	X	X
3	Neoxanthin	8.88	414 436 464	601 583 565	X	X	X	
4	Neochrome	9.35	400 421 448	601 565	X	X	X	X
5	Lutein-5,6-epoxide	9.73	417 440 469	585 567 549		X		X
6	ni	10.22	336 413 437 464	601 583		X		X
7	13*Z*-Antheraxanthin	10.91	334 (415) 440 465	585 567		X		X
8	Luteoxanthin	11.60	399 421 448	601 583				X
9	8'*R*-Auroxanthin	11.98	380 401 426	601 583 565		X	X	
10	Antheraxanthin	12.64	(421) 445 473	585 567 549		X	X	X
11	13*Z*-Capsanthin	13.73	336 467	601 583				X
12	Auroxanthin	15.01	380 402 426	601 583 565		X		
13	ni	16.22	358 467	585 567				X
14	13*Z*-Lutein	16.38	329 417 437 465	569	X			
15	Chlorophyll b	16.47	317 345 468 553 603 652	907	X		X	

16	Mutatoxanthin	16.51	405 428 455	585 567	X	X	X	
17	Capsorubin	16.75	445 474 501	585				
18	Chlorophyll b’	17.01	317 345 468 553 603 652	907			X	
19	Lutein	17.98	418 446 472	569 551	X	X	X	X
20	Capsanthin	19.62	474	585				X
21	Chlorophyll a	21.40	338 411 432 544 587 603 666	893	X		X	
22	Zeaxanthin	23.31	(425) 450 477	569 551	X	X	X	X
23	Zeaxanthin type	26.87	(425) 450 477	569				
24	13 or 15*Z*-β-Cryptoxanthin	29.53	339 421 444 473	553		X	X	X
25	Phytoene	29.59	(278) 288 298	545	X	X	X	X
26	ni	29.68			X			
27	9*Z*-Zeaxanthin	29.76	337 445 471	569				
28	ni	29.91	(422) 448 467	755				X
29	9'*Z*-Zeaxanthin	31.24	338 445 472	569				
30	Phytofluene	33.12	334 348 368	543		X		
31	13*Z*-α-Carotene	34.52	329 416 440 466	537		X		
32	Curcubitaxanthin	37.10	(421) 446 473	584 566 532				X
33	β-Cryptoxanthin	37.40	(427) 450 476	553	X	X	X	X

34	ni	37.71	334 442 467					X
35	Phytofluene	37.72	334 348 368	543		X		X
36	15*Z*-β-Carotene	40.28	338 447 471	537		X		X
37	α-Cryptoxanthin	41.11	(420) 446 470	553				X
38	Pheophytin a type	41.87	410 505 535 609 666					
39	13*Z*-β-Carotene	42.38	337 446 469	537	X	X	X	X
40	13*Z*-Capsanthin-C12	43.19	339 357 (425) 450 (474)	767 749 567				X
41	Antheraxanthin-C12	44.12	420 445 473	767 749 567				X
42	Pheophytin a type	45.03	409 506 535 609 668					
43	α-Carotene	45.57	(422) 445 473	537	X	X	X	X
44	9*Z*-α-Carotene	45.92	331 418 441 469	537		X		
45	Cabsorubin monester	47.03	339 358 447 474	783 765 583				X
46	Capsorubin-C14	47.83	475	811 793 583				X
47	Pheophytin b'	48.16	435 530 600 656	884	X	X	X	
48	Pheophytin b	48.42	436 530 600 656	885	X	X	X	X
49	13*Z*-Capsanthin-C14	48.85	349 357 448 470	795 777 567				X
50	Pheophytin a'	49.54	409 505 535 609 666	872	X	X	X	X
51	Lutein-C12	49.73	421 445 473	751 733 551	X			

52	Capsanthin-C12	49.86	473	767 749 567				X
53	*E*-β-Carotene	51.24	(427) 452 477	537	X	X	X	X
54	Pheophytin a	51.60	410 505 535 609 665	872	X	X	X	X
55	Capsorubin-C16	52.07	476	839 583				
56	Antheraxanthin-C14	52.81	(421) 447 474	795 777 567		X		X
57	9*Z*-β-Carotene	53.64	336 (423) 447 473	537	X	X	X	X
58	ni	53.85				X		
59	Zeaxanthin-C12	54.02	(425) 450 477	751 733 551	X			
60	Lutein-C14	54.13	420 446 472	779 761 551	X			
61	Capsanthin-C14	54.28	471	795 777 567				X
62	Capsanthin-C14	54.92	471	795 777 567				X
63	ni	56.07	359 480					X
64	ni	56.62	(421) 447 474			X		
65	ni	56.90	(421) 447 474			X		
66	ni	57.42	(421) 447 474			X		
67	Zeaxanthin-C14	58.01	(423) 451 477	779 761 551	X			X
68	Antheraxanthin-C16	58.92	(423) 449 474	823 805 567				X
69	Capsanthin-C16	59.90	475	823 805 567				X

70	Capsanthin-C16	60.20	473	823 805 567				X
71	Pheophytin a type	60.59	410 506 536 609 665				X	
72	9*Z*-Lutein-C16	60.94	329 417 440 467	807 789 551	X			
73	β-Cryptoxanthin-C12	61.32	(427) 452 479	735 535		X		X
74	Capsanthin-2C10	61.83	474	893 549				X
75	13*Z*-Capsanthin-2C12	63.00	358 474	949 749 549				X
76	Antheraxanthin-2C12	63.75	(423) 450 475	949 749 549				X
77	Capsanthin-C10-C12	63.98	474	921 749 721 549				X
78	Capsanthin-C12-C10	64.54	473	921 749 721 549				X
79	β-Cryptoxanthin-C14	65.81	(426) 452 478	763 535	X	X		X
80	13*Z*-Capsanthin-C12-C14	67.19	356 457 480	977 777 749 549				X
81	Capsanthin-2C12	68.08	359 474	949 749 549				X
82	Lutein-2C12	68.27	422 447 472	933 733 533	X	X		
83	Capsorubin-C12-C14	68.29	479 (513)	993 793 765 565				X
84	Mutatoxanthin-C12-C14	68.92	405 427 453	977 777 749 549				X
85	9*Z*-β-Cryptoxanthin-C14	69.07	338 445 473	763 535		X		
86	Antheraxanthin-2C14	69.19	(423) 450 475	1005 777 549		X		
87	ni	69.34	446 471	791 535		X		

88	ni	69.44	336 423 448 474	932 733 533		X	
89	Zeaxanthin-2C12	69.61	(428) 451 479	933 733 533		X	
90	13*Z*-Zeaxanthin-C12-C14	69.81	337 440 469	961 761 733 533		X	
91	Lutein-C12-C14	69.92	421 445 472	961 761 733 533	X		
92	ni	70.04	457				X
93	Capsanthin-C12-C14	71.18	475	977 777 749			X
94	Capsorubin-2C14	71.33	360 480	1021 793 565			X
95	β-Cryptoxanthin-C16	72.01	(425) 448 476	791 535		X	X
96	Zeaxanthin-C12-C14	72.54	(422) 447 474	961 761 733 533		X	
97	Zeaxanthin-C12-C14	72.79	(422) 447 474	961 761 733 533		X	
98	9*Z*-Zeaxanthin-C12-C14	73.03	338 423 444 474	961 761 733 533		X	
99	Mutatoxanthin-2C14	73.21	405 427 452	1005 777 549			X
100	Lutein-2C14	73.64	(422) 447 474	989 761 533	X		
101	Capsanthin-2C14	74.18	476	1005 777 549			X
102	Capsanthin-C12-C16	74.52	476	1005 805 749 549			X
103	Auroxanthin-diester	74.96	380 401 426				
104	*Z*-Capsanthin-C16-C12	75.16	357 475	1005 805 749 549			X
105	13*Z*-Zeaxanthin-2C14	76.04	337 440 468	989 761 533		X	X

106	13Z-Zeaxanthin-2C14	76.68	337 440 468	989 761 533		X	
107	Zeaxanthin-2C14	77.01	(428) 451 479	989 761 533		X	X
108	9Z-Zeaxanthin-2C14	77.10	338 440 468	989 761 533		X	
109	Zeaxanthin-C12-C16	77.26	(426) 451 478	989 789 733 533		X	
110	Zeaxanthin-C12-C16	77.39	(426) 451 478	989 789 733 533		X	
111	Capsanthin-C14-C16	77.43	477	1033 805 777 549			X
112	Capsanthin-C16-C14	77.77	477	1033 805 777 549			X
113	Zeaxanthin-C14-C16	79.84	(425) 453 478	1017 789 761 533	X	X	X
114	9Z-Zeaxanthin-C14-C16	80.70	(425) 453 478	1017 789 761 533		X	
115	Zeaxanthin-2C16	81.57	(425) 452 479	1045 789 533	X	X	X

Remarkable, 23 xanthophyll esters were identified for the first time in yellow peppers and their presence could be due to the advanced ripened stage of the peppers tested, since they had not been previously reported (Giuffrida, *et al.*, 2011). The green peppers were characterized by the characteristic chloroplast pigments, chlorophylls, lutein, and neoxanthin that decreased in concentration with ripening. Both xanthophyll mono- and diesters were identified in green (only in the G-Y type) and yellow bell peppers for the first time. In particular, lutein-C14:0 and lutein-C12:0 and C14:0 were the main esters detected, although in a small percentage, in green bell peppers (only in the G-Y type), and antheraxanthin-C14:0, β-cryptoxanthin-C14:0, β-cryptoxanthin-C16:0 and antheraxanthin-C14:0 and C14:0, and zeaxanthin-C10:0 and C14:0 were the main esters detected in yellow bell peppers. Red bell peppers were characterized by pigments that are biosynthesized de novo during the red bell pepper ripening, namely capsanthin, capsorubin, and curcubitaxanthin, and the most representative esters were capsanthin esters of myristic acid. The results showed that the unripe fruit significantly differs in composition from the ripe one, and that the presence of carotenoid esters is correlated to the ripeness stage of the fruit.

Table VIII-3. *List of pigments quantified (µg/g) in the four sweet bell peppers investigated.*

Pigment compounds	Quantitative curve	Chemical Class	Y-G	Y	R-G	R
Free xanthophylls and derivatives						
Neoxanthin	Neoxanthin	TOME	12.11	76.64	22.36	15.10
Neoxanthin type	Neoxanthin	TOME	Tr	Tr	Tr	Tr
Violaxanthin	Violaxanthin	DODE	26.39	45.43	41.48	
Neochrome	Neoxanthin	TOMF	9.03	83.75	12.70	1.00
Lutein-5,6-epoxide	Violaxanthin	DODE		4.27		1.28
13*Z*-Antheraxanthin	Antheraxanthin	DOME		6.01		1.26
Luteoxanthin	Violaxanthin	DODF				1.02
8'*R*-Auroxanthin	Violaxanthin	DODF		5.60	9.30	
Antheraxanthin	Antheraxanthin	DOME		1.52	13.34	13.07
13*Z*-Capsanthin	Capsanthin	DOMK				5.27
Auroxanthin	Violaxanthin	DODF		3.15		
13*Z*-Lutein	Lutein	DO	6.89			
Mutatoxanthin	Antheraxanthin	DOMF	5.33	5.59	4.93	
Capsorubin	Capsanthin	DODK				
Lutein	Lutein	DO	109.59	29.54	173.75	4.42

Capsanthin	Capsanthin	DOMK				33.38
Zeaxanthin	Zeaxanthin	DO	9.03	6.44	12.15	8.53
Zeaxanthin type	Zeaxanthin	DO				
13*Z*-β-Cryptoxanthin	β-Cryptoxanthin	MO		4.17	2.94	2.58
9*Z*-Zeaxanthin	Zeaxanthin	DO	Tr	Tr	Tr	Tr
9'*Z*-Zeaxanthin	Zeaxanthin	DO	Tr	Tr	Tr	Tr
β-Cryptoxanthin	β-Cryptoxanthin	MO	1.83	1.80	1.01	11.12
Curcubitaxanthin	Antheraxanthin	DOME				16.52
α-Cryptoxanthin	β-Cryptoxanthin	MO				3.00
TOT Free xanthophylls and deriv.			**171.17**	**273.92**	**293.96**	**117.55**
Chlorophylls and derivatives						
Chlorophyll b	Chlorophyll a		65.78		117.13	
Chlorophyll b’	Chlorophyll a				22.41	
Chlorophyll a	Chlorophyll a		0.66		0.82	
Pheophytin a type	Pheophytin a		Tr	Tr	Tr	Tr
Pheophytin a type	Pheophytin a		Tr	Tr	Tr	Tr
Pheophytin b'	Pheophytin a		7.39	3.18	4.59	
Pheophytin b	Pheophytin a		45.11	15.71	84.83	8.16

Pheophytin a'	Pheophytin a	33.19	3.68	66.99	2.31
Pheophytin a	Pheophytin a	224.41	23.24	511.12	7.82
Pheophytin a type	Pheophytin a	3.46			
TOT Chlorophylls and deriv.		**380.0**	**45.81**	**807.89**	**18.29**
Carotenes and derivatives					
Phytoene	Phytoene	4.16	66.72	3.73	14.26
Phytofluene	Phytofluene		0.92		
13*Z*-α-Carotene	β-Carotene		1.87		
ζ-Carotene	β-Carotene		4.30		2.08
15*Z*-β-Carotene	β-Carotene		2.03		2.83
13*Z*-β-Carotene	β-Carotene	1.84	5.60	2.36	12.16
α-Carotene	β-Carotene	9.27	18.94	1.40	15.17
9*Z*-α-Carotene	β-Carotene		2.60		
E-β-Carotene	β-Carotene	15.06	27.90	13.38	45.55
9*Z*-β-Carotene	β-Carotene	3.70	4.03	5.55	10.16
TOT Carotenes		**34.03**	**134.91**	**14.42**	**102.21**
Xanthophyll monoesters					
13*Z*-Capsanthin-C12					13.16

Antheraxanthin-C12				14.01
Cabsorubin ester				6.07
Capsorubin-C14				33.04
13*Z*-Capsanthin-C14				20.82
Lutein-C12	2.77			
Capsanthin-C12				37.99
Capsorubin-C16	Tr	Tr	Tr	Tr
Antheraxanthin-C14		12.93		46.09
Zeaxanthin-C12	2.18			
Lutein-C14	6.04			
Capsanthin-C14				71.88
Capsanthin-C14				29.04
Zeaxanthin-C14	3.04			14.40
Antheraxanthin-C16				8.69
Capsanthin-C16				20.10
Capsanthin-C16				11.51
9*Z*-Lutein-C16	3.46			
β-Cryptoxanthin-C12		3.82		16.56

β-Cryptoxanthin-C14	1.71	13.69	20.86
9Z-β-Cryptoxanthin-C14		5.16	
β-Cryptoxanthin-C16		11.85	6.85
TOT Xanthophyll monoesters	**19.20**	**47.45**	**371.07**
Xanthophyll diesters			
Capsanthin-2C10			12.72
13Z-Capsanthin-2C12			4.61
Antheraxanthin-2C12			9.03
Capsanthin-C10-C12	1.71	13.69	20.86
Capsanthin-C12-C10			12.79
13Z-Capsanthin-C12-C14			71.31
Capsanthin-2C12	4.37	11.20	
Lutein-2C12			23.58
Capsorubin-C12-C14			18.38
Mutatoxanthin-C12-C14		5.16	
Antheraxanthin-2C14		20.56	
Zeaxanthin-2C12		5.86	
13Z-Zeaxanthin-C12-C14		6.21	

Lutein-C12-C14	10.20		
Capsanthin-C12-C14			166.91
Capsorubin-2C14			71.86
Zeaxanthin-C12-C14		15.23	
Zeaxanthin-C12-C14		5.99	
9Z-Zeaxanthin-C12-C14		4.93	
Mutatoxanthin-2C14			5.85
Lutein-2C14	3.50		
Capsanthin-2C14			125.52
Capsanthin-C12-C16			43.31
Auroxanthin-diester			
Z-Capsanthin-C16-C12			10.74
13Z-Zeaxanthin-2C14		0.89	0.99
13Z-Zeaxanthin-2C14		3.37	
Zeaxanthin-2C14		7.94	8.79
9Z-Zeaxanthin-2C14		3.61	
Zeaxanthin-C12-C16		4.50	
Zeaxanthin-C12-C16		7.31	

Capsanthin-C14-C16			23.15
Capsanthin-C16-C14			29.03
Zeaxanthin-C14-C16	3.16	4.41	9.78
9*Z*-Zeaxanthin-C14-C16		2.68	
Zeaxanthin-2C16	1.57	2.14	0.91
TOT Xanthophyll diesters	**24.51**	**125.68**	**673.12**
TOT Xanthophyll Esters	**43.71**	**173.13**	**1044.19**

Tr, trace below LOQ; DO, Di-ol; MO, mono-ol; TO, Tri-ol; ME, mono-epoxy; DE, di-epoxy; MF, mono-furan; DF, di-furan; MK, mono-keton; DK, di-keton.

8.4. Conclusions

In this work, the ability of the off-line coupling of UPC^2 and RP-LC to analyze and characterize complex samples has been demonstrated. Such a technology provided significantly higher peak capacity respect to the conventional 1D-LC (1900 *vs.* 186, respectively), mainly due to the high degree of orthogonality of the two separation techniques employed. Furthermore, the enhanced separation power allowed a more reliable quantification of the samples investigated.

The characterization of the carotenoid stability and composition in overripe yellow and red bell peppers collected directly from the plant was reported, and a number of 115 different compounds belonging to chlorophylls, free xanthophylls, free carotenes, xanthophyll monoesters, and xanthophyll diesters were positively identified. (This chapter was adapted from Bonaccorsi, *et al.*, 2016).

REFERENCES

- Arab L., Steck S., Am. J. Clin. Nutr. 2000, 71, 1691S-1695S.
- Aubert M.C., Lee C.R., Krstulovic A.M., J. Chromatogr. 1991, 557, 47-58.
- Beutner S., Bloedorn B., Frixel S., Hernandez Blanco I., Hoffman T., Martin H.D., Mayer B., Noack P., Ruck C., Schmidt M., Schulke I., Sell S., Ernst H., Haremza S., Seybold G., Sies H., Stahl W., Walsh R., J. Sci. Food Agric. 2001, 81, 559-568.
- Bonaccorsi I., Cacciola F., Utczas M., Inferrera V., Giuffrida D., Donato P., Dugo P., Mondello L., J. Sep. Sci. 2016, 39, 3281-3291.
- Cacciola F., Donato P., Beccaria M., Dugo P., Mondello L., LC-GC Eur. 2012, 25, 15-24.
- Cacciola F., Donato P., Giuffrida D., Torre G., Dugo P., Mondello L., J. Chromatogr. A 2012, 1255, 244-251.
- Giddings J.C., McLaren L., Myers M.N., Science 1968, 159, 197-199.

- Giuffrida D., Dugo P., Dugo G., Torre G., Mondello L., Nat. Prod. Commun. 2011, 6, 1817-1820.
- Giuffrida D., Dugo P., Torre G., Bignardi C., Cavazza A., Corradini C., Dugo G., Food Chem. 2013, 140, 794-802.
- Herrero M., Cacciola F., Donato P., Giuffrida D., Dugo G., Dugo P., Mondello L., J. Chromatogr. A 2008, 1188, 208-215.
- Hornero-Mendez D., Minguez-Mosquera M.I., J. Agric. Food Chem. 2000, 48, 1617-1622.
- Lesellier E., Tchapla A., Marty C., Lebert A., J. Chromatogr. 1993, 633, 9-23.
- Lesellier E., Tchapla A., PeHchard M.R., Lee C.R., Krstulovic A.M., J. Chromatogr. 1991, 557, 59-67.
- Markus F., Daood H.G., Kapitany J., Biacs P.A., J. Agric. Food Chem. 1999, 47, 100-107.
- Minguez-Mosquera M.I., Hornero-Mendez D., J. Agric. Food Chem. 1994, 42, 640-644.
- Mokhtar M., Russo M., Cacciola F., Donato P., Giuffrida D., Riazi A., Farnetti S., Dugo P., Mondello L., Food Anal. Meth. 2016, 9, 1381-1390.
- Mokhtar M., Soukup J., Donato P., Cacciola F., Dugo P., Riazi A., Jandera P., Mondello L., J. Sep. Sci. 2015, 38, 171-178.
- Nishino H., Tokuda H., Satomi Y., Masuda M., Bu P., Onozuka M., Yamaguchi S., Okuda Y., Takayasu J., Tsuruta J., Okuda M., Ichiishi E., Murakoshi M., Kato T., Misawa N., Narisawa T., Takasuka N., Yano M., Pure Appl. Chem. 1999, 71, 2273-2278.
- O'Neil C., Schwartz S.J., J. Chromatogr. 1992, 624, 235-252.
- Rao A.V., Rao R.G., Pharmacol. Res. 2007, 55, 207-216.
- Sakaki K., Shinbo T., Kawamura M., J. Chromatogr. Sci. 1994, 32, 172-177.
- Schweiggert U., Kammerer D.R., Carle R., Schieber A., Rapid Commun. Mass Spectrom. 2005, 19, 2617-2628.
- Snodderly M.D., Am. J. Clin. Nutr. 1995, 62, S1448-S1461.
- Tee E.S., Lim C.L., Food Chem. 1991, 41, 147-193.

CHAPTER IX
On-line coupling of ultra performance convergence chromatography and ultra high pressure liquid chromatography for enhancing orthogonality in comprehensive separations

9.1. Introduction

The high complexity of many natural samples often overwhelms the separation capability of any 1D-LC approaches, given the high number of molecules that may be found, possibly with high degrees of structural similarity leading to co-elutions, often difficult to detect. Multidimensional chromatographic techniques provide improvements both in terms of peak capacity and resolving power (Dugo, *et al.*, 2008a; Dugo, *et al.*, 2008b; Dugo, *et al.*, 2008c; Dugo, *et al.*, 2006; François, *et al.*, 2009; Dugo, *et al.*, 2009), especially in the comprehensive mode. Of all LC×LC approaches, the combination of NP-LC and RP-LC is one of the most effective ways to increase the orthogonality, being the two separation mechanisms truly independent. However, the NP-LC×RP-LC coupling is not easy and straightforward to implement, mainly related due to the incompatibility of the mobile phases. RP-LC is carried out with aqueous mobile phases in which the apolar solvents, such as dichloromethane and *n*-hexane, eluting from the NP dimension are not miscible. Moreover, hyphenation of the two techniques is also complicated by the peak focusing at the head of the ^{2}D column, signal interferences and peak deterioration that may result in an elaborate data interpretation. The first dimension is usually restricted to micro- or narrow bore columns operated at low flow rates in order to minimize the volumes of the transferred fractions, resulting in reduced sample capacity.

A viable alternative is to replace the ^{1}D NP-LC dimension by SFC or subcritical fluid chromatography; such a combination alleviates immiscibility issues and further provides a number of advantages related to the use of supercritical CO_2 (e.g., shorter retention times, faster column re-equilibration).

The low viscosity of supercritical fluids together with increased diffusivity lead to shorter retention times, and faster column re-equilibration than NP-LC.

An on-line UHPSFC×RP-UPLC separation system is here described implemented in a fully automated fashion around two 2-position, six-port switching valves equipped with two packed octadecyl silica cartridges for effective trapping and focusing of the analytes after elution from ^{1}D. The addition of a water make-up flow to the SFC effluent prior to entering the loops permitted to efficiently focus the solutes on the sorbent material and to reduce interferences of expanded CO_2 gas on the second dimension separation (François, *et al.*, 2008).

Such a platform was demonstrated for the characterization of native carotenoids in a complex paprika sample, with photodiode array and time-of-flight mass spectrometry detection. The potential for IMS to resolve and characterize carotenoid isomers was also investigated using TWIMS on a Q-ToF MS.

9.2. Experimental section

9.2.1. Chemicals

Acetone, methanol, diethyl ether, and methyl-*tert*-butyl ether, all reagent grade, for sample preparation were supplied by Sigma-Aldrich (Milan, Italy). Optima LC/MS grade solvents for UHPSFC×RP-UPLC analyses, water, methanol, and acetonitrile, were purchased from Thermo Fisher Scientific (Milan, Italy); LC-MS grade 2-propanol was obtained from Sigma-Aldrich. CO_2, 99.99% purity, was a product of the Tirino Gas Vari di Di Carlo Roberto (Messina, Italy).

Powdered anhydrous sodium sulphate, sodium bicarbonate, and sodium chloride were obtained from Sigma-Aldrich. The standard β-carotene was purchased from Extrasynthese (Genay, France).

9.2.2. Sample and sample preparation

The paprika sample was purchased in a local market. The carotenoid pigments were extracted according to the recommended procedures (Rodriguez-Amaya, 2016). 10 grams of samples were mixed with 1 g of sodium bicarbonate, homogenized and extracted to colour exhaustion with acetone. The extracts were combined and the acetone was evaporated (under vacuum at 35°C) until a 50 mL final volume was attained. The concentrate was transferred into a separatory funnel with 100 mL of diethyl ether, shaken and left to settle. Enough NaCl solution (10%) was added to separate the phases and to transfer the pigments to the ether. This solution was treated several times with anhydrous Na_2SO_4 solution (2%) to remove all the water. The ether phase was evaporated to dryness at 30°C. The dry residue was then dissolved in a mixture of methanol/methyl-tert-butyl ether (MTBE) (1:1, *v/v*), filtered through a 0.45 μm Acrodisc nylon membrane filter (Pall Life Sciences, Ann Arbor, MI, USA), and analyzed.

9.2.3. Instrumental set-up

An Acquity UPC^2 instrument (Waters Corp., Manchester, England) was used for the UHPSFC experiments and consisted of a binary solvent manager (ccBSM), a convergence manager, a sample manager fixed-loop (SM-FL), and a column manager (CM). The latter can accommodate two columns, and the temperature of each column can be set independently, and was used for the ^2D columns. An additional oven was employed to allocate the longer ^1D column.

The second dimension analyses were carried out on an Acquity UPLC I-Class, including a binary solvent manager (BSM), an isocratic solvent manager (ISM), and a PDAeλ (500 nL). The two dimensions were connected by means of two 2-position, 6-ports switching valves, placed inside the column manager and equipped with two packed loops. The UPC^2×RP-UPLC system was coupled to a hybrid quadrupole-traveling wave ion mobility-time of flight mass spectrometer Synapt G2-Si HDMS (Waters Corp., Manchester, England) through an APCI source. Figure IX-1 shows a schematic of the system employed in this work.

9.2.4. Analytical conditions

UHPSFC experiments were performed on an Ascentis ES Cyano column, 250 mm × 1.0 mm I.D., 5.0 μm d_p (Supelco) at a temperature of 40 °C. The mobile phase consisted of supercritical CO_2 (solvent A) and methanol (solvent B); the flow rate was 0.05 mL/min; the gradient applied was 0-2 min, 0% B, 2-27 min to 20% B, hold for 13 min. The injection volume was 2 μL. The cartridges (packed loops) used for the trapping of the SFC effluent were Xbridge C18, 2.1 mm × 20 mm, 5 μm (Waters). The second dimension column was an Acquity UPLC BEH C18, 50 mm × 2.1 mm I.D., 1.7 μm d_p (Waters) and was operated at a flow rate of 0.7 mL/min with a mixture of acetonitrile/water (8:2, *v/v*) (solvent A) and isopropanol (solvent B) as mobile phases. The linear gradient program was as follows: 0-0.5 min, 20-50% B (hold for 0.3), 0.8-1.0 min, to 80% B (hold for 0.6), 1.61 min to 20% B (0.39 min for reconditioning). The gradient lasted for 2 min and it was repeated during the whole analysis time, thus, being 2 min the modulation time for the switching valves. Water was added to the SFC effluent prior to entering the cartridges at a flow rate of 1.3 mL/min, from the isocratic solvent manager.

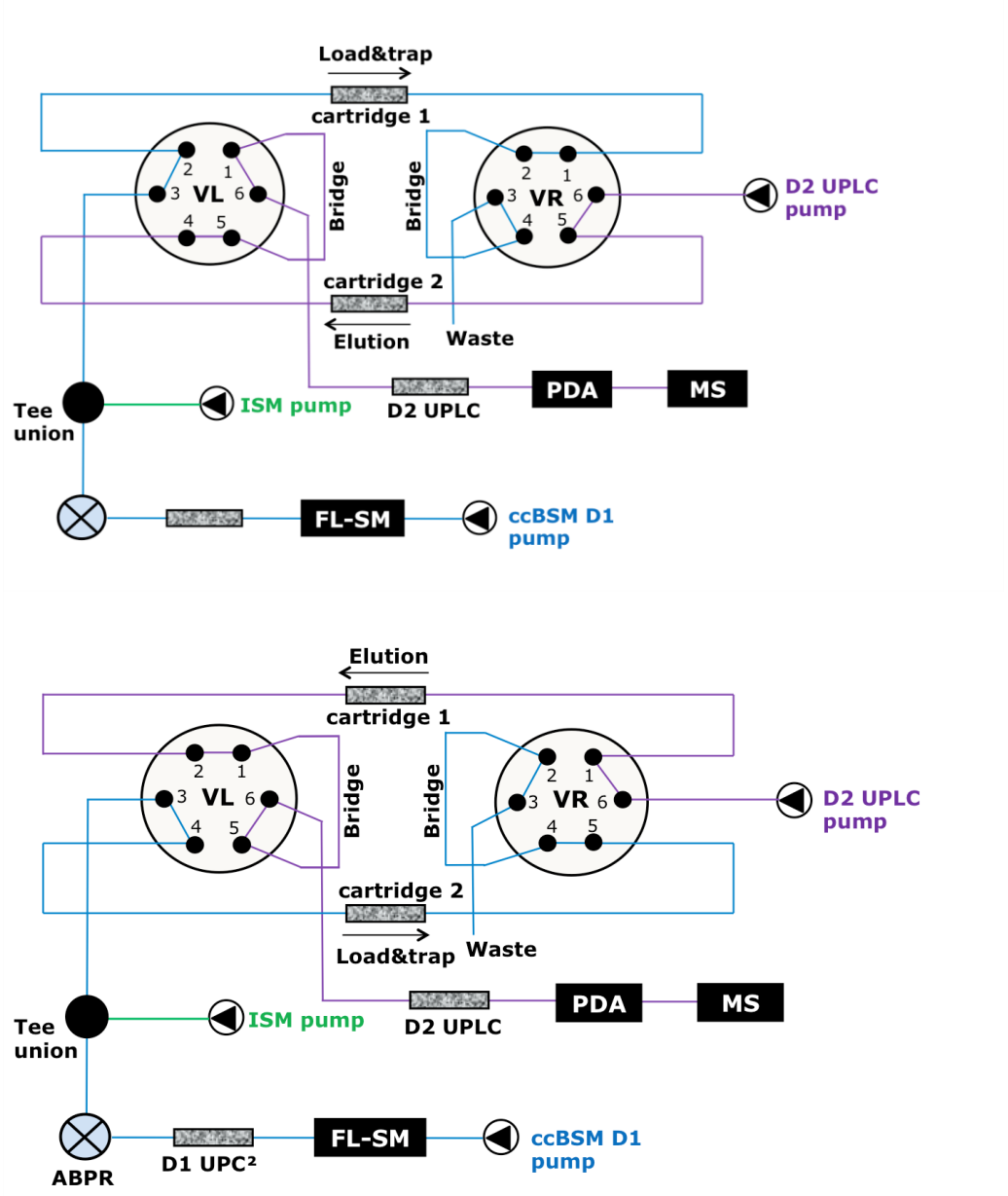

Figure IX-1. *Schematic of the UHPSFC×RP-UPLC system employed in this work, showing the routes for each second dimension separation, corresponding to different positions of the two 2-position, 6-ports switching valves.*

The PDA detector covered a wavelength range from 330-550 nm (sampling rate 40 Hz, resolution 1.2 nm), while the MS detector was working in APCI-negative mode. The parameters involving the ToF MS detection and APCI were: mass range *m/z* 100-1200; source temperature, 150 °C; probe temperature, 400 °C; desolvation gas flow (N_2), 600 L/h; corona current, 3 μA; sampling cone, 40 V.

For IM MSMS CID of β-carotene standard (*m/z* 536.4) experiment: transfer collision energy, 4 V; IM wave height 40 V; wave velocity, ramping 800-300 m/s.

9.2.5. Software

Both dimensions and the switching valve were controlled by the MassLynx V4.1 SCN916 (Waters). The UHPSFC×RP-UPLC data were converted to ASCII data using the DataBridge tool (Waters). Later on, this data were visualized and elaborated into 2D and 4D (four dimensions) using Chromsquare ver. 2.0 software (Chromaleont). IMS data were processed with DriftScope 2.7 (Waters).

9.3. Results and discussion

The carotenoid extract of a paprika sample was chosen to test the novel instrument because of its complexity, by far overwhelming the limited peak capacity provided by any 1D-LC technique. Carotenoids represent a challenging analysis task, due to a series of factors, such as high variability in the chemical structures, isomerisation, scarce stability, and the lack or the expensive cost of commercially available standards for comprehensive characterization real samples.

Results obtained from the UPC^2×RP-UPLC analysis of free carotenoids and

carotenoid esters in the paprika extract are shown in the contour plot of Figure IX-2.

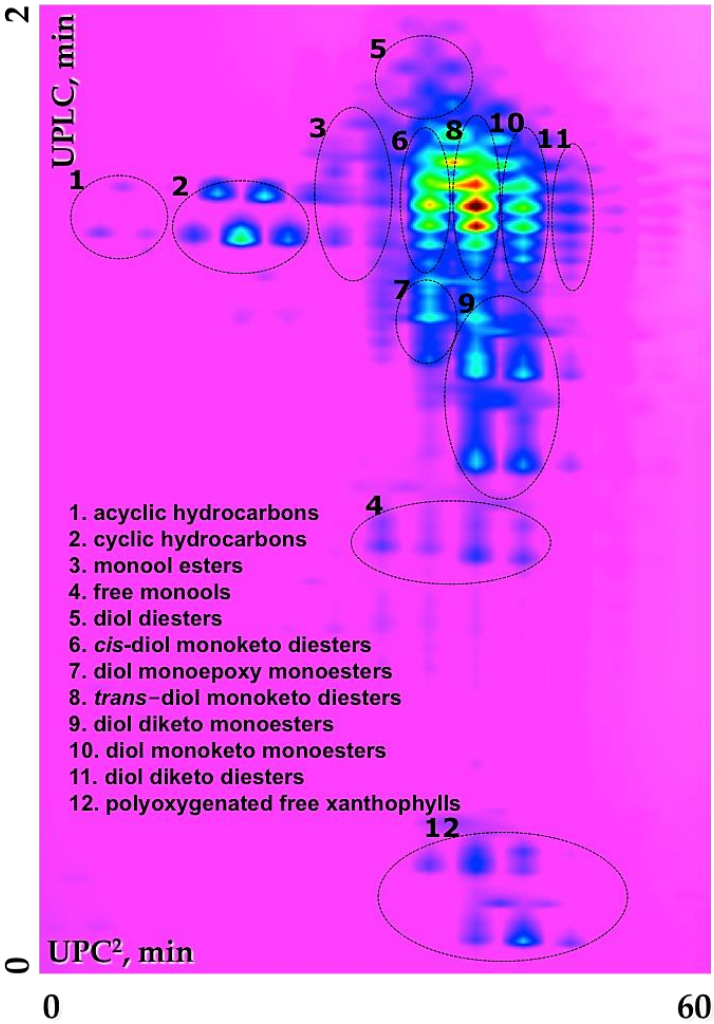

Figure IX-2. *UPC^2×RP-UPLC contour plot of free carotenoids and carotenoid esters in a paprika extract.*

Chromatography on the cyano stationary phase in ^{1}D allowed a good separation of the carotenoids into 12 chemical classes of polarity: 1. acyclic hydrocarbons, 2. cyclic hydrocarbons, 3. monool esters, 4. free monools, 5. diol diesters, 6.

cis-diol monoketo diesters, 7. diol monoepoxy monoesters, 8. *trans*-diol monoketo diesters, 9. diol diketo monoesters, 10. diol monoketo monoesters, 11. diol diketo diesters, 12. polyoxygenated free xanthophylls.

On the other hand, the C18 column in ^{2}D afforded the separation of compounds of increasing hydrophobicity and decreasing polarity within each class. Complete elution of each transferred fraction from ^{1}D was achieved, in on-line comprehensive analyses, within a modulation time of 2 minutes, including 0.39 min for column reconditioning from the gradient.

A water make-up fluid was added to the ^{1}D effluent by means of a T-junction and transferred to the interface. The addition of water is vital not only to eliminate the expanded CO_2 gas, avoiding the interferences of CO_2 in the ^{2}D separation after transfer ("solvent displacement" effect), but furthermore to ensure focusing in the trap, since the presence of small volumes of modifier, as strong RP solvent, would result in breakthrough of the cartridge and loss of the analytes.

The high separation power resulted from the coupling of orthogonal retention mechanisms in the two chromatographic dimensions, on the basis of the low correlation derived from solute retention vectors.

Identification of the separated compounds was achieved by the complementary information gathered from retention times, PDA spectra, and high resolution ToF MS data (Figure IX-3).

Spectra obtained under negative ionization mode are dominated by the presence of very intense pseudomolecular ions $[M]^{\cdot -}$, which make identification of minor components easier.

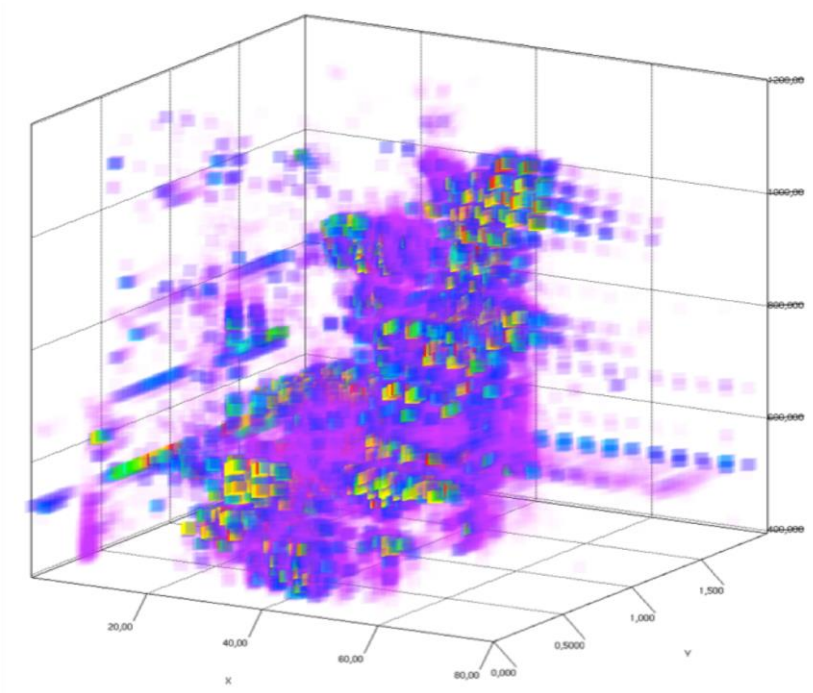

Figure IX-3. *4D Scatter plot displaying the mass distribution over the first and second retention time. Intensity is rendered by colour map.*

Moreover, enhanced information can be obtained by adding a fourth dimension with the use of IMS that allowed for the gas-phase separation of the ions in an electric field on the basis of their size and shape. Figure IX-4 shows the 2D UPC^2×RP-UPLC-IM-MS analysis of the paprika extract.

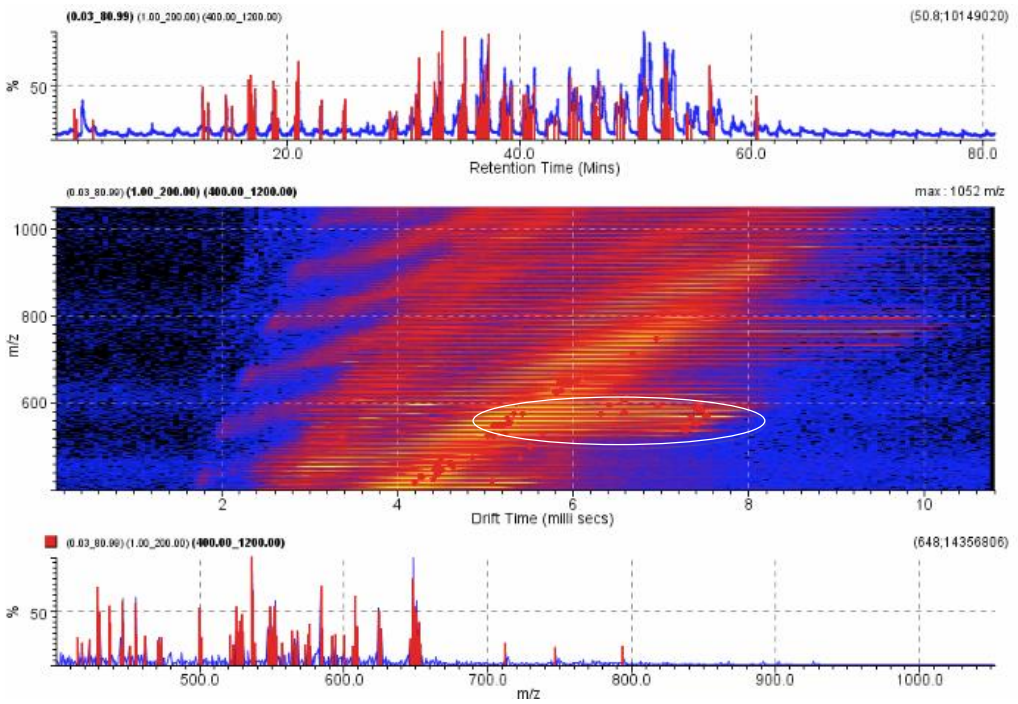

Figure IX-4. *2D UPC²×RP-UPLC-IM-MS analysis of a paprika extract: (A) UPC²×RP-UPLC-MS chromatogram; (B) 2D map of m/z (y) vs. IMS drift time (x); (C) total MS spectrum.*

The capability of IMS is more evident in Figure IX-5, in which is shown the separation of β-carotene isomers. The *trans*-β-carotene was separated by several milliseconds from the *cis*-isomer (the *trans*-isomer have a longer drift time than *cis*-isomer). Collision-induced dissociation MS/MS of ion mobility-resolved isomers indicated that *cis*- and *trans*-carotenoid isomers can be distinguished by their fragmentation patterns. The base peak of the tandem mass spectrum of the *trans*-β-carotene was observed at *m/z* 444 and corresponded to the loss of toluene, while the *cis*-β-carotene is characterized by an intense molecular ion *m/z* 536 according to Dong et al. (Dong, *et al.*, 2010).

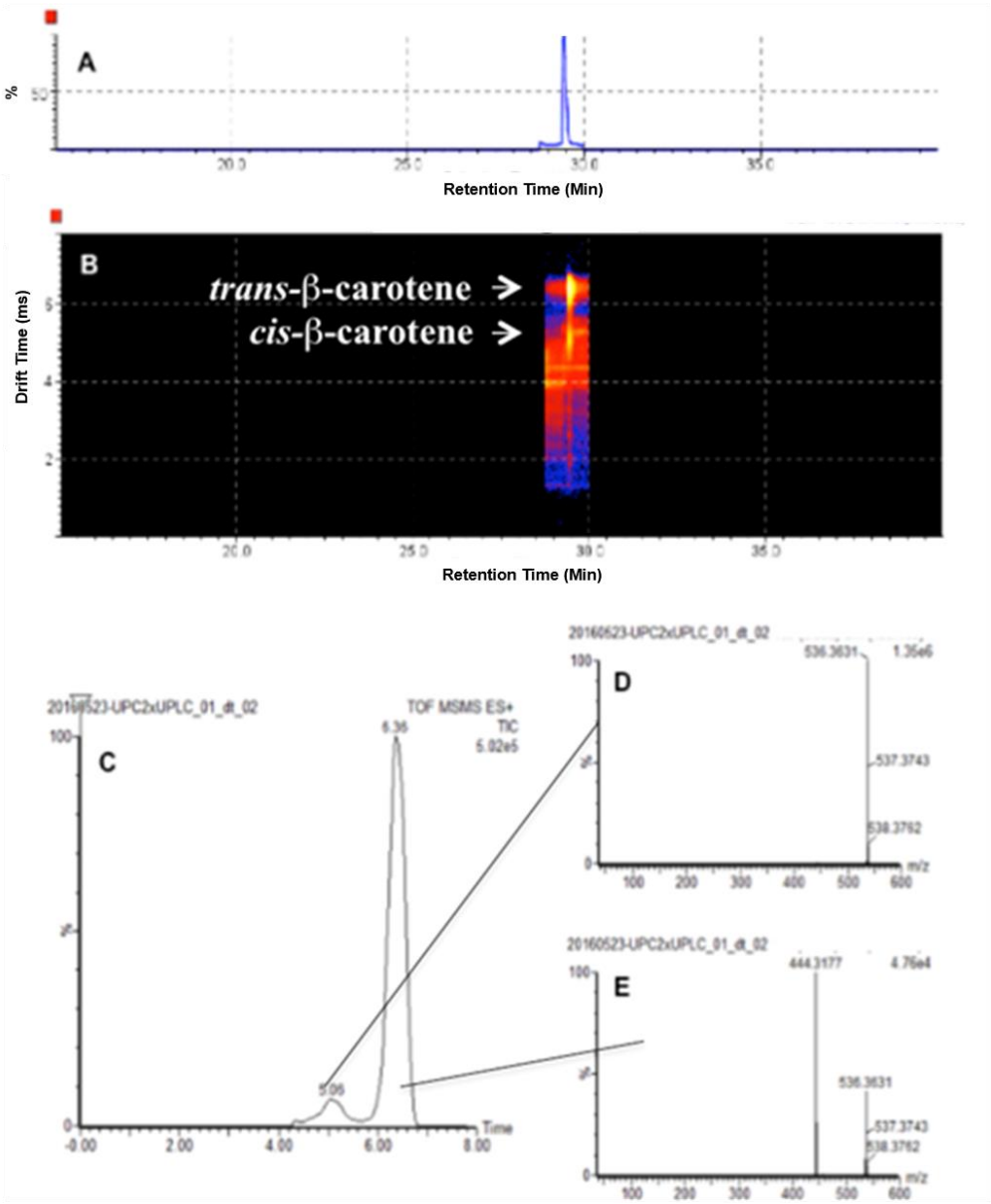

Figure IX-5. *2D UPC²×RP-UPLC-IM-MS-MS analysis of β-carotene isomers: (A) UPC²×RP-UPLC MS chromatogram of β-carotene molecular ions of m/z 536.4; (B) 2D map showing the ion mobility separation of β-carotene isomers; (C) IMS drift time distributions and the relative abundances of cis- (peak at 5.06 ms drift time) and trans- (peak at 6.36 ms drift time) β-carotene; (D) IM-MS-MS with CID of cis-β-carotene; (E) IM-MS-MS with CID of trans-β-carotene.*

9.4. Conclusions

In this work, the ability of the novel on-line UPC^2×RP-UPLC coupled to PDA, Q-ToF and IMS to analyze and characterize complex sample has been demonstrated. In particular, carotenoids fingerprint in a paprika sample was obtained in almost half the time with respect to conventional NP-LC×RP-LC, with great reduction in solvent consumption and suppression of signal interferences.

The separation of geometric isomers like *cis*/*trans* carotenoids using travelling wave ion mobility was also demonstrated.

REFERENCES

- Dong L., Shion H., Davis R.G., Terry-Penak B., Castro-Perez J., van Breemen R.B., Anal. Chem. 2010, 82(21), 1-17.
- Dugo P., Cacciola F., Kumm T., Dugo G., Mondello L., J. Chromatogr. A 2008, 1184, 353-368.
- Dugo P., Giuffrida D., Herrero M., Donato P., Mondello L., J. Sep. Sci. 2009, 32, 973-980.
- Dugo P., Herrero M., Giuffrida D., Kumm T., Dugo G., Mondello L., J. Agric. Food Chem. 2008, 56, 3478-3485.
- Dugo P., Herrero M., Kumm T., Giuffrida D., Dugo G., Mondello L., J. Chromatogr. A 2008, 1189, 196-206.
- Dugo P., Skerikova V., Kumm T., Trozzi A., Jandera P., Mondello L., Anal. Chem. 2006, 78, 7743-7750.
- François I., dos Santos Pereira A., Lynen F., Sandra P., J. Sep. Sci. 2008, 31, 3473-3478.
- François I., Sandra K., Sandra P., Anal. Chim. Acta 2009, 641, 14-31.
- Rodriguez-Amaya D.B., IFT Press, Wiley Blackwell, Chichester, West Sussex, UK, 2016.

CHAPTER X
Multidimensional preparative liquid chromatography to isolate flavonoids from Citrus products

10.1. Introduction

Preparative liquid chromatography (prep-LC) is the most extensively used technique for the isolation and purification of valuable products in the chemical and pharmaceutical industry as well as in biotechnology and biochemistry. Depending on the working area the amount of compound to isolate or purify differs dramatically. It starts in the µg range for isolation of enzymes in biotechnology (micro purification); for identification and structure elucidation of unknown compounds in synthesis or natural product chemistry it is necessary to obtain pure compounds in amounts ranging from one to a few milligrams. Larger amounts, in gram quantity, are necessary for standards, reference compounds and compounds for toxicological and pharmacological testing.

It is very common that a molecule isolated in a single preparative HPLC analysis shows a purity lesser than 95%. As a consequence, this compound must be subjected to a second purification step if higher purity is required (Zhang & Zeng, 2014). The choice of the second purification step is not simple, but surely preparative multidimensional liquid chromatography (prep-MDLC) can represent an optimum solution for purification of molecules in very complex samples. Coupling two preparative columns with different stationary phases or with different internal diameter leads to obtain compounds with high purity (Jin, *et al.*, 2013; Li, *et al.*, 2013; Qiu, *et al.*, 2014).

In the last decade, a number of articles described prep-MDLC techniques for the purification of complex samples (Jin, *et al.*, 2013; Su, *et al.*, 2013; Jiang, *et*

al., 2009; Wong, *et al.*, 2004; Jayaprakasha, *et al.*, 2013; Russo, *et al.*, 2014; Russo, *et al.*, 2015). As far as prep-MDLC techniques are concerned, several approaches have been employed, like preparative off-line (Jin, *et al.*, 2013; Li, *et al.*, 2013; Russo, *et al.*, 2014; Russo, *et al.*, 2015) and on-line heart-cutting (Su, *et al.*, 2013; Liu, *et al.*, 2013; Qiu, *et al.*, 2014) approaches. Some authors used medium pressure prep-LC in both dimensions (Jayaprakasha, *et al.*, 2013) or only in the first dimension (Qiu, *et al.*, 2014).

Flavonoids belong to a class of natural compounds that in the last two decades have been the subject of considerable scientific and therapeutic interest.

These molecules are a widely distributed group of polyphenolic compounds characterized by a common benzo-γ-pirone structure that have been reported to act as antioxidants in various biological systems (Benavente-Garcia, *et al.*, 1997). They occur as aglycones (without sugar moieties) and glycoside (with sugar moieties). Flavonoids have shown many biological properties: anticancer, antimicrobial, antiviral and anti-inflammatory activities, effects on capillary fragility, inhibition of human platelet aggregation and reduction of oxidative stress (Benavente-Garcia, *et al.*, 1997; Delle Monache, *et al.*, 2013; Navarra, *et al.*, 2014). The group of flavonoids includes several hundred compounds belonging to subgroups of flavanones, flavonols, flavan-3-ols (such as proanthocyanidins), flavonones, isoflavonoids, and anthocyanins.

Citrus fruits are rich in flavonoids, and these molecules typically include flavanones (e.g. hesperidin), flavonols (e.g. quercetin glycosides), and flavonones (e.g. tangeritin). In general, such compounds may contribute to fruit and juice quality in many ways, influencing the appearance, the taste and the nutritional value of the product from the plant, and their content may vary widely depending on the nature of the *Citrus* fruit.

LC coupled with UV and MS detectors represents the technique of choice for separation and characterization of flavonoids in *Citrus* fruits, as demonstrated by many literature data where bioactive molecules in *Citrus* fruits were analyzed by means of monodimensional (Gardana, *et al.*, 2008; Baldi, *et al.*, 1995; He, *et al.*, 2011) and multidimensional (Dugo, *et al.*, 2012; Russo, *et al.*, 2011) LC.

The purpose of this study, which is a part of a more extended project aimed to endorse the use of the waste produced by agro-food industries, is focused on the development of a method for the investigation, quantification, and isolation of flavonoids and other bioactive molecules (e.g. limonoids) in different *Citrus* products by means of prep-MDLC coupled with a photodiode array detector and a single quadrupole mass spectrometer (LC-LC-PDA-MS prep). This instrumental set-up allowed a simple and very efficient automated collection of fractions separated both in ^{1}D and ^{2}D using mass-triggered approach.

In this chapter will be presented two different applications: CASE 1. isolation of different flavonoids from bergamot juice; CASE 2. isolation of hesperidin from the by-product (waste water) of the industrial transformation of orange.

CASE 1.

10.2. Isolation of flavonoids from bergamot juice

Among *Citrus* fruits, bergamot presents a considerable abundance and variety of flavonoids, such as naringin, neohesperidin, and neoeriocitrin, which are present in the juice on the order of hundreds of milligrams per liter (Di Donna, *et al.*, 2009). According to these considerations, *Citrus* fruits, and in particular bergamot juice, represent an excellent raw material for the isolation of flavones and flavanones. Bergamot juice is considered a by-product of the bergamot essential oil production (Pernice, *et al.*, 2009), thus isolation of nutraceuticals

from bergamot juice represent a way for the valorization of this by-product. The LC-LC-PDA-MS preparative system was used for a thorough purification of all flavonoid content from concentrated bergamot juice.

10.2.1. Experimental section

10.2.1.1. Sample and chemicals

This research was carried out on a 48° Brix concentrated bergamot juice obtained from a *Citrus* plant located in Calabria (Italy). For the analytical determination of flavonoids, the concentrated bergamot juice required a dilution 1:40 *v/v* with distilled water, then was filtered using Acrodisc filter 0.45 μm (Sigma-Aldrich, Milan, Italy) and injected into RP-HPLC. The sample was analyzed in triplicate. For prep-MDLC analyses, the sample was analyzed without any pretreatment.

Formic acid was purchased from Riedel-de Haën (Hanover, Germany). Tetradeuteromethanol and DMSO-d_6 were purchased from Sigma-Aldrich. For HPLC-MS analyses, water and acetonitrile were obtained from Sigma-Aldrich. The standard compounds: narirutin, eriocitrin, and neohesperidin were obtained from Extrasynthese (Genay Cedex, France). Brutieridin, melitidin, naringin, and neoriocitrin were isolated from concentrated bergamot juice. Apigenin 6,8-di-*C*-glucoside and diosmetin 6,8-di-*C*-glucoside were previously isolated in our laboratory (Russo, *et al.*, 2014).

10.2.1.2. Instrumentation and software

HPLC analyses were carried out using a Shimadzu Prominence LC-20A system (Shimadzu, Milan, Italy), including a CBM-20A controller, two LC-20 AD dual-plunger parallel-flow pumps, a DGU-20A3 online degasser, and a CTO-20A column oven. As detectors, an SPD-M20A UV detector and a HPLC-MS

2020, through an ESI interface (Shimadzu, Kyoto, Japan), were employed, respectively, for quantification and characterization of bioactive molecules. MS data acquisition was performed by the LCMSsolution version 3.30 software (Shimadzu).

Prep-MDLC analyses were carried out using a Shimadzu Prominence LC-20A system, including a CBM-20A controller, one LC-20 AD dual-plunger parallel-flow pump, three LC-20 AP preparative pumps, a DGU-20A3R online degasser, one FCV-20AH2 valve, two FCV-14AH valves, and an APV Split. As detectors, an SPD-20A UV detector with a preparative cell (0.5 mm), an SPD-M20A UV detector, and an HPLC-MS 2020, through ESI interface (Shimadzu), were employed. As autosampler/autocollector a GX-281 Gilson was employed. MS data acquisition was performed by the LabSolution version 5.53 software (Shimadzu, Kyoto, Japan). The Figure X-1 illustrate the design of the prep-MDLC system. Figure X-1A shows 1D configuration: mobile phases pumped by the two preparative pumps collect the sample loaded in the autosampler; the eluate reaching the ^{1}D preparative column goes through one of the two FCV-14AH valves. In the ^{1}D preparative column the analysis starts, and fractions separated arrive to the detectors through the second FCV-14AH valve. Figure X-1B shows how it is possible to change the configuration from ^{1}D to ^{2}D, changing the position of the three valves (one FCV-20AH2 valve and two FCV-14AH valves). For 2D configuration, the eluate coming from the autosampler reaches the ^{2}D preparative column through one of the two FCV-14AH valves, and then to the FCV-20AH2 valve. As for the ^{1}D separation, molecules separated by ^{2}D preparative column reach the detector through the second FCV-14AH valve. The fraction collection was realized by means of the autocollector GX-281 Gilson. This kind of instrumentation provides the autocollection of fractions eluted from the preparative column in vials

according to MS signal based on MS triggering signal.

NMR spectra were obtained with a Varian instrument and spectra were recorded at 500 MHz, and all the flavonoids tested were dissolved in tetradeuteromethanol or DMSO-d_6. The fraction collected from preparative purification were concentrated by means of a high-performance solvent evaporation system EZ-2 (Genevac, Ipswich, UK).

10.2.1.3. RP-HPLC-PDA-MS analytical conditions

HPLC analyses were carried out on an Ascentis Express C18, 150 mm × 4.6 mm I.D., 2.7 μm d_p (Supelco, Bellefonte, PA, USA). Injection volume: 2 μL, mobile phases: water/formic acid (99.9:0.1, *v/v*; solvent A) and acetonitrile/formic acid (99.9:0.1, *v/v*; solvent B), gradient: 0 min, 5% B, 40 min, 25% B, 60 min, 100% B, 70 min, 100% B, 73 min, 5%, 80 min, 5% B. Flow rate: 0.7 mL/min, data were acquired using a PDA in the range of 190-400 nm and the chromatograms were extracted at 283 and 325 nm. Time constant was 0.64 s and sample frequency 1.5625 Hz. Data acquisition was performed by Shimadzu LCsolution software version 3.3.

MS acquisition was performed using ESI in negative mode: mass spectral range, *m/z* 100-800; interval, 0.5 s; scan speed, 938 amu/s; nebulizing gas (N_2) flow, 1.5 L/min; ESI temperature, 350 °C; heat block, 300 °C; desolvation line (DL) temperature, 300 °C; DL, voltage −34 V; probe voltage, +4.5 kV; Qarray voltage, 1.0 V; and detection gain, 1.05 kV.

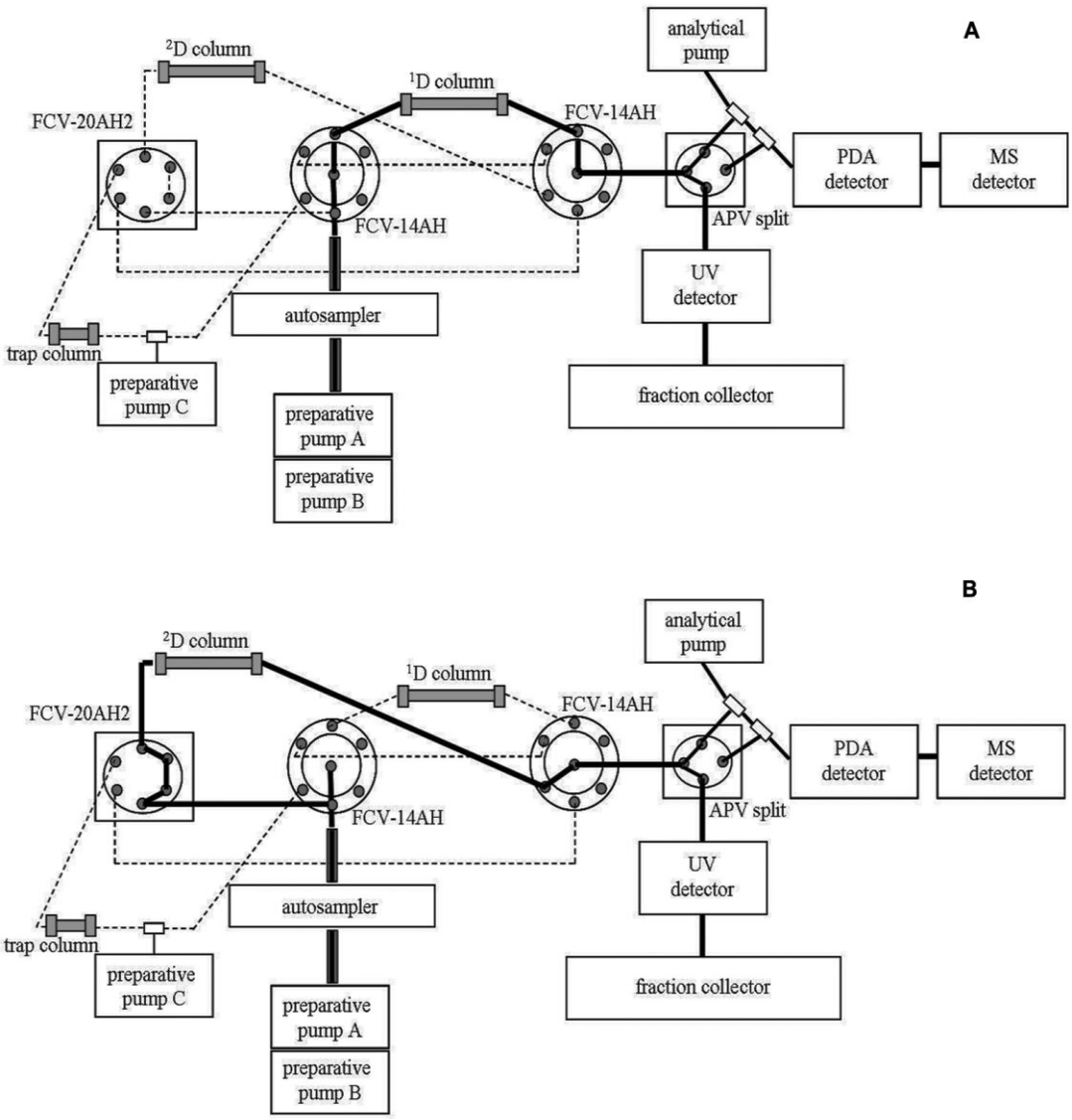

Figure X-1. *Schematic diagram of the 2D HPLC preparative column switching system: (A) system configuration for elution of the sample on ^{1}D column; (B) system configuration for elution of the collected fractions on ^{2}D column.*

10.2.1.4. Isolation of flavonoids by means of ^{1}D of prep-MDLC

After several sample overload tests of the preparative column, based on concentration or volume overloading, the best choice was to select a small volume of sample (4 mL) of a very concentrated bergamot juice. Concentration

overloading was possible because the sample compounds have good solubility in the mobile phase, and in this way the sample amount that can be separated was higher. Six aliquots of 4 mL each (24 mL total) of a concentrated bergamot juice (48° Brix) were subjected to prep-MDLC separation using an Ascentis Express C18 (250 mm × 21.2 mm I.D., 5 μm d_p; Supelco) preparative column. Mobile phases: water (solvent A) and acetonitrile (solvent B), flow rate: 10 mL/min; ^{1}D gradient: 0 min, 5%B, 40min, 25%B, 50min, 100%B, 60min, 100% B. Flow rate of analytical pump: 200 μL, the APV split was set to 1000:1 value. Data were acquired using a UV detector at 283 nm, a PDA in the range of 190-400 (chromatograms were extracted at 283), cell temperature was 40 °C, and slit width 1.2 nm. MS acquisition was performed using ESI, in negative mode: mass spectral range, m/z 100-800; interval, 0.35 s; scan speed, 938 amu/s; nebulizing gas (N_2) flow, 1.5 L/min; ESI temperature, 350 °C; heat block, 250 °C; DL temperature, 250 °C; DL, voltage −34 V; probe voltage, +4.5 kV; Qarray voltage, 1.0 V, and detection gain, 1.05 kV.

10.2.1.5. Isolation of flavonoids by means of ^{2}D of prep-MDLC

Fractions collected from ^{1}D were subjected to ^{2}D prep-MDLC separation using a Discovery HS F5-5 (250 mm × 21.2 mm I.D., 5 μm d_p; Supelco) preparative column. Mobile phases: water (solvent A) and acetonitrile (solvent B), flow rate: 10 mL/min. Flow rate of analytical pump: 200 μL, the APV split was set to 1000:1 value. Data were acquired using a UV detector at 283 nm, a PDA in the range of 190-400 (chromatograms were extracted at 283), cell temperature was 40 °C, and slit width 1.2 nm. Fractions 1-2 were combined and concentrated to 21 mL, fraction 3 was concentrated to 15 mL and fraction 4 was concentrated to 12 mL by means of the EZ-2 evaporator, and then subjected to 2D prep-MDLC separation. The fractions were injected three consecutive times and injection

volume was 7, 5, and 4 mL, respectively, each time. ^{2}D analyses were carried out in isocratic mode using water/acetonitrile 85:15 *v/v* for fractions 1-2, 70:30 *v/v* for fraction 3, and 65:35 *v/v* for fraction 4. MS acquisition was performed using ESI in negative mode. Mass detection was performed in SIM mode at the following *m/z* values: 593 (apigenin-6,8-di-*C*-glucoside), 623 (diosmetin-6,8-di-*C*-glucoside), and 595 (eriocitrin), for frac- tions 1-2; *m/z* values: 579 (naringin) and 595 (neoeriocitrin) for fraction 3; *m/z* values: 609 (neohesperidin), 723 (melitidin), and 753 (brutieridin) for fraction 4. The MS and ESI conditions are the same as those reported in the previous section. The collected fractions were evaporated by the EZ-2 evaporator to obtain apigenin 6,8-di-*C*-glucoside, diosmetin 6,8- di-*C*-glucoside, eriocitrin, naringin, neohesperidin, neoreiocitrin, brutieridin, and melitidin whose structures were confirmed by 1H NMR spectroscopy and ESI-MS. These data were in agreement with those reported elsewhere (Di Donna, *et al.*, 2009; Caristi, *et al.*, 2006; Gattuso, *et al.*, 2007).

10.2.1.6. RP-HPLC methods validation and statistical analysis

To determine the amount of flavones and flavanones present in the concentrated bergamot juice, calibration curves were constructed by using each available standard or previously isolated. Five different concentrations of each component, in the 0.2-100 mg/L concentration range, were prepared by diluting a stock solution of 1000 mg/L, using methanol as solvent, and analyzed for five times by HPLC, following a validated procedure adopted previously (Russo, *et al.*, 2014). Limit of detection (LOD) and limit of quantification (LOQ) values, following the guidelines, were also calculated using a method reported previously (Russo, *et al.*, 2014; EURACHEM Guide, 2014). The instrumental

intraday repeatability and the recovery were calculated on six replicated injections at one concentration level for all the analytes (1 mg/L).

10.2.2. Results and discussion

10.2.2.1. RP-HPLC-PDA analysis

To characterize flavonoids content in bergamot juice, the sample was analyzed by using the analytical RP-HPLC-PDA system, before the purification of the molecules through the prep-MDLC system. The analytical method used was previously applied in our laboratory (Russo, *et al.*, 2014; Russo, *et al.*, 2015) for the analyses of flavonoids in Citrus juices, and was validated both for the selection of mobile phases and stationary phase, and in terms of precision and reproducibility. Figure X-2 shows the chromatogram of flavonoids contained in the juice. Table X-1 reports concentration values (mg/L) of the compounds of our interest.

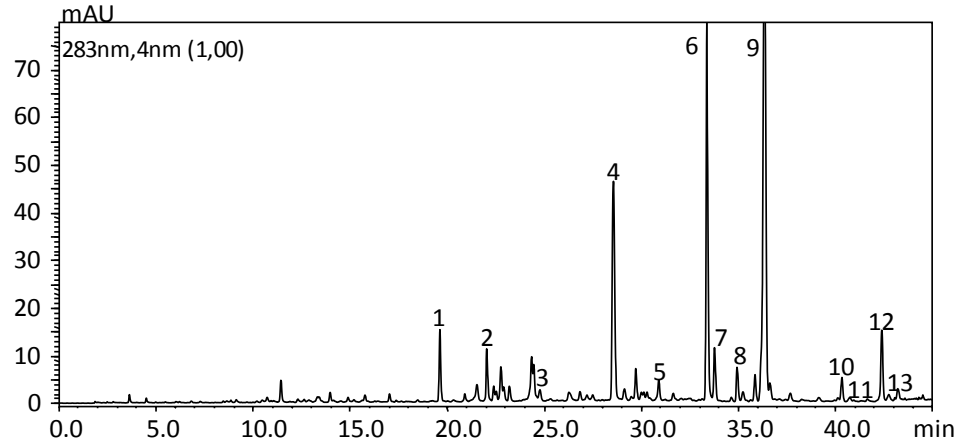

Figure X-2. *RP-HPLC-PDA analytical chromatogram of a concentrated bergamot juice.*

Table X-1. *Flavonoids composition (mg/mL) of a concentrated bergamot juice, regression equations, correlation coefficients (R^2), LOD (mg/L), LOQ (mg/L), recoveries values of analytes, and MS values for each flavonoids.*

N°	Compound	mg/mL	$(M–H)^-$	Regression line	R^2	LOD	LOQ	Recovery
1	Apigenin 6,8-di-*C*-glucoside	3.2 ± 0.06	593	$y = 23832x + 33947$	0.996	0.084	0.142	92%
2	Diosmetin 6,8-di-*C*-glucoside	2.8 ± 0.08	623	$y = 23169x - 10103$	0.996	0.105	0.174	90%
3	Eriocitrin	1.4 ± 0.01	595	$y = 1065.6x - 197.31$	0.999	0.098	0.164	90%
4	Neoeriocitrin	23.8 ± 0.48	595	$y = 24324x - 31888$	0.998	0.087	0.148	93%
5	Poncirin[a])	2.4 ± 0.02	593					
6	Naringin	68.7 ± 1.37	579	$y = 28090x - 21953$	0.998	0.085	0.142	87%
7	Narirutin	5.9 ± 0.12	579	$y = 932.21x - 750.79$	0.991	0.113	0.189	93%
8	Neodiosmin[a])	1.2 ± 0.01	607					
9	Neohesperidin	125.3 ± 3.13	609	$y = 1063.1x - 48.476$	0.998	0.098	0.164	90%
10	Melitidin	1.8 ± 0.02	723	$y = 18438x - 7778.8$	0.997	0.094	0.157	85%
11	Rhoifolin[a)]	0.2 ± 0.01	577					
12	Brutieridin	2.1 ± 0.03	753	$y = 10516x + 1385.1$	0.997	0.112	0.183	88%
13	Diosmin[a)]	0.9 ± 0.01	607					

[a)] Flavonoids were quantitatively determined based on calibration curves obtained with the correspondent standard compound, neohesperidin.

10.2.2.2. [1]D preparative analyses

The selection of mobile and stationary phases and the knowledge of the total amount of flavones and flavanones in the concentrated bergamot juice, obtained from the analytical systems, may be upgraded to a preparative scale for the purification process.

The main goals of any HPLC preparative process are: purity of products isolated, yield, and throughput. Unfortunately, the three parameters are dependent on each other, so it is not easy to optimize a preparative HPLC with respect to all parameters. The HPLC-HPLC-PDA-MS preparative method used in this work allowed an increased throughput, moreover, purity and yield are improved thanks to the automated collection of the molecules based on the mass-triggered approach. Usually, automated collections of fractions from preparative HPLC analyses are based on retention time and UV signals (Jin, *et al.*, 2013; Li, *et al.*, 2013; Xie, *et al.*, 2010), but this can lead to problems of peak purity. Using an automated collection of fraction based on the intensity of a signal generated from the MS detector, only a specific product can be targeted. Automated collection of fractions from the concentrated bergamot juice analysis was carried out using the signal generated from the MS. Since MS detector relies in principle on nebulization and ionization of the column eluate inside the detector, the targeted substances emerging from the detector cannot be recovered. To solve this problem, most of the column eluate is directed to the fraction collector, and the remaining micro-volume is introduced into the MS. As can be seen in Figure X-1A, the flow of mobile phase output from the [1]D preparative column is split by means of an APV splitter placed between the UV detector equipped with a preparative cell and the PDA and MS coupled in series. The split microflow (10 μL/min) reaches the PDA and then the MS, while the greatest part of the flow (9.990 mL/min) get to the waste or

to the autocollector. An analytical pump placed before the APV splitter generates a make-up flow to ensure a constant flow rate to the MS detector. According to the intensity threshold of fraction collection value, the system collected automatically four fractions (1, 2, 3, and 4). After six replicated injections of the concentrated bergamot juice, fractions were combined, concentrated, and subjected to analytical RP-HPLC-PDA analysis at the same chromatographic conditions optimized for the initial sample. In Figure X-3, the RP-HPLC-PDA chromatograms of each fraction purified by the preparative system are reported. As can be seen, the first fraction contained only apigenin 6,8-di-*C*-glucoside; fraction two included apigenin 6,8-di-*C*-glucoside, diosmetin 6,8-di-*C*-glucoside, and eriocitrin; fraction three contained neoeriocitrin, poncirin, naringin, narirutin, and neodiosmin; and fraction four comprised neohesperidin, brutieridin, and melitidin. Fractions 1 and 2 were combined together. Because none of the three fractions contained a pure compound, each fraction was subjected to a second purification step.

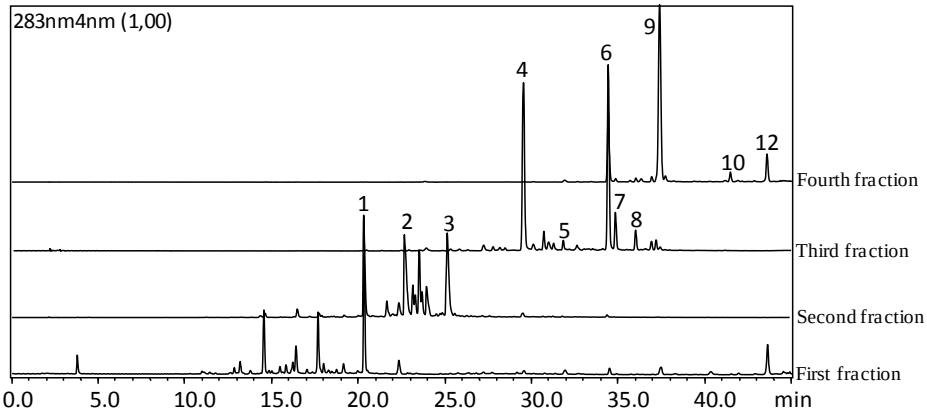

Figure X-3. *RP-HPLC-PDA chromatograms of the four fractions purified by means of the 1D HPLC-prep system.*

10.2.2.3. ^{2}D preparative analyses

A pentafluorophenylpropyl stationary phase was used to isolate pure compound from ^{1}D fractions. This stationary phase displayed a good separative capacity for bioactive molecules, higher retention for polar molecules compared to a C18 column; it represents a valid alternative to the common stationary phases used for flavonoids isolation in natural matrices.

In general, the ^{1}D preparative column is subjected to sample overloading, while ^{2}D preparative column is subjected to an injection of a semipurified fraction. The three fractions subjected to a second purification step were analyzed under isocratic conditions using water and acetonitrile. For fractions 1-2, 15% of acetonitrile was used; for fraction 3, 30% of acetonitrile; for fraction 4, 35% of acetonitrile. Moreover to efficiently use the preparative HPLC-MS fractionation, ^{2}D preparative analyses were performed in SIM mode (as reported in 10.2.5. section). In this way, only specific compounds can be targeted, thus MS only considers the target ions and is very sensitive. According to the intensity threshold value set in the method, the system automatically collected pure compounds. Subsequently, the molecules isolated and purified were crystallized and subjected to RP-HPLC-PDA analytical analysis under the same chromatographic conditions optimized for the bergamot juice, to determine the purity degree. All compounds presented a purity higher than 95%. The molecular structure of all the bioactive molecules purified were also confirmed by 1H NMR and ESI-MS data. From prep-MDLC analyses of 24 mL of the concentrated bergamot juice were purified: 30 mg of apigenin-6,8-di-*C*-glucoside (97.5% pure), 25 mg of diosmetin-6,8-di-*C*-glucoside (98.0% pure), 10 mg of eriocitrin (97.9% pure), 200 mg of naringin (99.9% pure), 100 mg of neoeriocitrin (99.9% pure), 250 mg of neohesperidin (99.9% pure), 15 mg of melitidin (97.3% pure), and 20 mg of brutieridin

(98.1% pure). To quantify flavanones in real sample, compounds isolated in this work were used to construct calibration curves of naringin, neoeriocitrin, brutieridin, and melitidin, considering the signal produced by PDA detector, as reported in Table X-1.

10.2.3. Conclusions

The LC-LC-PDA-MS preparative system used in this work allowed, in six analyses in the first dimension and 2-3 analyses for each fraction in the second dimension, the isolation of eight pure compounds present at very different concentration in the original sample with high purity and yield (from 10 to 250 mg), in a relatively short analysis time (11 h), showing how the system is efficient and versatile.

CASE 2.

10.3. Isolation of hesperidin from orange's waste waters

The waste products, derived from the local industrial plants in Sicily, represent a growing problem, while the cost to send this material for disposal greatly compromise the commercial trade, with a strong impact on the final cost of the primary product (orange juice). In order to minimize waste and to re-use the by-products it is necessary to deeply characterize their composition, with particular regards to bioactive molecules.

10.3.1. Experimental section

10.3.1.1. Samples and chemicals

This study was carried out on an orange juice, and on the by-products resulting from the entire industrial process: waste waters, solid residue (peels and pulps)

and seeds. The samples were collected at a local *Citrus* plant located in Barcellona Pozzo di Gotto (Messina, Italy).

The standard compounds: p-hydroxybenzoic acid, caffeic acid, eriocitrin, narirutin and hesperidin were obtained from Extrasynthese (Genay Cedex, France). Apigenin 6,8-di-*C*-glucoside was isolated in our laboratory (Russo, *et al.*, 2014). Methanol and *n*-hexane employed for the extraction procedure were obtained from VWR (Milan, Italy). Formic acid was purchased from Riedel-de Haën (Germany). For LC and preparative LC-LC analyses, water, acetonitrile and ethanol were obtained from Sigma-Aldrich.

10.3.1.2. Sample preparation

For the determination of bioactive molecules the samples of waste water was diluted 1:4, while orange juice required a dilution 1:5 with distilled water, then they were filtered on Acrodisc filter 0.45 μm and injected into HPLC.

The solid residues (peels and pulps) and the seeds were subjected to solvent extraction before HPLC analysis. The extraction procedure was carried out on 4 g of each dried sample, extracted with three aliquots of 40 mL of *n*-hexane, in order to remove the lipids present in the sample. The samples were extracted four times with aliquots of 40 mL of methanol, then they were dried with anhydrous sodium sulfate, filtered on filter paper, and brought to dryness in a rotary evaporator; the extract thus obtained was dissolved in 8 mL of a mixture of methanol/acetonitrile (3:1, *v/v*), filtered on Acrodisc filter 0.45 μm and injected into HPLC. Each sample was analyzed in triplicate.

10.3.1.3. RP-HPLC-PDA-MS analytical conditions

The instrumentation and software employed for this research are the same as for the CASE 1. For the HPLC conditions refer to 10.2.1.3. section.

MS acquisition was performed using both APCI, in positive mode, and ESI, in negative mode. In the latter case only 200 μL of the entire LC flow rate were directed to the interface. The total flow was switched to waste (500 μL) and to interface (200 μL) by means of a flow splitter. ESI conditions: mass spectral range, *m/z* 100-700; interval, 0.5 s; scan speed, 938 amu/s; N_2 flow, 1.5 L/ min; ESI temperature, 350 °C; heat block, 300 °C; DL temperature, 300 °C; DL, voltage −34 V; probe voltage, +4.5 kV; Qarray voltage, 1.0 V and detection gain, 1.05 kV. APCI conditions: mass spectral range, *m/z* 100-700; interval, 0.5 s; scan speed, 1500 amu/s; N_2 flow, 4.0 L/min; Interface temp., 350 °C; heat block, 300 °C; DL temp., 300 °C; DL, volt. −34 V; probe volt., +4.5 kV; Qarray volt., 1.0 V, detection gain, 1.05 kV.

10.3.1.4. Methods validation

Recovery of flavones, flavanones, and phenolic acids was performed on the orange solid residue (peel and pulp) samples. The extraction procedure was carried out after addition of known amounts of: p-hydroxybenzoic acid, caffeic acid, eriocitrin, narirutin and hesperidin on the sample, following a validated procedure previously adopted (Russo *et al.*, 2014). Each fortification was carried out on two different samples and every extract was analyzed in triplicate. Recovery was calculated using the following formula:

$$\text{Recovery \%} = [(\text{Cfs} - \text{Cuf})\, f] \times 100$$

where Cfs is the concentration of fortified sample, Cuf is the concentration of the unfortified sample, and *f* is the fortification.

In order to determine the amount of flavones, flavanones and limonoids present in orange-processing by-products, calibration curves were constructed by using

each available standard or previously isolated. The procedure for the analytical method validation was the same to that previously reported for bergamot juice.

10.3.1.5. Isolation of hesperidin from waste waters

Fifty milliliters of orange waste waters have been subjected to a preparative LC-LC/MS using two different preparative columns: Ascentis Express C18 (250 mm × 21.2 mm I.D., 5 μm d_p) was used as ^{1}D, and Discovery HS F5-5 (250 mm × 21.2 mm I.D., 5 μm d_p) as ^{2}D. Injection volume was 25 mL. As mobile phase water (solvent A) and ethanol (solvent B) were employed and the flow rate was 10 mL/min for both ^{1}D and ^{2}D. ^{1}D elution gradient was: 0min, 0%B, 5min, 0%B, 30min, 100%B, 40min, 100%B. ^{2}D elution gradient was: 0 min, 20% B, 5 min, 20% B, 30 min, 100% B, 40 min, 100% B.

MS acquisition was performed using ESI in negative mode. ESI conditions: mass spectral range, *m/z* 100-800; interval, 0.35 s; scan speed, 2143 amu/s; nebulizing gas (N_2) flow, 1.5 L/min; ESI temperature, 350 °C; heat block, 300 °C; DL temperature, 250 °C; DL, voltage −34 V; probe voltage, +4.5 kV; Qarray voltage, 1.0 V and detection gain, 1.05 kV. The fraction collection was realized by means of the autocollector GX-281 Gilson. As already described for the CASE 1, the auto-collection of fractions eluted from the preparative column was in accord with MS signal based on MS triggering signal. Fractions with hesperidin eluted from the ^{1}D preparative column were combined, concentrated with a rotary evaporator (up to 10 mL), and re-injected two times onto the ^{2}D preparative column with an injection volume of 5 mL each. The collected fractions were evaporated by a rotary evaporator to obtain hesperidin (40 mg), whose structure was confirmed by FTIR as described below.

10.3.1.6. FTIR analysis of hesperidin

In order to confirm the presence of hesperidin in the collected fraction an FTIR experiment was carried out using a Bruker Vertex 80 FT-IR system (Bruker Italia, Milan, Italy) equipped with a RT-DLaTGS detector operating a 40 kHz scanner velocity. Spectra were collected at 4 cm^{-1} resolution covering the range from 3700 to 700 cm^{-1}. The sample containing the solvent used for making the solution (acetonitrile) was placed between two IR-transparent KBr plates that were placed in a dedicated sample holder. After the evaporation of the solvent a spectrum of the sample was acquired (30 scans). The molecule was confirmed by comparison of the resulting spectrum obtained from authentic standard.

10.3.2. Results and discussion

In all the the products generated from the industrial processing of sweet orange significant amounts of bioactive molecules were determined. In Table X-2 are reported the quantitative values (mg/kg ± standard deviation) of bioactive molecules in the sample analyzed. As can be noted, flavanones are more abundant than phenolic acids, flavones and limonoids, both in the orange juice and in the by-products. Thirteen compounds belonging to four different classes of components (six different flavonoids, two phenolic acids and five limonoids) were detected (Figure X-4). Seeds were the richest source of bioactive molecules, with flavanones being the most abundant, followed by phenolic acids (238 mg/kg). The solide residue (exhausted peels and pulps) was characterized by higly content of p-hydroxybenzoic acid and caffeic acid (560 mg/kg). Among all the samples analysed, in the juice, the primary product of the industrial transformation of orange, was detected the lowest amounts of total bioactive compounds (1,8 g/kg). Limonoids were determined exclusively in seeds (560 mg/kg), while hesperidin was the most abundant compound in all

the sample investigated. In particular the highest amount of such compound was determined in seeds, followed by the waste water (20 g/kg). On the basis of this result, an eco-compatible friendly preparative LC-LC-MS method for the recovery and purification of hesperidin from the waste water was developed. The isolation of such compound was performed by using only water and ethanol as LC eluents, which are compatible with human consumption. The prep-LC-LC-MS method developed permitted to purify and isolate 40 mg of hesperidin with a yield of 4% that allowed obtaining hesperidin 99.9% pure.

Table X-2. *Concentration values (mg/kg) of phenolic acids, limonoids and flavonoids content in orange-processing by products.*

N°	Compounds	Juice	Seeds	Pulps	Waste water
1	p-Hydroxybenzoic acid *4-hydroxybenzoic acid*	19.6 ± 0.97	153.6 ± 9.96	367.7 ± 18.71	-
2	Caffeic acid *3-(3,4-Dihydroxyphenyl)- 2-propenoic acid*	95.4 ± 3.78	84.7 ± 3.38	192.7 ± 11.37	-
3	Apigenin 6,8-di-*C*-glucoside *5,7,4'-Trihydroxyflavone-6,8-di-C-β-glucoside*	9.9 ± 0.26	32.3 ± 2.16	22.3 ± 0.93	-
4	Apigenin7-(malonylpiosyl)-glucoside[a] *5,7,4'- Trihydroxyflavone 7-O- (malonylpiosyl)glicoside*	11.0 ± 0.74	36.0 ± 2.46	32.8 ± 1.82	318.8 ± 0.3
5	Eriocitrin *5,7,3',4'-tetrahydroxyflavonone-7- β-rutinoside*	165.1 ± 9.16	747.0 ± 35.07	404.5 ± 12.02	1167.7 ± 0.2
6	Narirutin *5,7,4'-trihydroxyflavanone7- β-rutinoside*	442.6 ± 24.81	4704.7 ± 309.34	5452.0 ± 352.04	1479 ± 4.3
7	Hesperidin *5,7- Trihydroxy-4'-methoxy flavone7- β-rutinoside*	986.3 ± 24.91	40399.7 ± 1876.28	14864.6 ± 841.38	19640.9 ± 322.25
8	Didimin[b] *5,7,3'-Dihydroxy-4'-methoxyflavonone7-O-rutinoside*	63.8 ± 4.48	1584.3 ± 86.96	1576.9 ± 44.40	942.7 ± 42.39
9	Ichangin	-	1.3 ± 0.03	-	-
10	Deacetylnomilin *1-Hydroxy-1,2-dihydroobacunoic acid ε-lactone*	-	< LOQ	-	-
11	Limonin *7,16-dioxo-7,16-dideoxylimondiol*	-	75.1 ± 2.09	-	-
12	Nomilin *1-(Acetyloxy)-1,2-dihydroobacunoic acid ε-lactone*		21.9 ± 1.04	-	-
13	Obacunone *Obacunoic acid ε-lactone*	-	15.9 ± 0.67	-	-

Phenolic acids	*115*	*238*	*560*	-
Flavons	*21*	*68*	*55*	*318*
Flavanones	*1658*	*47436*	*22298*	*23230*
Limonoids	-	*114*	-	-
BIOACTIVE MOLECULES	**1,794**	**47,856**	**22,914**	**23,549**

For quantitative determination of all the identified polyphenolic compounds were calculated calibration curve of: [a]apigenin 6,8-di-*C*-glucoside, [b]hesperidin; quantitative determination of limonoids were based on correction factor equal to 1.

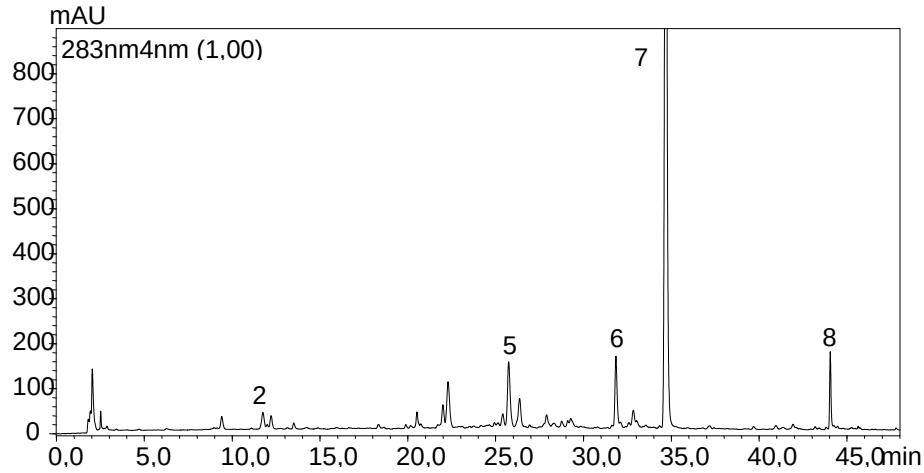

Figure X-4. *RP-HPLC-PDA chromatogram of polyphenols content in orange waste water. For peak identification see Table X-2.*

Figure X-5 depicted the UV preparative chromatogram (A), the HPLC-MS total ion chromatogram (B) of orange waste water analyzed in the first dimension, and (C) the MS spectra of the fraction isolated in the first dimension. Figure X-6 showed the UV preparative chromatogram (A), the HPLC-MS total ion chromatogram (B) of the fraction containing hesperidin purified on the first dimension analyzed in the second one, and (C) the correspondent MS spectra. The compound isolated was then analyzed by FTIR in order to characterize it (Figure X-7).

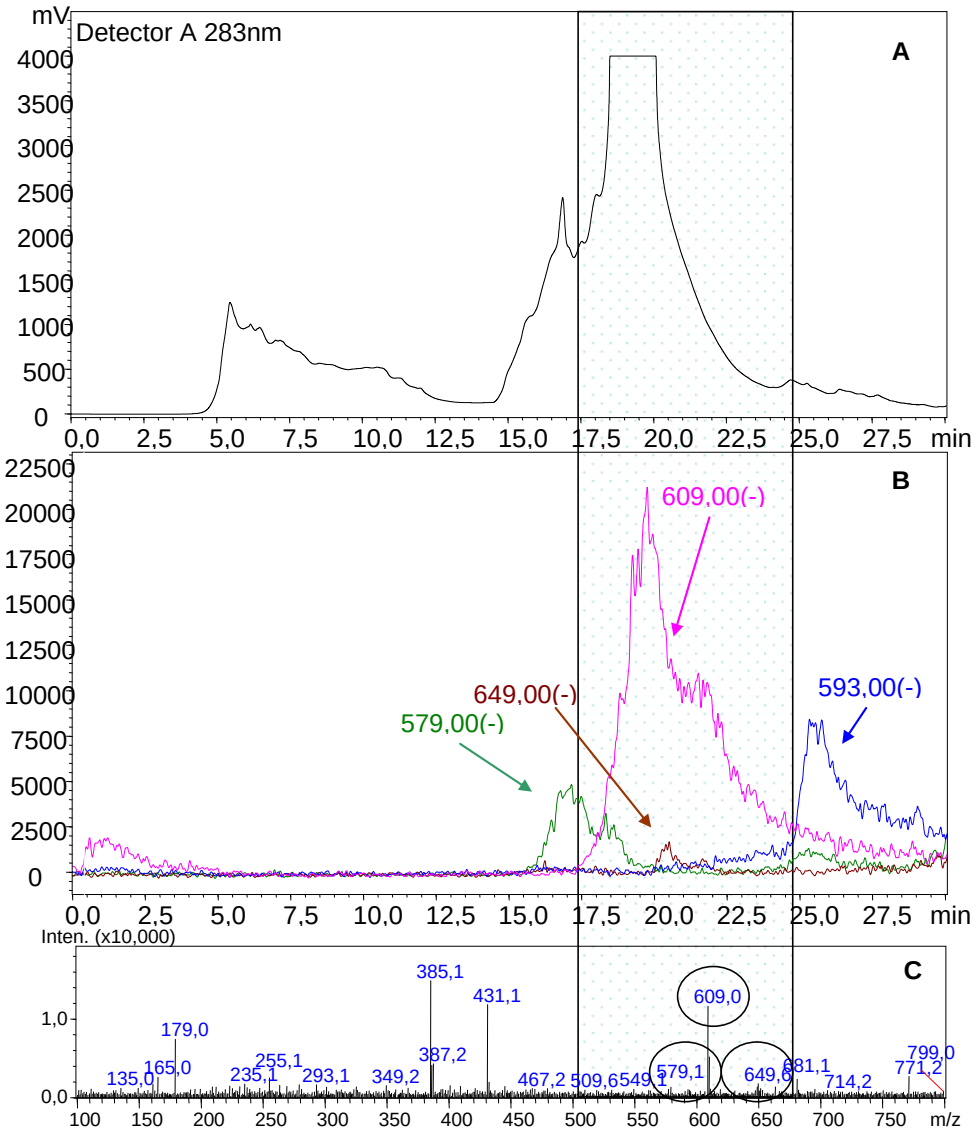

Figure X-5. *UV preparative chromatogram (A), HPLC-MS total ion chromatogram (negative ion mode) (B) of orange waste water analyzed in the first dimension, and (C) MS spectra of fraction isolated in first dimension. Narirutin (579), Hesperidin (609), Didimin (593), Apigenin7-(malonylpiosyl)-glucoside (649).*

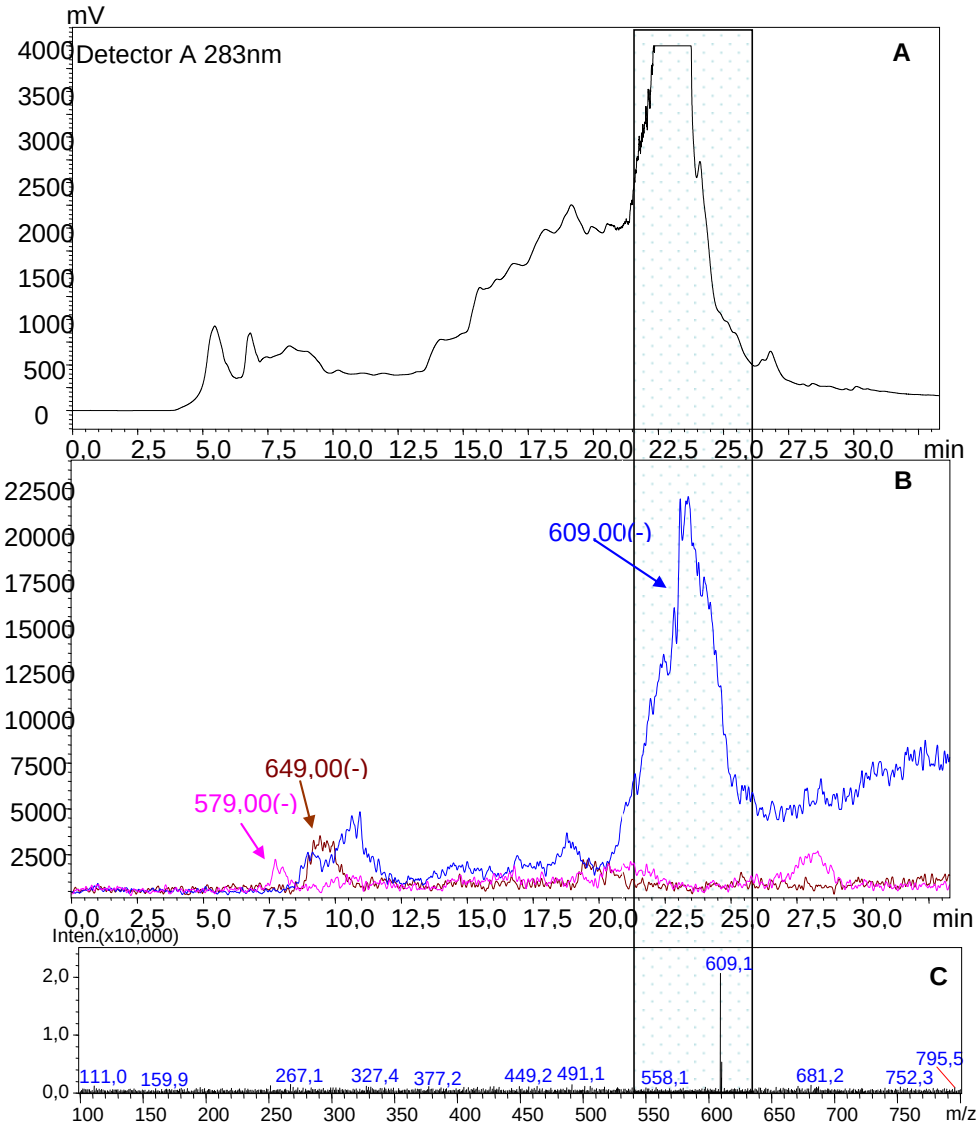

Figure X-6. *UV preparative chromatogram (A), HPLC-MS total ion chromatogram (negative ion mode) (B) of the fraction collected from the preparative analysis of the orange waste water and (C) MS spectra of hesperidin isolated in second dimension. Narirutin (579), Hesperidin (609), Apigenin7-(malonylpiosyl)-glucoside (649).*

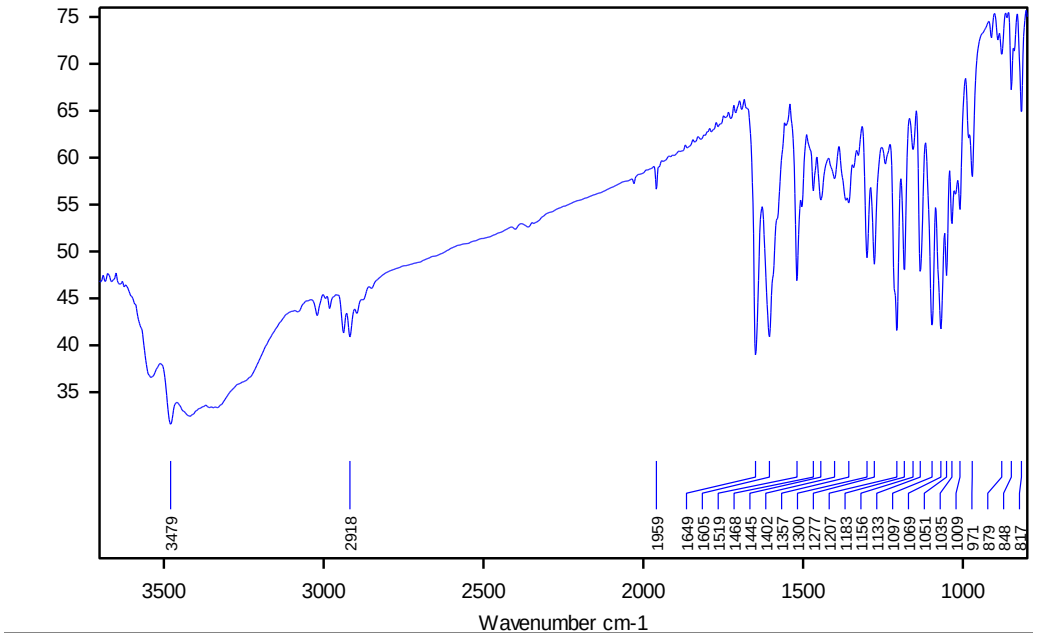

Figure X-7. *FTIR spectrum of the pure hesperidin.*

10.3.3. Conclusions

From the results presented, it is possible to conclude that all the by-products, generated by the Citrus industrial transformation, represent a rich source of bioactive molecules, so they can potentially find applications in the nutraceutical, cosmeceutical, food and feed industry. In particular, water can be easily treated to isolate important amounts of flavanone, which can be used as antioxidant and prebiotics in different functional food preparations. The prep-LC-LC-MS method developed allowed to purify and isolate a great amount of hesperidin (40 mg) with high yield (4%) and purity (99.9%). (This chapter was adapted from Russo, *et al.*, 2016; Russo, *et al.*, 2015).

REFERENCES

- Baldi A., Rosen R.T., Fukuda E.K., Ho C.T., J. Chromatogr. A 1995, 718, 89-97.
- Benavente-Garcia O., Castillo J., Marin F.R., Ortuno˜ A., Del Rìo J.A., J. Agric. Food Chem. 1997, 45, 4505-4515.
- Caristi C., Bellocco E., Gargiulli C., Toscano G., Lezzi U., Food Chem. 2006, 95, 431-437.
- Delle Monache S., Sanità P., Trapasso E., Ursino M.R., Dugo P., Russo M., Ferlazzo N., Calapai G., Angelucci A., Navarra M., PLoS ONE 2013, 8, 1-14.
- Di Donna L., De Luca G., Mazzotti F., Napoli A., Salerno R., Taverna D., Sindona G., J. Nat. Prod. 2009, 72, 1352-1354.
- Dugo P., Russo M., Saro` M., Carnovale C., Bonaccorsi I., Mondello L., J. Sep. Sci. 2012, 35, 1828-1836.
- EURACHEM, The Fitness for Purpose of Analytical Methods: A Laboratory Guide to Method Validation and Related Topics, EURACHEM Guide, 2014.
- Gardana C., Nalin F., Simonetti P., Molecules 2008, 13, 2220-2228.
- Gattuso G., Barreca D., Gargiulli C., Lezzi U., Caristi C., Molecules 2007, 12, 1641-1673.
- He D., Shang Y., Wu Y., Liu G., Chen B., Yao S., Food Chem. 2011, 127, 880-885.
- Jayaprakasha G.K., Nagana Gowda G.A., Marquez S., Patil B.S., J. Chromatogr. B 2013, 937, 25-32.
- Jiang Y., Zhao W., Feng C., Zhou T., Fan G., Wu Y., Biomed. Chromatogr. 2009, 23, 1064-1072.
- Jin H., Liu Y., Feng J., Guo Z., Wang C., Zhong Z., Peng X., Dang J., Tao Y., Liang X., J. Sep. Sci. 2013, 36, 2414-2420.
- Li K., Zhu W., Fu Q., Ke Y., Jin Y., Liang X., Analyst 2013, 138, 3313-3320.
- Liu Q., Shi S., Liu L., Yang H., Su W., Chen X., J. Chromatogr. A 2013, 1304, 183-193.

- Navarra M., Ursino M.R., Ferlazzo N., Russo M., Schumacher U., Valentiner U., Fitoterapia 2014, 95, 83-92.
- Pernice R., Borriello G., Ferracane R., Borrelli R.C., Cennamo F., Ritieni A., Food Chem. 2009, 112, 545-550.
- Qiu Y.K., Chen F.F., Zhang L.L., Yan X., Chen L., Fang M.J., Anal. Chim. Acta 2014, 820, 176-186.
- Russo M., Bonaccorsi I., Inferrera V., Dugo P., Mondello L., J. Funct. Foods 2015, 12, 150-157.
- Russo M., Bonaccorsi I., Torre G., Saro` M., Dugo P., Mondello L., J. Funct. Foods 2014, 9, 18-26.
- Russo M., Cacciola F., Bonaccorsi I., Dugo P., Mondello L., J. Sep. Sci. 2011, 34, 681-687.
- Russo M., Dugo P., Marzocco S., Inferrera V., Mondello L., J. Sep. Sci. 2016, 38, 4196-4203.
- Su W., Liu Q., Yang Q., Yu J., Chen X., J. Sep. Sci. 2013, 36, 3338-3344.
- Wong V., Sweeney A.P., Shalliker R.A., J. Sep. Sci. 2004, 27, 47-52.
- Xie Y., Zhao W., Zhou T., Fan G., Wu Y., Phytochem. Anal. 2010, 21, 473-482.
- Zhang Y., Zeng L., Pham C., Xu R., J. Chromatogr. A 2014, 1324, 86-94.

List of original papers

1) Supercritical Fluid Chromatography for Lipid Analysis in Foodstuffs
Paola Donato, **Veronica Inferrera**, Danilo Sciarrone, Luigi Mondello
In Press J. Sep. Sci.

2) High informative multiclass profiling of lipid by ultra-high pressure liquid chromatography- quadrupole mass spectrometry by using ESI and APCI interfaces
Marco Beccaria, **Veronica Inferrera**, Francesca Rigano, Krzysztof Gorynski, Giorgia Purcaro, Paola Dugo, Luigi Mondello
Sent to J. Chromatogr. A

3) Characterization of the pigment fraction in sweet bell peppers (*Capsicum annuum* L.) harvested at green and overripe yellow and red stages by off-line multidimensional convergence chromatography/liquid chromatography-mass spectrometry
Ivana Bonaccorsi, Francesco Cacciola, Margita Utczas, **Veronica Inferrera**, Daniele Giuffrida, Paola Donato, Paola Dugo, Luigi Mondello
J. Sep. Sci. 2016, 39, 3281-3291.

4) Multidimensional preparative liquid chromatography to isolate flavonoids from bergamot juice and evaluation of their anti-inflammatory potential
Marina Russo, Paola Dugo, Stefania Marzocco, **Veronica Inferrera**, Luigi Mondello
J. Sep. Sci. 2016, 38, 4196-4203.

5) Underestimated sources of flavonoids, limonoids and dietary fiber: Availability in orange's by- products
Marina Russo, Ivana Bonaccorsi, **Veronica Inferrera**, Paola Dugo, and Luigi Mondello
J. Funct. Food 2015, 12, 150–157.